An Improved Model To Simulate Pollutant Dispersion From Roadways

By

ANTHONY EDWARD HELD
B.S. (University of Texas, Austin) 1994
M.S. (University of California, Davis) 1998

DISSERTATION
Submitted in partial satisfaction of the requirements for the degree of
DOCTOR OF PHILOSOPHY

in

Civil and Environmental Engineering
in the
OFFICE OF GRADUATE STUDIES
of the
UNIVERSITY OF CALIFORNIA
DAVIS

Approved:

_____

_____

_____

Committee in Charge
2001

Table of Contents

List of Tables

List of Figures

Dedication

This dissertation is dedicated to my mother Gayle, father David and sister Heidi. Thank you for a lifetime of loving support.

Acknowledgements

A number of organizations provided support for my doctoral research that lead to the creation of the UCD 2001 model. I would like to thank Dr. Pat Mokhtarian and the National Science Foundation (NSF) for their support through the Integrative Graduate Education and Research Training (IGERT) program. In addition, this research would not have been possible without funding from the Federal Highway Administration (FHA) and the Dwight David Eisenhower Transportation Fellowship Program.

I would also like to thank Dr. Desmond Lawler and Dr. Richard Corsi at the University of Texas, Austin for their kind words and inspiration that resulted in my interest in graduate studies. Special thanks are also in order for Dr. Kyaw Tha Paw U and Dr. John Carroll of the University of California, Davis (UCD) atmospheric science department for their help in developing the UCD 2001 model. In addition, I am indebted to Whitney Leeman for her tireless efforts in proofreading and editing my dissertation. Last but not least, I would like to thank my advisors, Dr. Daniel Chang, Dr. Debbie Niemeier, and Dr. Roger Shaw for the countless meetings, advice, and nurturing that they provided during my graduate studies.

Abstract

An improved dispersion model, UCD 2001, designed to estimate pollutant concentrations near roadways was developed and its performance evaluated. The UCD model internally represents a highway link as a three-dimensional array of point sources which simulates a roadway mixing zone that extends 2.5m above a highway link. Dispersion from each point source is estimated with the Huang dispersion equation. The Huang equation is a simplified solution to the semi-empirical advection diffusion equation (SEADE) whose derivation requires that the vertical profiles of wind speed and eddy diffusivity in the boundary layer be approximated by power law functions.

Several independent studies concluded that the atmosphere is well mixed and neutrally stratified immediately downwind of a roadway with significant vehicular activity. The UCD 2001 model was calibrated with one-half of the General Motors (GM) SF_6 tracer study database. This calibration resulted in a selection of eddy diffusivity parameters that did not vary with ambient meteorology which suggests pollutant mixing immediately downwind of an active roadway depends more on vehicle activity than upon ambient meteorology. Consistent with these findings, UCD 2001 assumes a neutral downwind profile and does not compensate for ambient stability effects downwind of an active highway.

UCD 2001 model performance was evaluated and compared to the CALINE3 and CALINE4 dispersion models using the GM database. UCD 2001 adequately simulates near parallel, low wind speed (less than 0.5 m/s) meteorological conditions, whereas the CALINE models significantly over predict most receptor concentrations for these conditions. The UCD 2001 model results in approximately 80 to 90 percent reduction in

least squared residual error when compared to the CALINE3 and CALINE4 models. In addition, the UCD 2001 model shows better agreement in simulating the top forty observed concentrations than either CALINE model. Lastly, the UCD 2001 model requires less user input and modeler expertise than most roadway dispersion models and should result in more consistent and robust pollutant field estimations.

Chapter 1. Introduction and Background

Overview and Thesis Organization

The central focus of this thesis is the development and evaluation a novel dispersion model named UCD 2001. UCD 2001 is designed to predict roadway pollutant concentrations in the near field (less than 100m) region downwind of a highway in a more robust and accurate manner than existing regulatory models.

Chapter 1 addresses the regulatory basis of roadway dispersion analysis. The Gaussian and Huang dispersion equations are presented in Chapter 2. These equations are solutions to the semi-empirical advection diffusion equation and are used extensively in roadway dispersion modeling. A discussion of variables thought to influence pollutant transport near roadways is presented in Chapter 3. Chapter 4 contains the findings of a literature review of major roadway dispersion experiments. Selected roadway dispersion models are described in Chapter 5.

The UCD 2001 dispersion model is introduced in Chapter 6. An analysis of UCD 2001, contrasted with the CALINE3 and CALINE4 dispersion models performance, is presented in Chapter 7. A summary of findings and conclusions are presented in Chapter 8.

Air Quality Regulations

The primary reason air pollution specialists and transportation engineers model dispersion from proposed and existing roadways is to comply with state and federal environmental regulations. In this section regulations pertaining to roadway dispersion analysis are reviewed.

Environmental laws typically do not specify or contain all the details necessary for their practical use (US EPA 2000). For instance, the Clean Air Act does not specify each step that a transportation project manager must take to ensure that air pollution standards will be met near a proposed roadway. "In order to make the laws work on a day-to-day level, Congress authorizes certain governmental agencies, including EPA, to create regulations. Regulations set specific rules as to what is legal and what isn't" (US EPA 2000).

To facilitate the application of these regulations, the Federal Highway Administration (FHWA) and the Federal Transit Administration (FTA) published "Transportation Conformity: A Basic Guide for State & Local Officials (FHWA 1997)" which is a distillation of regulations necessary for transportation/ air quality analysis.

"By 1990, Congress recognized that, despite previous efforts, there were still about 100 million Americans living in urban areas that did not meet EPA standards for healthful air" (Cooper and Alley 1994). The CAAA of 1990 was created in part to reduce the number of Americans living in unhealthful air by introducing new amendments that make NAAQS attainment possible and enforceable. The need to model pollutant fields near roadways to ensure NAAQS are not violated was the impetus for the research conducted in this dissertation. The CAAA promulgated "hot spot" (or microscale conformity) regulations as defined below.

- **Hot-spot analysis**: "… is an estimation of likely future localized CO and PM_{10} pollutant concentrations and a comparison of those concentrations to the national ambient air quality standards. Hot-spot analysis assess impacts on a scale smaller than the entire nonattainment or maintenance area, including, for example, congested roadway intersections and highways or transit terminals, and uses an air quality dispersion model to determine the effects of emissions on air quality" (40 CFR Parts 51 and 93 1997).

Hot spot analysis is typically considered for carbon monoxide (CO) and particulate matter (PM) with an aerodynamic diameter of 10 microns or less. The CFR sections that directly relate to modeling CO and PM hotspots are listed below:

- 40 CRF 93.105 Consultation
- 40 CRF 40 CRF 93.116 Criteria and procedures: Localized CO and PM10 violations (hot spots)
- 40 CRF 93.117 Criteria and procedures: Compliance with PM10 control measures
- 40 CRF 93.123 Procedures for determining localized CO and PM10 concentrations (hot spot analysis)
- 40 CFR Appendix W to Part 51 – Guideline on Air Quality Models

Sections 40 CRF 93.116 states that a "FHWA/FTA project[s] must not cause or contribute to any new localized CO or PM_{10} violations or increase the frequency or severity of any existing CO or PM10 violations in CO and PM_{10} nonattainment and maintenance areas" (40 CFR Parts 51 and 93 1997). Furthermore, 93.116 states that "each FHWA/FTA project must eliminate or reduce the severity and number of localized CO violations in the area substantially affected by the project [in CO nonattainment areas]" (40 CFR Parts 51 and 93 1997). These two conditions must be demonstrated according to the consultation requirements of 93.105 and the methodology requirements of 93.123.

40 CFR 93.123 states that "CO hotspot analysis …must be based on quantitative analysis using the applicable air quality models, data bases, and other requirements specified in 40 CFR part 51, Appendix W (Guideline on Air Quality Models) … unless different procedures developed through the interagency consultation process required in § 93.105 and approved by the EPA Regional Administrator are used." In the state of California, an interagency consultation process was conducted and resulted in the report titled "Transportation Project-Level Carbon Monoxide Protocol" (hereafter referred to as the CO Protocol). The CO Protocol was completed by the Institute of Transportation Studies at the University of California, Davis (UCD ITS) under contract to the California Department of Transportation (Caltrans). Thus, in California, transportation planners use the CO Protocol to verify project level conformity, whereas in most other states, planners must show compliance with § 93.123 using CFR part 51, Appendix W to determine conformity.

Roadway Dispersion Models Approved for Regulatory Purposes

Transportation projects must demonstrate conformity with state and local air pollution goals to be federally approved. Specific guidance regarding how dispersion models may be used to show hot-spot conformity is given in 40 CFR part 51. In the state of California, it is sufficient to use the guidelines set forth in the CO Protocol to show project conformity. This section will introduce the dispersion models that are listed in these two documents. In addition, basic modeling terms such as "screening model" will be defined to facilitate interpretation of the CFR and CO Protocol.

Levels of Model Sophistication

EPA defines two levels of sophistication for utilizing air-quality models. "The first level consists of general, relatively simple estimation techniques that provide conservative estimates of the air quality impact of a specific source" (40 CFR Appendix to Part 51 1997). A model used for this purpose is commonly referred to as a *screening model*. The purpose of a screening model is "to eliminate the need of further more detailed modeling for those sources that clearly will not cause or contribute to ambient concentration in excess of … the NAAQS" (40 CFR Appendix to Part 51 1997). An example of a screening technique would be to estimate a worst case modeling parameter, such as a wind speed of 0.5 m/s, rather than attempting to estimate a reasonable wind speed for the modeled air pollution event. If it can be shown that an air pollution event would not violate a NAAQS for a worst case modeling parameter it is reasonable to forego the additional effort one would have to invest to perform a more realistic modeling scenario.

"If a screening technique indicates that the concentration contributed by the source exceeds … the NAAQS, then the second level of more sophisticated models should be applied" (40 CFR Appendix to Part 51 1997). EPA refers to the second level of sophistication as a *refined model.* Refined models "consists of those analytical techniques that provide more detailed treatment of physical and chemical atmospheric processes, require more detailed and precise input data, and provide more specialized concentration estimates. As a result they provide a more refined and, at least theoretically, a more accurate estimate of source impact and the effectiveness of control strategies" (40 CFR Appendix to Part 51 1997).

EPA indicates "the use of screening techniques followed by a more refined analysis is always desirable" (40 CFR Appendix to Part 51 1997). However, the following passage indicates that a refined technique is not always feasible.

> There are situations where the screening techniques are practically and technically the only viable option for estimating source impact. In such cases, an attempt should be made to acquire or improve the necessary data bases and to develop appropriate analytical techniques. Source: (40 CFR Appendix to Part 51 1997)

40 CFR part 51, Appendix W (Guideline on Air Quality Models)

40 CFR part 51, Appendix W (hereafter referred to as the Guideline) is a comprehensive document that provides guidelines on a wide spectrum of air quality models. "The guideline recommends air quality modeling techniques that should be applied to SIP revisions for existing sources and to new source reviews … it should serve as a basis by which air quality managers, supported by sound scientific judgment, have a common measure of acceptable technical analysis" (40 CFR Appendix to Part 51 1997).

Appendix A of the Guideline identifies CALINE3 as an EPA preferred model for use in regulatory applications. Furthermore, section 3.1.2 indicates that CALINE3 "may be used without a formal demonstration of applicability as long as [CALINE3 is] …used as indicated in [its] model summary of Appendix A" (40 CFR Appendix to Part 51 1997). Section 6.2.2 indicates "for analyses of highways characterized by uninterrupted traffic flows, CALINE3 is recommended, with emissions input from the latest version of the MOBILE model" (40 CFR Appendix to Part 51 1997).

The following excerpt is from section 6.2.2 of the Guideline, which indicates the EPA approved models for intersection modeling.

> For analyzing CO impacts at roadway intersections, user should follow the procedures in the 'Guideline for Modeling Carbon Monoxide from Roadway Intersections'. The recommended model for such analyses is CAL3QHC. This model combines CALINE3 … with a traffic model to calculate delays and queues that occur at signalized intersections. In areas where the use of either TEXIN2 or CALINE4 has previously been established, its use may continue.
>
> The capability exists for these intersection models to be used in either a screening or refined mode. The screening approach is described in reference (EPA 1992a); a refined approach may be considered on a case-by-case basis. Source: (40 CFR Appendix to Part 51 1997)

Thus, according to the Guideline, CALINE3 and CAL3QHC are endorsed for roadway dispersion, and CALINE4 and TEXIN2 are qualitatively recommended for use in certain regions of the U.S. Using these models presumably would facilitate EPA acceptance of a project level conformity report, however the following quote from Section 3.0 of the guideline makes it clear that EPA will consider other models and analysis approaches as well.

> It should not be construed that the preferred models identified here are to be permanently used to the exclusion of all others or that they are the only models available for relating emissions to air quality. The model that most accurately estimates concentrations in the area of interest is always

> sought. However, designation of specific models is needed to promote consistency in model selection and applications.

The California CO Protocol

The CO Protocol outlines procedures and guidelines "for use by agencies that sponsor transportation projects, to evaluate the potential local level CO impacts of a project" (Garza et al. 1997). The Protocol has been approved by EPA region IX as an acceptable alternative to 93.123 of the 1997 conformity regulation (1997; Garza et al. 1997).

CALINE4 is the dispersion model specified in the CO Protocol for hot spot analysis. The CO Protocol recommends receptor placements similar to those indicated in the 'Guideline for Modeling Carbon Monoxide from Roadway Intersections'. Thus, the dispersion algorithms and receptor placement for California hot-spot analysis are essentially identical to those used outside California.

Guideline for Modeling Carbon Monoxide from Roadway Intersections

The Guideline for Modeling Carbon Monoxide from Roadway Intersections (hereafter referred to as Intersection Guideline) was "designed to evaluate air quality impacts at one or more roadway intersections where vehicular traffic will cause or contribute to increased emissions of carbon monoxide (CO)" (EPA 1992a). It is designated in section 6.2.2 of the Guideline for use in intersection hot-spot analyses. According to the report,

> [The Intersection Guideline] is appropriate for project level analyses in accordance with SIPs, including conformity analyses. This guidance may also be used for Environmental Impact Statements (EISs). Development projects such as street and intersection reconfigurations, mall constructions, and other construction projects that could significantly affect traffic patterns will require air quality impact assessment. For such studies, the effect of the project on traffic, congestion, and subsequent air quality impacts must be studied. This guideline offers guidance for applying dispersion and emission modeling techniques for such analyses.

The Intersection Guideline makes it clear that the dispersion models that are approved for intersection modeling use CALINE3 algorithms (e.g. CAL3QHC) or slight modifications of the CALINE3 algorithms (e.g. CALINE4 & TEXIN2) for dispersion modeling.

> Several states have developed their own models for project level analysis. The models TEXIN and its update, TEXIN2 (Hlavinka et al. 1987), were developed by Texas in 1983 and 1987, respectively; the Georgia Intersection Model (GIM) was developed by Georgia in 1985; the CAL3Q model was developed by EPA Region I in 1987; and successive versions of the CALINE model were developed by California, with CALINE3 (Benson 1979) in 1979 and CALINE4 (Benson 1984) in 1984. Most of these models have been used in areas of the country outside the state in which they were originally developed. It should be noted that CALINE3 is simply a dispersion model and does not contain an emissions or traffic component as do the other models mentioned. In fact, the dispersion components of these other models is essentially CALINE3 with, in some cases, very minor modifications.
>
> Because of its widespread use nationally, CALINE3 became the EPA recommended dispersion model for highway project level analysis in 1986 … CAL3QHC (Version 2.0) (EPA 1992b) has been selected as the recommended CO intersection model in the Guideline on Air Quality Models for intersection modeling. CAL3QHC contains the CALINE3 dispersion model and utilizes procedures in the 1985 Highway Capacity Manual to calculate queue length. The latest version of the MOBILE emissions model is used to calculate emissions input to the CAL3QHC model.

The 3-m Receptor Location Requirement

According to the EPA guidelines, hot-spot analysis requires, with some qualifications, that NAAQS must be met 3 m from any traveled way at a location near breathing height where the public is likely to have public access. Ground, and near ground level, pollutant concentrations are likely to decrease as receptor distance is increased from the traveled way. Thus, compliance with the NAAQS standard at 3 m is a necessary, and likely a sufficient condition, for project level conformity.

Chapter 2. Review of Dispersion Algorithms

Introduction

To model air pollution from first principles one needs to derive a coupled set of differential equations based on our understanding of the underlying physics of atmospheric fluid dynamics and chemistry. This set of equations consists of 1) Newton's law of motion, 2) the first law of thermodynamics, 3) mass continuity, and 4) the equation of state. Direct solution of these equations requires a detailed knowledge of both the initial and boundary conditions of an atmosphere and powerful computing resources to simulate even the most simple air pollution scenarios. To avoid the overhead of these advanced techniques, a variety of simplistic equations and relationships have been developed to provide insight into the transport of atmospheric pollutants.

Two simplified dispersion equation will be developed in this chapter. The first is the Huang dispersion equation that is the foundation of the UCD 2001 dispersion model.

The second is the Gaussian equation, selected because it is the foundation of the CALINE3 & CALINE4 dispersion algorithms.

The Semi-Empirical Advection Diffusion Equation

The Semi-Empirical Advection Diffusion Equation (SEADE) is a typical starting point for the derivation of simplified dispersion algorithms as Equation 2-1. For a detailed derivation and description of each term in the SEADE readers are encouraged to consult "An Introduction to Boundary Layer Meteorology" (Stull 1988).

$$\frac{\partial \overline{c}}{\partial t} + \overline{u}_j \frac{\partial \overline{c}}{\partial x_j} = \frac{\partial}{\partial x_j}\left(K_{jj} \frac{\partial \overline{c}}{\partial x_j} \right) + S_C \qquad (2\text{-}1)$$

This equation indicates that time dependent evolution of the concentration field of a non-reactive pollutant will be known over a volume of interest if the wind field, eddy diffusivity coefficients, and source terms are also fully specified over the same domain and time period. The terms of the SEADE are explored in the following sub sections.

Dependence of SEADE Terms on Stability

Atmospheric transport processes are strongly dependent upon vertical temperature gradients. Correspondingly, the eddy diffusivity coefficients, and wind speed variables in the SEADE are commonly parameterized in terms of these gradients. Temperature gradients are formed at the surface layer due to complex interactions of radiative heating and thermal advection. The presence of temperature gradients may serve to increase or decrease turbulent mixing processes. As a practical matter, many dispersion modeling algorithms are dependent upon a stability class scheme developed in the early 1960's rather than directly using temperature gradients to address mixing processes.

Most stability schemes define a neutral atmosphere as a reference condition. For atmospheric dispersion purposes, a neutral atmosphere is defined as having a temperature profile that is in thermodynamic equilibrium. For this equilibrium to exist the atmosphere would have to be completely mixed or void of any boundary temperature forcings. Given that radiative heat processes always occur, and atmospheric mixing processes usually do not result in a completely mixed atmosphere, the neutral stability

class is rarely attained for long periods of time. Based on a literature review presented in Chapter 4, it is assumed that the intense mechanical and thermal mixing above a roadway result in either a well mixed neutral temperature profile or a profile too complex for standard stability classifications. At some point significantly downwind of the roadway (e.g. 5 km) one would expect that the atmosphere would relax back to its original stratification. However, since most roadway dispersion experiments were exclusively based on near field measurements (<100m), there is little experimental data available to characterize the atmosphere's transition from neutral to ambient stratification.

SEADE Wind Field Terms

An analytical solution to Equation 2-1 is possible, at least in theory, if one could determine the wind field as an analytical function of x, y, z, and t. To facilitate the mathematics of Equation 2-1, one typically aligns the horizontal wind direction with the x-axis. This re-alignment requires that the horizontal resultant wind vector direction is uniform. This assumption can be quite accurate for certain engineered systems, but it is a poor approximation of a natural system with obstructions or complex terrain. Since vertical wind speeds are generally insignificant for near surface dispersion modeling, it is typical to assume that the mean vertical wind speed is equal to zero. The coordinate rotation and vertical wind speed assumption results in Equation 2-1 being approximated by Equations 2-2 and 2-3.

$$\frac{\partial \overline{c}}{\partial t} + \overline{u}_1 \frac{\partial \overline{c}}{\partial x_1} = \frac{\partial}{\partial x_j}\left(K_{jj} \frac{\partial \overline{c}}{\partial x_j} \right) + S_C \qquad (2\text{-}2)$$

$$\overline{u}_1 = fn(x_1, x_2, x_3, t) \qquad (2\text{-}3)$$

There are a variety of methods used to parameterize Equation 2-3. By far the easiest parameterization is to assume that the average horizontal wind speed is constant and thus not a function of x_1, x_2, x_3, or t. This assumption is only valid where there is no wind shear in either the horizontal or vertical direction over the domain of interest. One could only reasonably expect the wind field to be uniform if the flow field is significantly separated from physical boundaries. For most purposes it is invalid to assume that the wind field in the surface layer is a constant function with no x_3 dependence.

Surface layer wind data have been satisfactorily parameterized by equations that have no functional dependence on x_1, x_2, or t but retain dependence on x_3. These parameterizations can accurately simulate wind fields where the mean horizontal wind speed varies with height while discounting horizontal wind shear or temporal effects. It is commonly assumed that the functional dependence of wind speed with height can be approximated by algebraic or logarithmic formulae.

An equation that relates a wind speed at one elevation to a wind speed measured at a different elevation is presented as Equation 2-4. This equation is typically referred to as the power law wind profile. Interested readers can consult Sutton for a review of the development of this equation (Sutton 1953). EPA recommendations for estimating the variable 'p' for differing stability classes are shown in Table 2-1 (EPA 1995).

$$\frac{u_2}{u_1} = \left(\frac{z_2}{z_1}\right)^p \qquad (2\text{-}4)$$

Where:

z_1 & z_2 are elevations 1 and 2
u_1 & u_2 are wind speeds at z_1 and z_2
p is an exponent based on ambient stability class

Table 2-1. Power law wind profile exponents for rough surfaces (urban).

Stability Class	Class Description	Exponent (p)
A	Very unstable	0.15
B	Moderately unstable	0.15
C	Slightly unstable	0.20
D	Neutral	0.25
E	Slightly stable	0.30
F	Stable	0.30

It should be noted that Equation 2-4 can be re-written as Equation 2-5 if one combines the u_1 and z_1 terms into a aggregate parameter as shown in Equation 2-6.

$$u_2 = a z_2^p \tag{2-5}$$

$$a = u_1 z_1^{-p} \tag{2-6}$$

An alternative expression for the wind velocity profile can be derived from dimensional analysis arguments. It can be shown that for a neutral atmosphere, the following relationship is valid (Stull 1988):

$$\frac{\partial \bar{u}}{\partial z} = \frac{u_*}{kz} \tag{2-7}$$

Where:

u_* is the friction velocity
k is von Karman's constant (typically considered 0.4)

If u_1 and u_2 are the wind speeds at elevations z_1 and z_2, respectively, the solution of Equation 2-7 is found to be:

$$u_2 - u_1 = \frac{u_*}{k} \ln \frac{z_2}{z_1} \tag{2-8}$$

The elevation at which u_1 apparently vanishes is referred to as the roughness length and typically denoted as z_0. The literature typically recommends that the roughness length should be considered a property of the surface terrain and not of the fluid flow. With this notation, Equation 2-7 can be written in the familiar form of Equation 2-9.

$$u_2 = \frac{u_*}{k} \ln \frac{z_2}{z_0} \tag{2-9}$$

It is desirable to find a relationship between parameters in the log and power wind profiles. The parameters u*, p, and k can be interrelated by combining the derivative of Equation 2-4 (shown as Equation 2-10) and Equation 2-7 which results in Equation 2-11. Since the wind speed u in Equation 2-11 is not defined at a specific elevation, Equation 2-11 is non-physical because it indicates that u_* is not constant for a given wind profile. Equation 2-11 suggests that the power law profile and the log profile do not have an

analytic relationship given the empirical nature of the power law equation. However, if one attempts to numerically relate the wind profile parameters, it can be inferred from Equation 2-11 that there exists a linear relationship between u_* and wind speed at a specific reference elevation as shown in Equation 2-12 .

$$\frac{\partial \overline{U}}{\partial z} = \frac{p\overline{U}}{z} \tag{2-10}$$

$$u_* = puk \tag{2-11}$$

$$u_* = \alpha u_{REF} \tag{2-12}$$

To determine if Equation 2-12 is valid for neutral stability, a range of neutral power law wind profiles were best fit to the log wind profile. Figures 2-1 and 2-2 show two such wind profiles that were generated with the power wind law equation with p = 0.25 and a reference wind speed (measured at 10m) of 2 and 14 m/s. In these plots, the blue circles were determined from the power law profile (Equation 2-4) and the red dashed line is the curve-fit log wind associated with the plotted points. The dashed line was found by linearly fitting the wind speed versus the natural logarithm of elevation. Given the form of Equation 2-9, the slope and intercept of the transformed data can be used to determine the surface roughness and u_*. Figure 2-3 is a plot of u* versus u_{REF} which demonstrates that for the data sets considered Equation 2-12 is valid and that α is approximately 0.075 for a reference elevation of 10m when $z_0 \approx 0.05$ m. The UCD 2001 beta model used this u* estimation technique to specify vertical eddy diffusivity parameters. However, during model calibration it was determined that the vertical eddy diffusivity profile was not well correlated with either u* or u_{REF} immediately downwind of a roadway. In the final version of the UCD 2001 model the relationship between u* and u_{REF} derived above was not used, however, for completeness, its derivation is still included in this thesis.

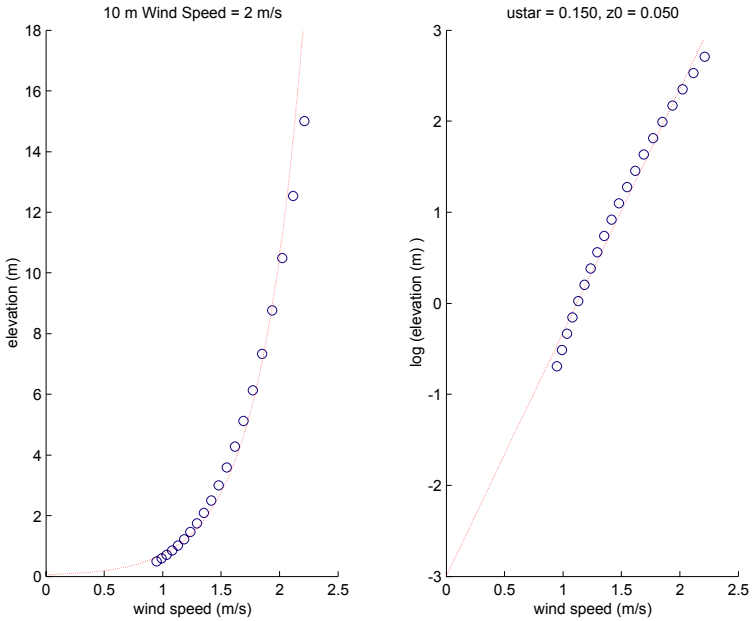

Figure 2-1. A relationship between power law and log wind profiles for a wind speed of 2 m/s at a reference height of 10 m. The blue circles are based on a power law exponent of 0.25, the dashed red line is the curve fit approximation of the power law data.

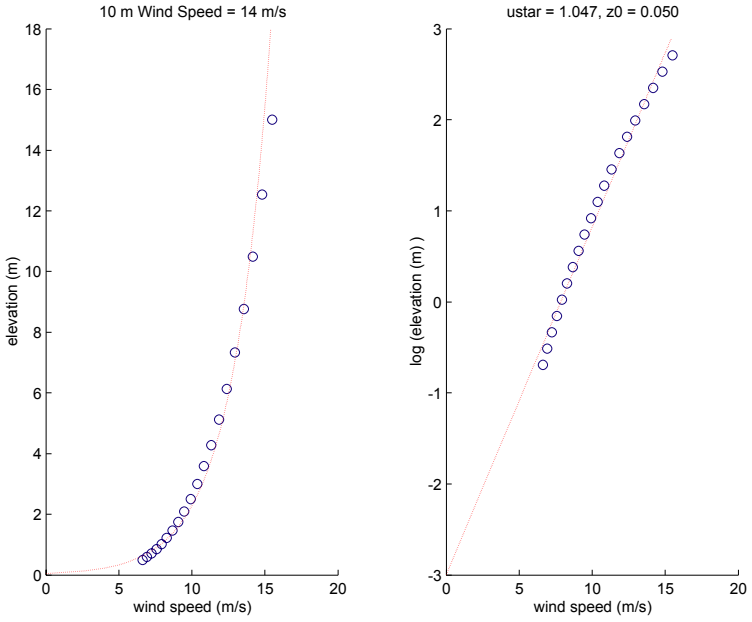

Figure 2-2. A relationship between power law and log wind profiles for a wind speed of 14 m/s at a reference height of 10 m. The blue circles are based on a power law exponent of 0.25, the dashed red line is the curve fit approximation of the power law data.

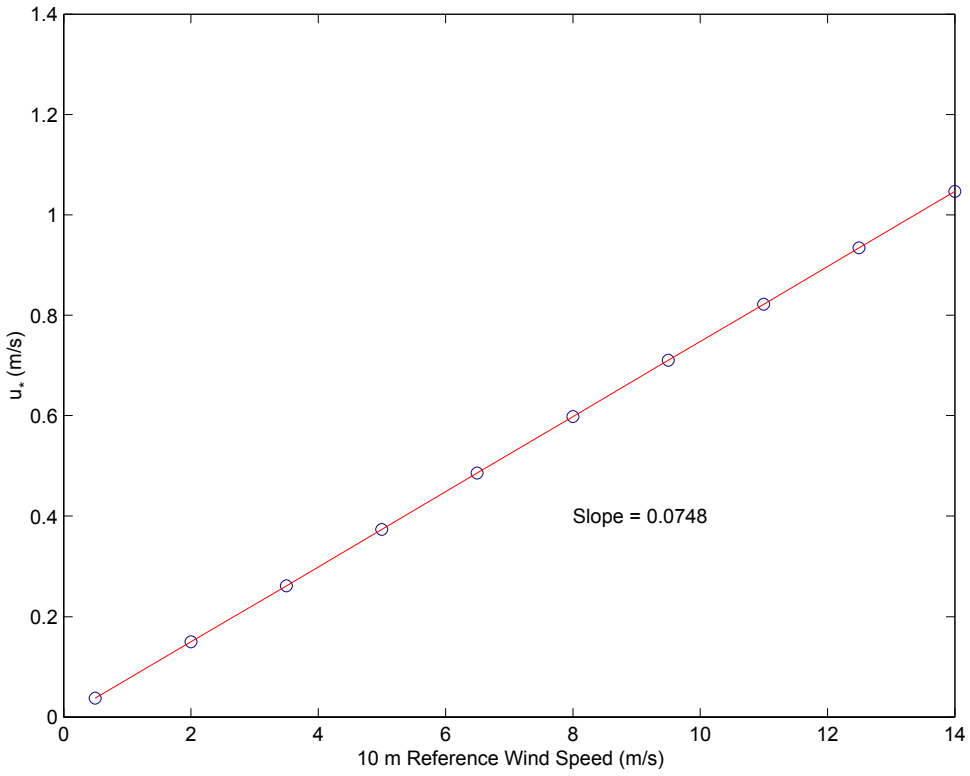

Figure 2-3. Relationship between u* and the 10 m elevation wind speed for neutral stability (p=0.25) and $z_0 \approx 0.05$ m.

SEADE Eddy Diffusivity Terms

Boundary layer literature is replete with techniques and approaches available to parameterize the eddy diffusivity terms of Equation 2-1. One such theory is based on the mixing-length arguments proposed by Prandtl in 1925 (Stull 1988). Essentially, this theory indicates that eddy diffusivity terms can be equated to the product of a local velocity shear and a representative mixing length. This relationship was derived assuming that the eddy diffusivity transport occurred over small distances in a neutrally stratified mechanically generated turbulent field. Although the assumptions necessary for the development of mixing length theory are restrictive, the result of the analysis provides insight in to the nature of turbulent transport and mixing processes. Based on Prandtl's work, we can deduce that "the magnitude of [K] should increase as the shear increases (i.e., a measure of the intensity of turbulence) and as the mixing length increases (i.e., a measure of the ability of turbulence to cause mixing)" (Stull 1988).

Stull has stipulated that "parameterizations for K should satisfy the following constraints:

- K=0 where there is no turbulence.
- K=0 at the ground (z=0).
- K increases as the turbulent kinetic energy of the flow increases.
- K varies with static stability… In general one would expect to find "Kstatically unstable > Kneutral > Kstatically stable.
- K is non-negative ". (Stull 1988)

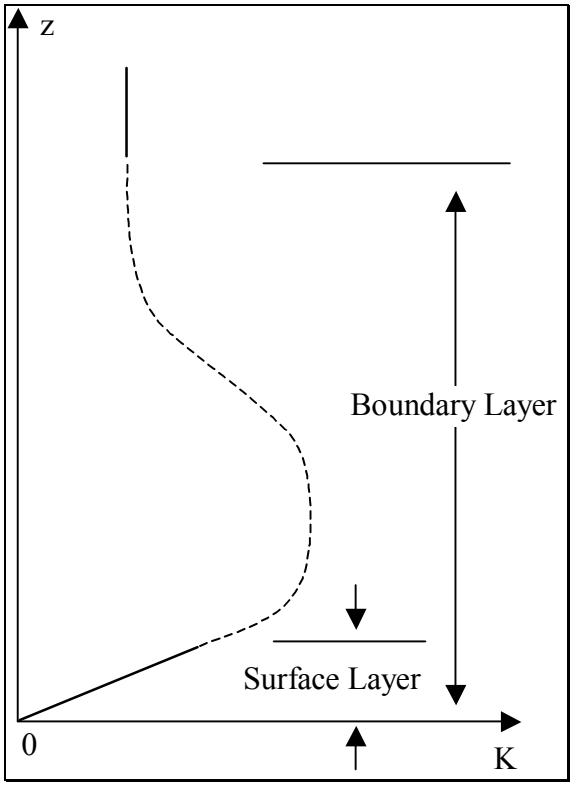

Figure 2-4. Typical variation of K_z with height in the boundary layer. Source: (Stull 1988).

Figure 2-4 presents a typical variation of eddy diffusivity as a function of height in the boundary layer (Stull 1988). The variation of K_z is heavily influenced by the presence of the earth's surface and the capping inversion that marks the top of the boundary layer. These two surfaces restrict the range of vertical fluid motions, and therefore eddy sizes, that are able to form in the boundary layer. Near the center of the boundary layer no such barriers exist and the scale of vertical motions is considerably larger. The profile of K_z over the entire boundary layer is quite complex, however, in the surface layer, simple relationships have been found to adequately specify vertical turbulent parameters as a function of elevation. Two such relations are presented as Equations 2-13 and 2-14. It should be noted that Equation 2-13 is identical to Equation 2-14 when n=1 and b= k u_*.

$$K_z = kzu_* \tag{2-13}$$

$$K_z = bz^n \tag{2-14}$$

Lateral diffusivity coefficients differ in nature to their vertical counterparts because they are not bound by capping inversions or the earth's surface. The lack of boundaries makes it difficult to determine appropriate scales and dimensionless groups to parameterize K_y.

One approach to parameterizing pollutant diffusivity coefficients was derived by Batchelor (Batchelor 1949). His derivation was Lagrangian in nature and assumed a homogeneous turbulent field that was statistically stationary. The analysis resulted in the definition of "apparent lateral eddy diffusivity" which is presented in Equation 2-15 (Batchelor as quoted in (Huang 1979)). Here it is assumed that Taylor's hypothesis holds, which allows one to relate time derivatives to space derivatives.

$$K_y = \frac{1}{2}\frac{d}{dt}\sigma_y^2 = \frac{u}{2}\frac{d}{dx}\sigma_y^2 \tag{2-15}$$

Where:

σ_y^2 is the mean square particle displacement, along the y-axis, of particles released from an upwind point source.

Equation 2-15 does not explicitly relate lateral eddy diffusivity with elevation. Furthermore, it is clear that the surface layer is neither stationary nor homogeneous.

These are significant limitations in the applicability of Equation 2-15, however, given that this equation is effectively a starting point for the curve-fitting of the sigma function, this equation appears to be commensurate with the rigor used to develop Equation 2-5 through 2-9.

A variety of formulae have been developed to determine the lateral standard deviation. Most of these parameterizations were based on passive tracer releases over uniform terrain that bear little resemblance to the intense mechanical and thermal turbulence near a roadway. Equation 2-16 represents one approach to determine mean square particle displacement that accounts for vehicular mixing effects. This equation is based on the Brookhaven National Laboratory (BNL) formulation presented in Huang (Huang 1979) and its applicability for use in roadway dispersion modeling will be explored in a subsequent section.

$$\sigma_y = a + bx^c \tag{2-16}$$

Huang and Gaussian Solutions to the SEADE

A steady state solution to the SEADE for a continuous point source, which accounts for shear in the vertical wind profile and variation of eddy diffusivity with elevation, was developed by Huang and is presented in Equation 2-17 (Huang 1979). The terms of Equation 2-17 are defined as follows: "Q is the source strength; the origin of the point source is expressed by y_s and z_s in the y and z directions; and δ is the Dirac delta function" (Huang 1979). Huang's solution is based on a power law approximation of the wind and vertical eddy diffusivity profiles (see Equations 2-5 and 2-14). The lateral eddy diffusivity was based on the result of Batchelor's result represented by Equation 2-15. Note: the variable α used in this equation is not the same as the α used in previous sections

$$\overline{C} = \frac{Q}{\sigma_y\sqrt{2\pi}}\exp\left[-\frac{(y-y_s)^2}{2\sigma_y^2}\right]\frac{(zz_s)^{\left(\frac{1-n}{2}\right)}}{xb\alpha}\exp\left[-\frac{a\left(z^\alpha + z_s^\alpha\right)}{xb\alpha^2}\right]I_{-v}\left[\frac{2a(zz_s)^{\frac{\alpha}{2}}}{xb\alpha^2}\right] \tag{2-17}$$

$$S_C = Q\delta(x)\delta(y-y_s)\delta(z-z_s) \tag{2-18}$$

Where

$$\alpha = 2 + p - n \tag{2-19}$$

$$\nu = \frac{1-n}{\alpha} \tag{2-20}$$

The Huang solution states "that the concentration distribution in the crosswind direction is … Gaussian" (Huang 1979). The vertical concentration distribution is considerably more complex and dependant upon a modified Bessel function of the first kind of order -ν.

One can derive the conventional Gaussian point source diffusion equation (Equation 2-21) from Huang's SEADE solution (Equation 2-17) if one assumes that p=n=0. Designating the power law parameters is this way indicates that the wind field and eddy diffusivities are constant with elevation. Therefore, the Gaussian equation (Equation 2-21) is a special case solution of the more general Huang solution.

$$\overline{C} = \frac{Q}{2\pi\sigma_y\sigma_z u}\exp\left[-\frac{(y-y_s)^2}{2\sigma_y^2}\right]\left\{\exp\left[-\frac{1}{2}\left(\frac{z-z_s}{\sigma_z}\right)^2\right]+\exp\left[-\frac{1}{2}\left(\frac{z+z_s}{\sigma_z}\right)^2\right]\right\} \tag{2-21}$$

Where

$$K_y = \frac{u}{2}\frac{d}{dx}\sigma_y^2 \tag{2-22}$$

$$K_z = \frac{u}{2x}\sigma_z^2 \tag{2-23}$$

The assumption that wind speed and eddy diffusivity are constant with height is a poor assumption near the earth's surface. In theory, this should restrict the usage of the Gaussian dispersion equation to elevations where the wind and eddy diffusivity profiles are relatively constant. In practice, however, the Gaussian dispersion equation is frequently used to estimate pollutant concentration near ground level.

Gaussian Finite Line Source Approximation

Based on the Gaussian dispersion equation developed for a point source, one can derive a dispersion equation that is applicable for a finite line source. This formulation is used extensively in the CALINE dispersion models. The derivation of the finite line source is not explicit in CALINE user manuals and is included here to complement the CALINE model discussion that follows.

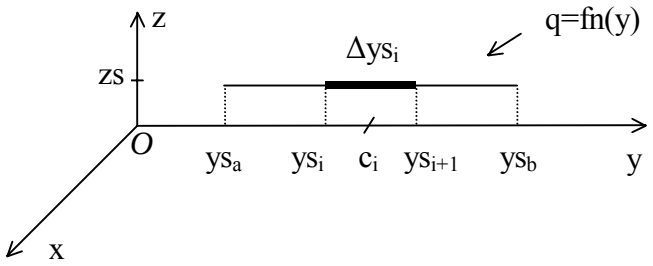

Figure 2-5. Finite line source coordinate system and terminology.

As shown in Figure 2-5, let a line source emission strength, q, be a continuous function defined on the closed interval [ys_a, ys_b] where c_i is any point in the *i*th subinterval Δys_i such that

$a = ys_0 < ys_1 < ys_2 < \ldots < ys_{n-1} < ys_n = b$

and

$ys_{i-1} < c_i < ys_i$.

The emissions from any subinterval can be estimated as the product of the interval size and the average emission strength q over the interval. To a first approximation, one can assume that the emissions released from a subinterval can be modeled as a point source centered at the subinterval centroid as shown in Equation 2-24.

$$\overline{C}(x,y,z) \approx \frac{\beta q(c_i)\Delta ys_i}{2\pi\sigma_y\sigma_z u}\exp\left[-\frac{(y-ys)^2}{2\sigma_y^2}\right] \tag{2-24}$$

where

$$\beta = \left\{\exp\left[-\frac{1}{2}\left(\frac{z-zs}{\sigma_z}\right)^2\right] + \exp\left[-\frac{1}{2}\left(\frac{z+zs}{\sigma_z}\right)^2\right]\right\} \tag{2-25}$$

If the wind is perpendicular to a level line source, then the downwind fetch distance, x, will be the same for any subinterval and the source height, zs, will be constant. For this case, one can use the superposition principle to show that the total downwind concentration is the sum of the subinterval contributions as shown in Equation 2-26.

$$\overline{C}_{Total}(x,y,z) \approx \sum_{i=1}^{n}\frac{\beta q(c_i)\Delta ys_i}{2\pi\sigma_y\sigma_z u}\exp\left[-\frac{(y-ys)^2}{2\sigma_y^2}\right] \tag{2-26}$$

If one considers the limit as a subinterval becomes infinitesimally small, the point source approximation becomes exact. Recognizing that the total downwind concentration, C_{Total}, has the same form as a Riemann sum, the summation in Equation 2-26 can be replaced with a definite integral as shown in Equation 2-27.

$$\begin{aligned}\overline{C}_{Total}(x,y,z) &= \lim_{\|\Delta\|\to 0}\sum_{i=1}^{n}\frac{\beta q(c_i)\Delta ys_i}{2\pi\sigma_y\sigma_z u}\exp\left[-\frac{(y-ys)^2}{2\sigma_y^2}\right] \\ &= \int_a^b \frac{\beta q(ys)}{2\pi\sigma_y\sigma_z u}\exp\left[-\frac{(y-ys)^2}{2\sigma_y^2}\right]dys\end{aligned} \tag{2-27}$$

If the source strength q is a known function of y_s, one can numerically or analytically evaluate the integral in Equation 2-27 and determine the concentration at some downwind receptor location. It is typically assumed that q is constant over the interval [a,b], resulting in the following equation.

$$\overline{C}_{Total}(x,y,z) = \frac{\beta q}{2\sqrt{2\pi}\sigma_z u}\left(erf\left[\frac{y-b}{\sqrt{2}\sigma_y}\right] - erf\left[\frac{y-a}{\sqrt{2}\sigma_y}\right]\right) \tag{2-28}$$

For numerical efficiency, the CALINE model evaluates Equation 2-27 differently than shown in Equation 2-28 so that error function calculations are avoided. The CALINE solution algorithm recasts the integral in Equation 2-27 to a form similar to the standard normal probability density function shown in Equation 2-29. Based on the variable transformation shown in Equations 2-30 and 2-31, the total downwind concentration can be calculated by Equation 2-32. The CALINE algorithm uses an internal coordinate system where y and y_s are transformed so that y will always be zero as shown in equation 2-33. Here the offset is defined as $y\text{-}y_s$ and $offset_2 > offset_1$ so that C_{Total} is always positive.

$$f(p) = \frac{1}{\sqrt{2\pi}}\exp\left(\frac{-p^2}{2}\right) \tag{2-29}$$

$$p = \frac{y-ys}{\sigma_y} \tag{2-30}$$

$$dp = -\frac{dys}{\sigma_y} \tag{2-31}$$

$$\overline{C}_{Total}(x,y,z) = -\frac{\beta q}{2\pi\sigma_z u}\int_{\frac{a-ys}{\sigma_y}}^{\frac{b-ys}{\sigma_y}} \exp\left[-\frac{p^2}{2}\right]dp \tag{2-32}$$

$$\overline{C}_{Total}(x,0,z) = \frac{\beta q}{2\pi\sigma_z u}\int_{\frac{ffset_2}{\sigma_y}}^{\frac{offset_1}{\sigma_y}} \exp\left[-\frac{p^2}{2}\right]dp \tag{2-33}$$

Summary

The SEADE equation is the foundation of the Huang and Gaussian equations developed in this section. A simplified SEADE is presented as Equation 2-34. The assumptions made in the derivation Equation 2-34 relevant to this study are shown in Table 2-2.

$$\frac{\partial\overline{C}}{\partial t} + \overline{U}_1\frac{\partial\overline{C}}{\partial x_1} = \frac{\partial}{\partial x_2}\left(K_{22}\frac{\partial\overline{C}}{\partial x_2}\right) + \frac{\partial}{\partial x_3}\left(K_{33}\frac{\partial\overline{C}}{\partial x_3}\right) + S_C \tag{2-34}$$

Table 2-2. Important assumptions made in the derivation of the simplified SEADE equation.

- It is appropriate to Reynolds average the governing atmospheric equations.
- The covariance terms that result from Reynolds averaging can be adequately parameterized by their K-theory equivalents for all atmospheric processes.
- Molecular diffusion is insignificant compared to turbulent diffusion.
- The wind field is horizontally homogeneous and is only a function of elevation.
- The wind and eddy diffusivity coefficients are invariant with time (i.e. steady state).
- The slender plume assumption is valid.

In a typical boundary layer, it is quite unlikely that all of these assumptions will be valid. However, if used with care, the SEADE is helpful in deriving practical dispersion algorithms for use in screening models.

The Huang dispersion equation assumes that the variation of wind speed and eddy diffusivity is approximated by power law relationships. The Gaussian equation was shown to be a special case of the Huang equation and is only valid when the wind and eddy diffusivity fields are constant. Based on the point source equation, a Gaussian-based equation to predict pollutant concentrations from a level finite line source perpendicular to wind direction can be derived. Given that wind shear near the earth's surface is significant, the Huang equation appears more suitable for roadway dispersion modeling purposes than the Gaussian-based formulations.

Chapter 3. Physical Phenomena Associated with Roadway Dispersion Modeling

Introduction

Vehicular emissions are actively released into the atmosphere in such a way that the wind and temperature fields are altered over and downwind of a roadway. To properly model the active release pollutant field near a roadway one needs to know the following:

- Where, when, quantity, and how emissions are released into the atmosphere.
- How are these emissions transported from the tail pipe to downwind receptors.

This chapter will focus on the second concept by identifying the meteorological, roadway, and vehicular variables important for pollutant transport. In reality, it is not easy to separate how the emissions are released from how they will be transported. For instance, vehicle speed will affect both emission rates and the dispersive properties in the atmosphere.

The information presented in this chapter will be largely qualitative in nature and serve merely to introduce the physical processes and phenomena generally thought to be relevant to roadway dispersion modeling. A quantitative description of the wind, temperature, and turbulence fields will be introduced in the Chapter 4.

Processes and Variables Affecting Roadway Pollutant Dispersion

Table 3-1 is a partial list of atmospheric properties that are thought to be significant for pollutant transport. This is not an exhaustive list, as it does not include parameters such as the standard deviation of the wind direction. Furthermore, the properties are interrelated and their separation is somewhat arbitrary. For instance, the mean wind profile and the TKE of the flow field are strongly dependant on the stability of the atmosphere. Nonetheless, Table 3-1 is a convenient grouping of properties that affect roadway pollutant transport. Table 3-2 is a partial list of the variables, and variable groups, that affect the atmospheric properties listed in Table 3-1. Our current understanding of how Tables 3-1 and 3-2 are related will be presented in the following subsections.

Table 3-1. Selected atmospheric properties significant for pollutant transport.

Atmospheric Property
Mean Wind Field
Atmospheric Stability (Temperature Structure)
TKE of the Flow Field
Eddy Diffusivity Field

Table 3-2. Variables which influence atmospheric properties listed in Table 3-1.

Variable Groups
Surface Roughness (Both Roadway and Non-Roadway)
Surface Heat Flux (Both Roadway and Non-Roadway)
Vehicular Exhaust Heat Flux
Vehicle Size and Shape
Vehicle Density
Vehicle Speed & Orientation

Surface Roughness and Heat Flux Effects of a Roadway

Even if one did not consider the effects of the vehicles directly, the presence of the roadway would significantly alter atmospheric profiles due to differences in land use. Specifically, roadway surface roughness and heat flux (not considering the waste emissions) is likely to be different from surrounding terrain. The current understanding of how equilibrium profiles are affected by an abrupt change in land use is explored in this section.

Relationships, such as Equation 2-8, which describe wind speed as a function of height, are not time dependant and therefore represent an equilibrium condition. These equilibrium relationships represent a dynamic balance between boundary conditions (BCs), such as surface heat flux and roughness, and the equations of motion.

If wind travels over a uniform fetch for long enough, equilibrium profiles of wind and temperature profiles would fully develop. A sharp change in BCs will result in the development of new equilibrium profiles, which will take time to fully develop. In between these fully developed profiles, one would expect the establishment of transition regimes.

The structure of the surface layer near a step change in surface roughness was simulated by a higher-order turbulence closure theory in the early 1970's (Rao et al. 1974). As shown in Figure 3-1, a change in surface roughness results in the formation of a new equilibrium relationships and a transitional boundary layer. "The height-to-fetch ratio of the new equilibrium layer is approximately 1/100 for a smooth-to-rough transition, and 1/200 for a rough-to-smooth transition" (Rao et al. 1974). Because it takes a considerable distance for the new equilibrium condition to be fully formed, the wind profile downwind of a roadway will likely be a combination of the upwind equilibrium profile, the downwind equilibrium profile, and the internal boundary layer.

A sudden change in land usage would likely result in different sensible and latent heat flux densities. One would assume that a new equilibrium and internal boundary layer would develop similarly to a step change in surface roughness. However, the change in heat flux due to a change in land usage is probably not significant when compared to the buoyancy flux associated with vehicular emissions.

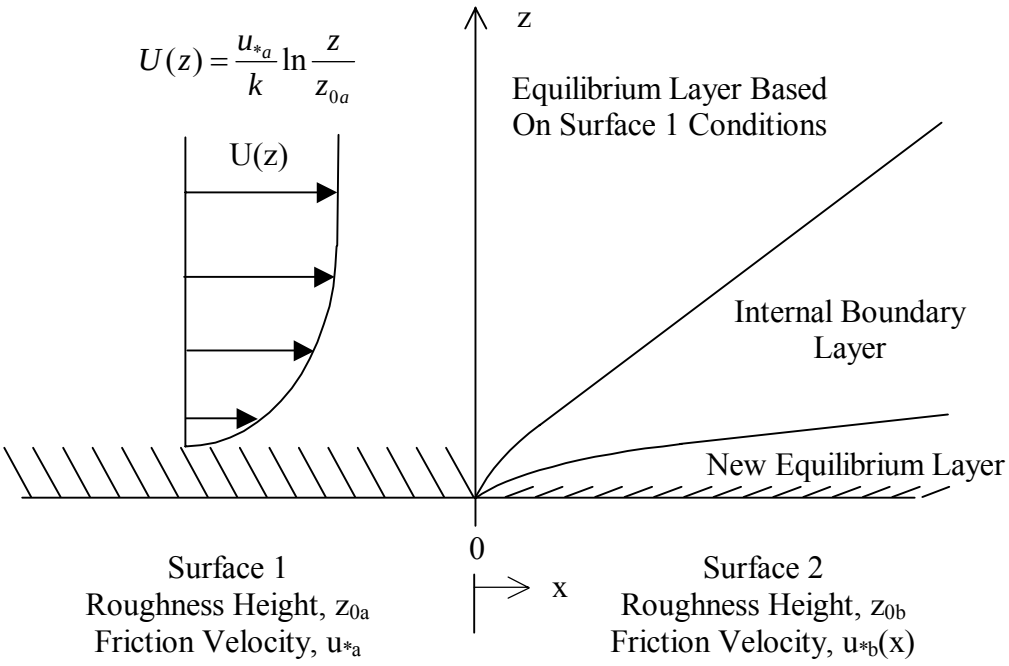

Figure 3-1. Diagram depicting equilibrium and internal boundary layers formed downwind of a step-change in surface roughness (based on (Rao et al. 1974)).

The Shelterbelt Effect

Whether the cars on a roadway are moving or stationary, their presence will significantly alter the wind profile over and downwind of a roadway because the vehicles form a significant obstruction to the mean wind flow. This deflection has been termed by Dabberdt as the "shelterbelt" effect because "individual vehicles, as well as the composite stream of vehicles on the roadway, present a barrier to the wind in much the same way as a row of trees or a fence used as an agricultural windbreak" (Dabberdt et al. 1981). The shelterbelt effect would presumably be a function of vehicle size, shape, and how densely packed the vehicles were relative to one another.

Based on wind tunnel experiments and atmospheric studies of wind flow around trees, the presence of ground based obstructions results in a reduction of the downwind mean wind speed near the surface. This results in greater wind shear, and "in turn, leads to larger diffusivity values and an increase in the rate of transfer of momentum and mass" (Dabberdt et al. 1981). This increased mixing and turbulent transport will reduce gradients in virtual potential temperature as well. An illustration of the shelterbelt effect is presented in Figure 3-2.

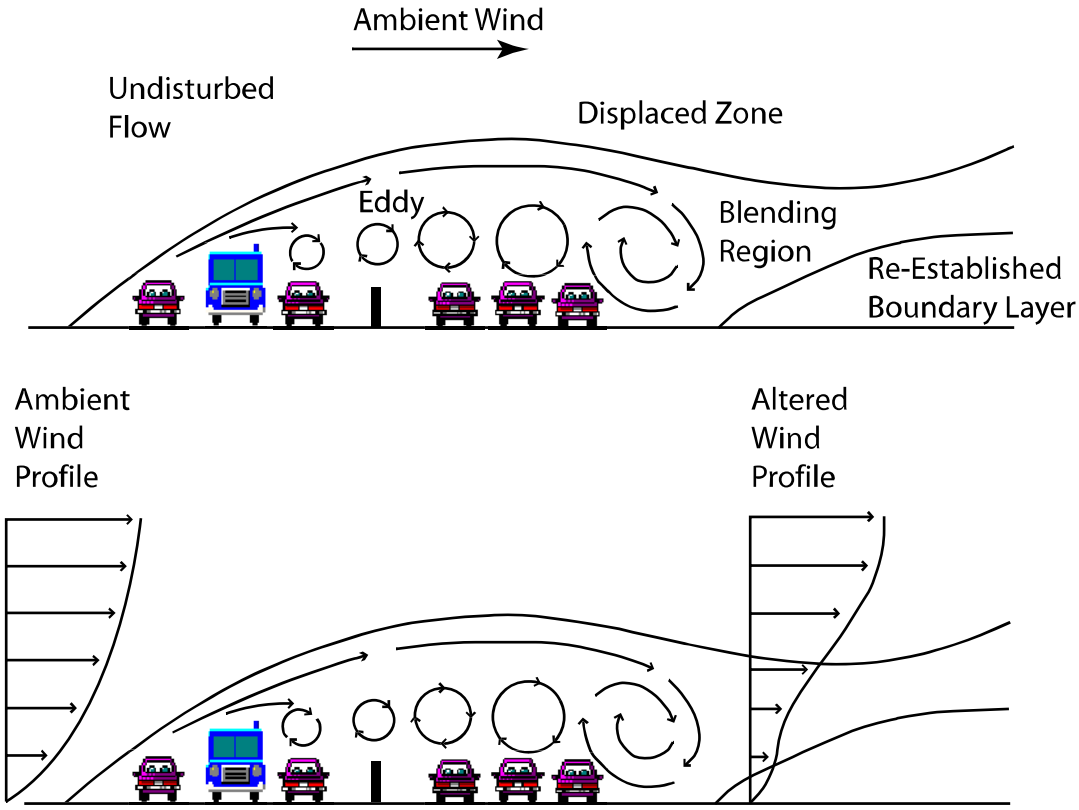

Figure 3-2. Illustration of the roadway-shelterbelt effect on wind and turbulence profiles (based on (Dabberdt et al. 1981)).

Vehicular Drag

Vehicular drag is a function of the vehicle speed, spacing, shape, roughness, and orientation. Since the "surface of a vehicle is aerodynamically rough … it drags with it the adjacent layers of air" (Dabberdt et al. 1981). Based on the conservation of momentum, one would expect that the vertical and cross wind components of the drag flow would be zero. It is expected that the energy imparted into the atmosphere by drag flow would initially increase the mean flow of turbulent kinetic energy above a roadway.

The turbulent eddies formed by flow over and around a vehicle will result in a three-dimensional eddy field. It has been estimated that the lateral dimensions of a turbulent eddy formed by vehicular drag would be one to two times the car width, with a vertical dimension of approximately two to three car heights (Dabberdt et al. 1981).

Dabberdt notes the following about vehicular drag flow:

> It is an effective factor in diffusing pollutants over the roadway. One way this occurs is through the horizontal transport of the drag flow that aids in producing a uniformly mixed layer along the roadway axis. Vertical mixing over the roadway occurs in two ways: One is through vertical

diffusion from the shear in the vertical profile of drag flow; more significant is the turbulent mixing that occurs above and behind the moving vehicles (Dabberdt et al. 1981).

Waste Heat from Vehicle Emissions

Based on conservation of energy arguments, the energy released from the combustion of fuel will ultimately be introduced into the atmosphere. A vehicle may heat up during operation thereby acting as a thermal reservoir. However, if a vehicle is at a thermal equilibrium, essentially all the energy released from combustion will be converted to sensible and latent heat fluxes to the atmosphere.

It has been estimated that the waste heat flux from a six-lane suburban freeway ranged from approximately 100 Wm^{-2} to 250 Wm^{-2} based on traffic loading. By way of comparison, "peak summer daytime heat fluxes from grass fields would be around 200 Wm^{-2} in the mid-latitudes of the United States, while a nighttime minima would typically be about –70 Wm^{-2}" (Dabberdt et al. 1981). As mentioned in a previous subsection, the composition of the roadway (e.g. asphalt) may act to enhance or diminish the overall energy flux over the roadway.

"Waste heat emissions are sufficiently large to modify the atmospheric stability over the roadway"(Dabberdt et al. 1981). This change in stability will act to enhance turbulent mixing process and result in increased dispersion of pollutant. One would expect that the effects of waste heat emissions on the wind and transport fields near a roadway would be most significant when ambient wind speed approach zero. Under these free-convection conditions, the waste heat emissions would result in additional vertical mixing of pollutants and would reduce ground level concentrations of pollutants near roadways.

Summary

The atmospheric properties presented in Table 3-1 are the mean wind field, atmospheric stability, TKE, and eddy diffusivity field. It is expected that roadway characteristics (i.e. vehicle speed and surface roughness) presented in Table 3-2 will significantly alter the atmospheric properties listed in Table 3-1. Four mechanisms were listed (roadway surface and heat flux changes, shelterbelt effect, drag effect, and waste heat emissions) that qualitatively express relations between roadway characteristics and atmospheric properties.

With the exception of the step change in land usage, the interrelation of the mechanisms presented in this chapter makes it difficult to determine the effect of one mechanism in isolation. Thus, the mechanisms presented are most helpful in qualitatively describing aspects of the complex atmospheric field surrounding a roadway. Dabberdt theorizes that the drag phenomenon is most significant over the roadway, which results in uniform horizontal mixing of pollutants near the vehicles. The shelterbelt effect "is suspected to have the most significant effect on the initial vertical dispersion over the roadway" (Dabberdt et al. 1981). For calm conditions, buoyancy effects due to waste heat emissions may be a significant source of vertical mixing of pollutants, however, for windy conditions, buoyancy forces would be most significant downwind of the roadway.

Chapter 4. Literature Review of Roadway Dispersion Experiments and Wind Tunnel Studies

Introduction

In the previous chapter the physical processes thought to be important for roadway dispersion modeling were introduced. In this chapter, published findings regarding wind fields, temperature profiles, and TKE profiles near roadways will be presented. Since most of these studies were conducted 20-30 years ago, many of the early reports and data sets are no longer in circulation; however, almost all of the peer reviewed journal articles are easily obtainable.

Two studies, one conducted by FHWA, and the other by General Motors, are key to our understanding of roadway dispersion and will be covered in detail (Cadle 1976; Dabberdt et al. 1981). The FHWA study was conducted by Dabberdt and provides a wealth of observations pertaining to tracer gas experiments conducted on California highways and wind tunnel dispersion studies. Unfortunately, neither the authors nor the FHWA have an archive of the experimental data set. The GM study was one of the most carefully conducted roadway dispersion analysis studies, the results of which were the determination of sulfate, temperature, and SF_6 fields near a four-lane closed test track. Luckily, a paper copy of the GM results survived which was digitized and archived by for this study by the author.

Other smaller scale studies, such as the sonic anemometer studies and tracer gas experiments conducted in New York in the late 1970's will also be introduced in this

chapter. Additional roadway dispersion studies were known to have been conduced near Los Angeles and Sacramento, however, experimental findings were not available and their results were not published in peer reviewed journals. Interested readers are referred to Benson for information on these studies (Benson 1984).

Early Dispersion Modeling Studies

"Field measurements of near-roadway carbon monoxide levels have been available since the early 1920's" and a review conducted by Wilkins (1956) "gives a succinct, comprehensive review of this earlier work" (Benson 1980). In the early 1960's the U.S. Surgeon General (SG) concluded that mobile source emissions were a human health concern in urban transportation corridors (Benson 1980). The SG's findings resulted in "a resurgence of interest in auto-related air pollutants [and] led to many new field investigations" (Benson 1980). One such study was conducted by McCormick and Xintaras that identified the importance of background concentration, traffic volume, and wind speed on curbside CO concentrations (McCormick and Xintaras 1962).

Drivas and Shair

In the winter of 1972-73 a tracer release study was conducted on Interstate 405 near San Diego, CA by Drivas and Shair (Drivas and Shair 1974). The section of highway studied ran parallel to the Pacific Ocean and was approximately 6 km inland. The sampling location was selected because "during the afternoon a brisk sea breeze normally blows inland perpendicularly across the highway" (Drivas and Shair 1974). SF6 was released in a quasi-instantaneous line source and concentrations at downwind distances of 0.4 to 2.3 km at a height of 1.5 m were recorded. Thus, the site was ideal to determine the dispersion characteristics of roadway pollutants from an infinite line source with a perpendicular wind.

Based on the downwind SF_6 time traces, Drivas and Shair concluded "the Gaussian model does not provide a good description of the dispersion from an instantaneous line source" (Drivas and Shair 1974). For certain sample periods, Gaussian equations overestimated peak concentrations "by a factor of 20; and the time associated with the movement of the concentration peak downwind was grossly in error" (Drivas and Shair 1974). Drivas explains, "the experimental results of non-Gaussian

concentration profiles … can be interpreted by the effect of wind shear, i.e. a horizontal wind velocity which increases with height. As the cloud of tracer grows vertically with time, the effective mean wind velocity which is transporting the cloud increases" (Drivas and Shair 1974).

Drivas and Shair concluded "the semi-empirical diffusion equation, using the power-law velocity and eddy diffusivity profiles, works quite well in predicting dispersion from an urban ground-level cross-wind line source" (Drivas and Shair 1974). Lastly, even though Drivas and Shair felt that a quasi-instantaneous line source was not well modeled by Gaussian techniques, they observe that in other studies "the Gaussian model does provide an adequate description of dispersion from continuous source releases" (Drivas and Shair 1974).

New York I-495 Dispersion Study

In the fall of 1976, tracer experiments were conducted on a 1.5 km straight segment of I-495 near New York City. I-495 is commonly called the Long Island Expressway and is a high volume roadway with three lanes traveling in each direction separated by a wide median. "A comprehensive sampling network was employed to monitor wind speed and direction, air quality, traffic and temperature structure" including conventional meteorological instruments mounted on towers and one sonic anemometer (Sistla et al. 1979). The "simulation of a line source was achieved by releasing [SF_6] at a constant rate near the tail pipes of six station wagons" (Sistla et al. 1979).

In 1978, Sistla published a summary of the tracer data and compared these results with several roadway dispersion models in use at the time (Sistla et al. 1979). Sistla grouped sampling runs by the wind angle. A perpendicular wind angle was considered to make a 60 to 90 degree angle with the roadway and a parallel wind was within 30 degrees of the roadway. The average absolute cross wind speed for the parallel and perpendicular periods were approximately 1 and 2.5 m/s respectively. When the normalized 2-m SF_6 concentrations as a function of downwind distance were plotted, the downwind concentrations for the parallel wind sample periods were on average significantly lower (for the same perpendicular distance from the roadway) than the perpendicular wind sample periods. A plot of the normalized concentration versus elevation at a given distance perpendicular to the roadway demonstrated that the concentrations attenuated

much more rapidly for perpendicular winds than for parallel winds. Both of these plots highlight increased vertical mixing under parallel winds.

When data were grouped by wind angle Sistla made the following observations:

"Parallel wind-road angles ($0 < \theta < 30$)

- The observed concentrations fall off to 50% of the maximum at about 40 m downwind [of the roadway].
- For a road-side receptor, at 16 m height no variation in the normalized observed concentration is found.

Perpendicular wind-road angles ($60 < \theta < 90$)

- The observed concentrations fall off to 50% of the maximum at a downwind distance of about 60 m.
- For a road-side receptor beyond 8 m height there is no variation in the normalized observed concentration" (Sistla et al. 1979).

Based on a scatter plot of observed vertical standard deviation for SF_6 and CO, Sistla states "that the dispersion of SF_6 is similar to that of CO. Hence, the models validated using SF_6 as a tracer gas can be confidently applied for modeling carbon monoxide" (Sistla et al. 1979).

Rao conducted a study designed "to asses the effect of traffic on the turbulence structure and to infer the time and space scales generated by the traffic" (Rao et al. 1979) based on the New York data set. In is important to note that the New York study only used a single sonic anemometer (Kaijo Denki Model 311). When Rao compares upwind and downwind wind spectra, in actuality, he is comparing measurements gathered during different sample periods. Comparisons of this type are more suspect than interpreting simultaneous upwind and downwind measurements because vehicle flow rates and ambient meteorological fields are not the same for both sample periods. For instance, Rao et. al. sometimes compared upwind and downwind spectra by analyzing the wind field at the same location for two periods with differing wind direction. In one period the sonic was upwind of the roadway and in the second it was downwind. If the fetch conditions on either side of the road are not identical, it is not clear if the data collected are meaningful.

"In order to isolate the contribution of the moving traffic to the turbulent energy, spectra with and without traffic influence are compared under otherwise similar

atmospheric conditions" (Rao et al. 1979). In all, Rao et. al. published results from 22 one-hour sampling periods. One comparison that received considerable attention was the comparison of Runs 1 and 2. Runs 1 and 2 were conducted on separate days in the late afternoon, and were considered unstable based on measurements of cloud cover, wind speed, radiation and temperature readings. The sonic anemometer was mounted 3 m above the ground at the same tower for both runs. For the first run, the wind speed was 1.6 m/s and the sonic was downwind of the roadway with a wind angle of 320. The wind direction orientation was such that a 0 or 180 degree wind was perpendicular to the road whereas a 90 or 270 degree wind was parallel. In the second run, the sonic anemometer was downwind of the roadway with an average wind speed of 2.2 m/s at a 155 degree wind angle. The total vehicles per hour for the first and second runs were 2100 and 1800 respectively.

Rao et. al. plotted the difference of the normalized spectra for the u, v, and w components from the first and second runs to determine the effects of roadway traffic. The spectra differences appeared to follow a log normal distribution with a pronounced peak at approximately 0.25 Hz. Rao et. al. concluded that the "range of frequencies affected by the traffic seems to be 0.1-1.0 Hz" and contends that an eddy with dimensions of 4 to 8 meters is consistent with the spectral data (Benson 1980).

Rao also concluded "that there are no significant convective motions induced by the traffic under stable atmospheric conditions. It appears that any heat input from the automobile exhaust is quickly destroyed by the mechanical turbulence generated by the moving traffic" (Rao et al. 1979). To demonstrate this point, Rao plotted the normalized heat and momentum fluxes versus frequency for Run 11. In Run 11 the sonic was downwind of the roadway with a wind speed of 1.7 m/s and a wind direction of 320. It is important to note that Run 11 was conducted at approximately 2 a.m. when the traffic flow rate was 756 vph and that the heat flux determined by the covariance of vertical wind and temperature perturbations was negative. Since the traffic flow rate was so low for this period, it is not clear that enough waste heat from vehicles was generated to result in a buoyant pollutant plume. In addition, it is not clear what the sonic anemometer's footprint is near a roadway. In actuality, the momentum flux spectra downwind of a roadway will have components from both the roadway and the fetch upwind of the

roadway. In general, the interpretation of the heat fluxes over non-uniform terrain is complex (readers are referred to (Wilson and Swaters 1991) for a comprehensive discussion). Lastly, since the sign of the momentum flux was negative, one would not expect convective conditions at all. Thus, care must be used in interpreting Rao's claim without further specification regarding how he reached his conclusions.

Rao et. al. also conducted 11 experiments which compared the upwind and downwind profiles of wind speed. Approximately 2 m south of the eastbound traffic wind speed and direction were measured at heights of 1.5, 2, 3, 5, 8, 11 m. Approximately 37 m north of the westbound traffic the same wind measurements were made at 2, 3, 5, and 8 meters elevation. Rao contends that "the most striking effect of the traffic on the wind profiles is the aerodynamic drag of the moving vehicles ... [which] exhibit strongly accelerated winds at the lower levels of the downwind tower". When the average wind direction is parallel to the direction a vehicle is traveling, one would expect elevated wind speeds downwind. However, inspection of the figures presented by Rao show significant scatter, and at times, the aerodynamic drag effects appear to accelerate the wind in the opposite direction that the vehicles are traveling. In a separate analysis of the wind data from the GM study Rao concludes “that the aerodynamic drag factor must be a function of the wind-road orientation angle. This is because the amount of acceleration in the lower layers is most significant under parallel wind-road orientation” (Rao and Kienan 1980). Lastly, Rao indicates the “mechanical turbulence generated by the vehicles extends at least up to 8 m height” (Sistla et al. 1979).

In a publication titled “Suggestions for Improvement of the EPA-HIWAY Model” Rao and Keenan noted, “That Rao and Eskridge clearly demonstrated that the dispersion in the near-field is completely dictated by the locally generated turbulence and that the ambient atmospheric stability plays an insignificant role in dispersing pollutants in the immediate vicinity of the roadway” (Rao and Kienan 1980). Also based on the findings of Petersen “the ambient turbulence mechanisms will be properly represented when on-site turbulence data are used” (Rao and Kienan 1980). Thus, even though it is rare that one would have on-site, near-field turbulence data, if it were available, one presumably would be able to model near field turbulent transport accurately independent of ambient stability.

Dabberdt FHWA Study

A comprehensive set of wind tunnel and field measurement studies were conducted by Dabbertdt in the mid to late 1970's to understand "how traffic, meteorology, and the geometry of the roadway and nearby buildings interact to influence the transport and diffusion of pollutants on the local or micro-scale (i.e., within the roadway right-of-way)" (Dabberdt et al. 1981). In the FHWA study, wind tunnel experiments were conducted to determine "the influences of roadway geometry, meteorology, surface roughness, and traffic and vehicle motion" upon microscale pollution-dispersion (Dabberdt et al. 1981). Three full-scale tracer release roadway studies were conducted to complement the wind tunnel study and form a database for model calibration purposes. "In all, 16 different roadway configurations were investigated; these included various types of at-grade, elevated, and depressed sections with both rough and smooth adjacent terrain. Three tests were conducted in the controlled environment of a wind tunnel. These scale model tests had the advantage of flexibility in that wind, traffic, and geometric variables could be easily varied. On the other hand, the atmospheric tests permitted the analysis of impacts due to diabatic stability conditions and vehicular thermal emissions" (Dabberdt et al. 1981).

Description of Wind Tunnel Experiments

A highway was simulated in a wind tunnel by releasing helium (He) from vehicles mounted on a conveyer belt-type apparatus and measuring its concentration at 20 locations "averaged over the equivalent of a one-hour period in full scale" (Dabberdt et al. 1981). The gas sampling and operation of the model roadway were fully described in the FHWA report; a summary of the model is provided below for convenience.

> "The model roadway had two moving belts to which model vehicles were attached. The belts could be driven in the same or in opposite directions by an electronic speed controller. The belts passed over elevated plenum chambers filled with He to supply simulated vehicle exhaust and were sealed by metal guides attached to the surfaces at the sides of the chambers. The complete unit was constructed to fit into the 2.24 m diameter turntable of the Claspan Atmospheric Simulation Facility (ASF).
>
> Two scales of model vehicles were used in the tests. For mixed traffic, consisting of autos and trucks, a scale of 1 in 300 was used, with each belt carrying two lanes of traffic. An additional series of tests was run with only automobiles, a single lane to each belt, at 3.5 times the above scale (1:85) … The small-scale cars and trucks were mounted on belts with two different spacing configurations: high density, with an average spacing between vehicles of two car lengths; and a

> low-density spacing of four car lengths. Only a high-density (1.5 car-length spacing) configuration was used with the large-scale vehicles. The probability distribution of the vehicles in each lane has been taken as a gamma semi-Poisson function where the particular sequence of spacing was chosen randomly" (Dabberdt et al. 1981).

In the Dabberdt study, "a matched fence/rough-floor combination was used … to generate the appropriate logarithmic mean velocity profile, as well as a turbulence spectrum representative of that in the neutral atmosphere" (Dabberdt et al. 1981). Careful consideration was given to the helium-in-nitrogen mixture so that tracer buoyancy or initial emission velocity did not corrupt the data set.

In all, a series of 18 wind tunnel configurations were conducted resulting in a total of 357 tests. The various configurations for each of the tests are shown in Table 4-1.

Table 4-1. Summary of wind tunnel test features in the Dabberdt FHWS study, source (Dabberdt et al. 1981).

Roadway Configuration	Surface Roughness	Traffic			Wind		Number of Tests
		Density	Flow	Speeds (mph)	Speeds (mph)	Directions (deg)	
At grade	Smooth	Hi-Hi	2-way	1.25,3.75, 15,30,50	10,20	0,15,30, 60,90	49
At grade	Smooth	Hi-Hi	2-way	1.25,12.5, 50	10,20	0,15,30, 60,90	30
At grade	Smooth	Hi-Lo	2-way	12.5,50	20	0,15,30, 90	18
At grade	Smooth	Hi-Hi	1-way	12.5,50	10,20	0,30,90	15
At grade, narrow right-of-way	Rough	Hi-Hi	1-way	12.5,25, 50	5,10,20	0,30,90	15
At grade, narrow right-of-way	Rough	Hi-Lo	1-way	25,50	5,10	0,30,90	16
At grade, narrow right-of-way	Rough	Hi-Lo	2-way	12.5,50	2.5,10	0,15,30, 90	18
At grade, narrow right-of-way	Rough	Hi-Hi	2-way	1.25,12.5, 25,50	2.5,5,10	0,15,30, 60,90	32
At grade, narrow right-of-way	Rough	Lo-Lo	2-way	1.25,12.5, 25,50	2.5,5,10	0,15,30, 60,90	20
At grade, wide right-of-way	Rough	Lo-Lo	2-way	1.25,12.5, 25,50	2.5,5,10	0,15,30, 60,90	20
Cut section, vertical side walls	Smooth	Lo-Lo	2-way	1.25,12.5, 25	10,20	0,15,30, 90	16
Cut section, sloping side walls	Smooth	Lo-Lo	2-way	1.25,12.5, 25	10,20	0,15,30, 90	16
Elevated, fill section	Smooth	Lo-Lo	2-way	1.25,12.5, 25	10,20	0,15,30, 90	16
Elevated, viaduct section	Smooth	Lo-Lo	2-way	1.25,12.5, 25	10,20	0,15,30, 90	16
At grade, wide right-of-way	Smooth downwind, rough upwind	Lo-Lo	2-way	1.25,12.5, 25	10,20	0,15,30, 90	16
At grade, wide right-of-way	Rough downwind, smooth upwind	Lo-Lo	2-way	1.25,12.5, 25	10,20	0,15,30, 90	16
Side of hill	Smooth	Lo-Lo	2-way	1.25,12.5, 25	10	0,90	12
Vertical cut section with adjacent air-right structure	Smooth	Lo-Lo	2-way	1.25,12.5, 25	10,20	0,30	16

Tunnel Study Findings

The wind tunnel experiments were conducted to establish a connection between traffic, winds, surface roughness, and roadway geometry upon the dispersion of pollutants. Various statistical tests and procedures including scatter plots, linear regression, factor analysis and multiple regression were used to determine these connections. The principal focus of the FHWA wind tunnel experiments was to explore the effects of traffic density, traffic speed, and traffic density on pollutant transport.

In general, when the terrain surrounding a roadway was relatively smooth, variations in traffic density had little effect on the concentration field above and adjacent to the model roadway. For oblique wind angles, Dabberdt found no correlation between pollutant concentrations and traffic density. However, "the parallel-wind cases indicate a tendency for the higher density traffic to result in slightly higher average ambient concentrations. This is contrary to intuition in that it would normally be assumed that the more dense traffic flow would result in increased turbulent mixing and, consequently, lower concentrations" (Dabberdt et al. 1981).

The effect of traffic direction on pollutant dispersion was also found to be counterintuitive because concentrations tended to decrease when traffic is moving in a single direction rather than in opposing directions. "This may mean that the drag flow induced by the stream of vehicles is more effective in increasing the vertical dispersion than the increased mechanical turbulence that results from the interaction of two opposing traffic streams. This could indeed be the case if the mechanical mixing from the unidirectional traffic stream were sufficiently vigorous to (initially) uniformly diffuse the exhaust in the air layer immediately above the roadway; then the added turbulence … from two-way traffic would not affect the magnitude of the dispersion. On the other had, the vertical wind profile generated by the Couette-type drag flow from the vehicle movement would have an effect on the vertical extent and intensity of the dispersion" (Dabberdt et al. 1981). The traffic direction data showed considerable scatter but on average, two-way traffic resulted in 18% higher normalized concentrations compared with one-way traffic.

"Variations in traffic speed show no effect on concentrations over the roadway, while farther away 10% averaged reductions are noted with 50 mph speeds compared to

12.5 mph traffic speeds. The pattern was independent of the wind/roadway orientation. Comparison of concentrations from idling vehicles and traffic moving steadily at 50 mph indicated an overall increase in concentrations from the idling vehicles of about 25%; the increase was independent of sampling locations and wind conditions" (Dabberdt et al. 1981). Since the downwind concentrations vary only slightly and with significant scatter over average vehicle speeds of 12.5 to 50 mph, one would expect that vehicle speed dependence could be safely ignored for a screening model, which would greatly simplify roadway dispersion analysis.

Description of Field Experiments

Three detailed field studies for level, cut, and elevated freeways were conducted. The level freeway study was conducted "in the San Francisco Bay Area on a stretch of U.S. Highway 101, midway between the Lawrence and San Tomas Expressways in Santa Clara, California" (Dabberdt et al. 1981). The cut-and-fill freeway studies were conducted on various sections of interstate 280 near San Jose, CA. The details of the Santa Clara study are representative of all three studies and will be presented in this section. For additional details of the San Jose study readers are referred to the FHWA report titled "Analyses, Experimental Studies, and Evaluations of Control Measures for Air Flow and Air Quality on and Near Highways. Volume 1: Experimental Studies, Analyses and Model Development" (Dabberdt et al. 1981).

The Santa Clara study was designed to achieve the following goals.

- "Investigate the impact of freeway traffic on the atmospheric wind and turbulence structure on and near the roadway.
- Determine the in-situ rate of emission from traffic flows of varying speed, density, and mix.
- Investigate freeway and nearby CO and hydrocarbon concentrations in relationship to traffic and meteorological conditions" (Dabberdt et al. 1981)."

The sampling site was relatively flat surrounded by level fields of grass. The section of I-280 studied had three eastbound and three westbound lanes separated by a median strip. Traffic flow was heavy with approximately 100,000 vehicles per day with a speed and velocity varying significantly throughout the day. "Comprehensive traffic information was recorded throughout the study, consisting of speed and axle number for

each vehicle, segregated on a lane-by-lane basis … Two inert tracer gases were released from vehicles driven in the traffic stream; one tracer was released exclusively from the westbound lanes, the other from the eastbound" (Dabberdt et al. 1981).

Meteorological instruments were mounted on five towers approximately 15 m in height. One tower was located in the median strip, and the other four were placed approximately 10 and 20 meters from the nearest traveled way on either side of the highway. Combinations of three-component anemometers and propeller vane systems profiled the wind field at up to four elevations for each tower. Temperature profile measurements were obtained from the two towers adjacent to the roadway. Both towers measured ambient temperature near the base (2.0 m) and the temperature differential at three heights (3.8 m, 7.5 m, and 14.2 m). FHWA site maps are presented as Figures 4-1 and 4-2, exact instrument locations are shown in Table 4-2.

Tracer gas was released from vans continuously driven in the center lane of both the west and eastbound traffic. In the west direction SF_6 was released and in the east direction $F_{13}B_1$ was released simulating a line source. In addition to the tracer gas analysis, CO, methane and total hydrocarbons were measured with a chromatograph. In total, 48 one-hour sampling tests were conducted.

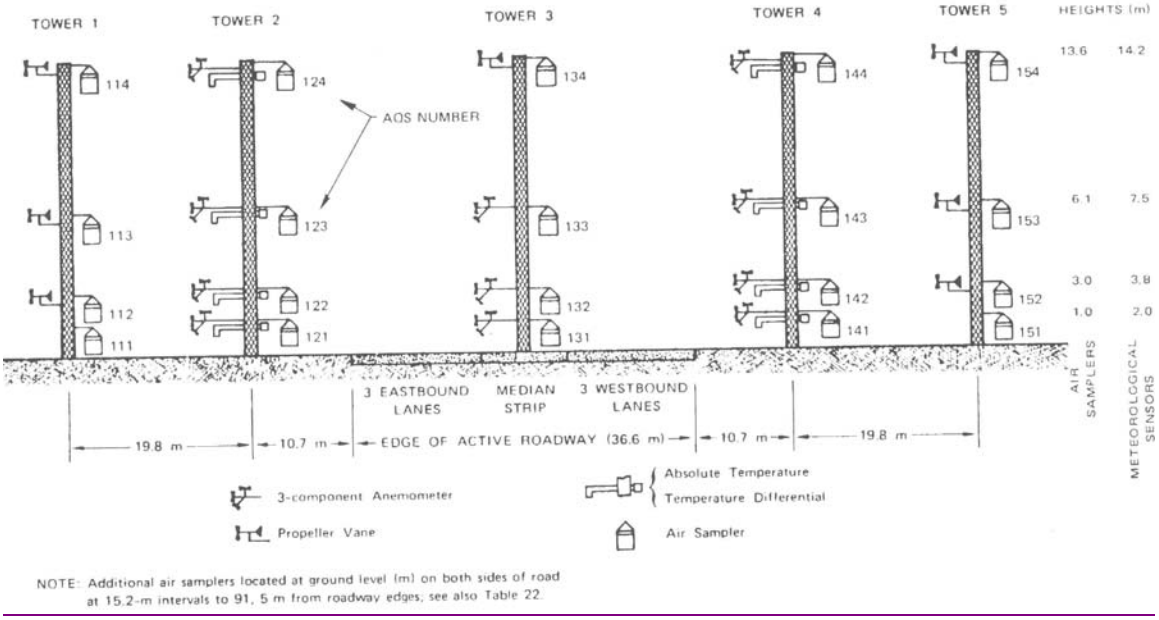

Figure 4-1. Instrument and tower locations for the at-grade roadway dispersion study conducted by Dabberdt, source (Dabberdt et al. 1981).

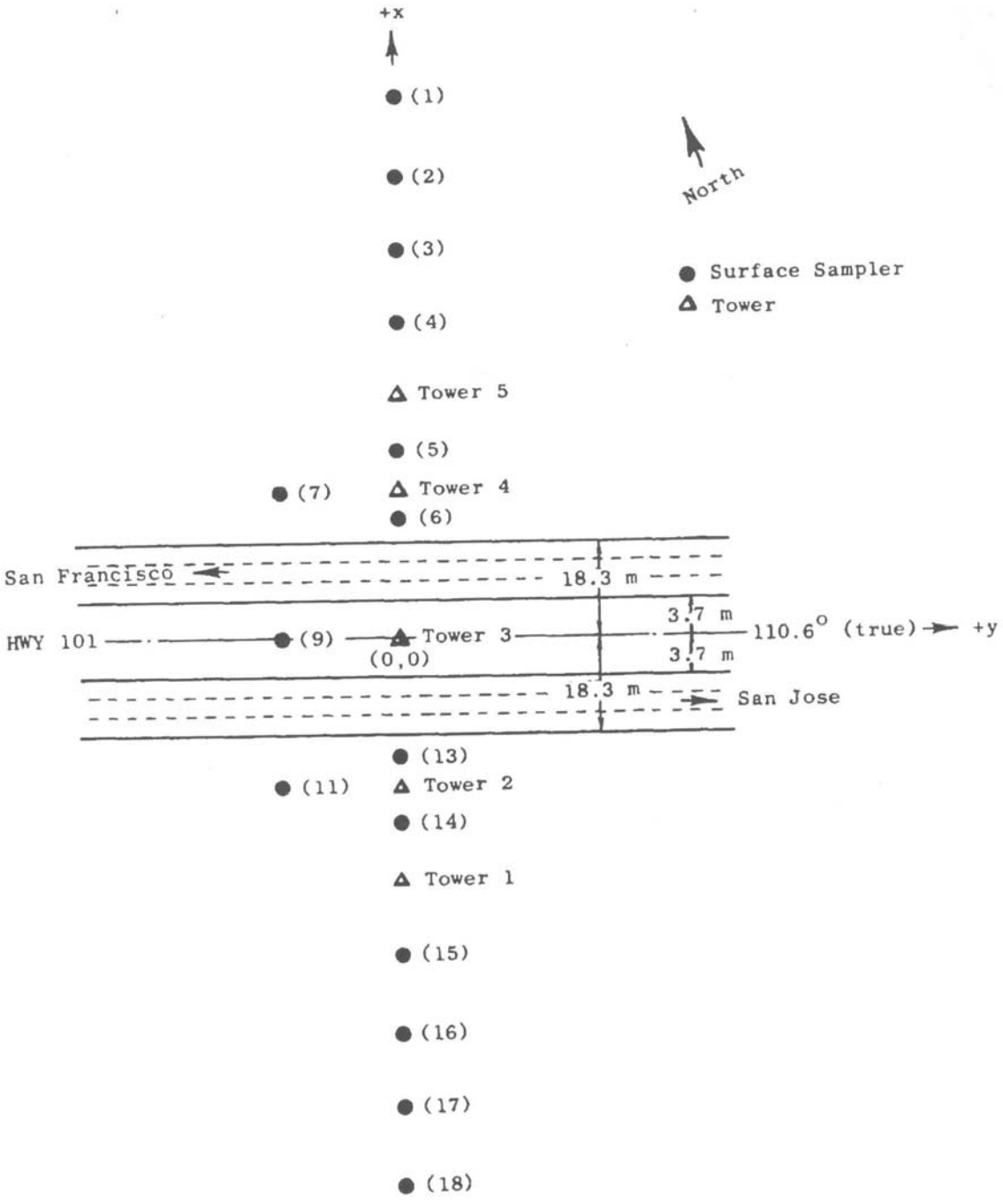

Figure 4-2. Plan view of tower locations for the at-grade roadway dispersion study conducted by Dabberdt, source (Dabberdt et al. 1981).

Table 4-2. Exact instrument and tower locations for the at-grade roadway dispersion study conducted by Dabberdt, source (Dabberdt et al. 1981).

Coordinates*			
Receptor Number	X (M)	Y (M)	Z (M)
1	109.8	0	0†
2	94.5	0	0
3	79.3	0	0
4	64.0	0	0
5	38.7	0	0
6	24.4	0	0
7	29.0	-22.9	0
9	0	-22.9	0
11	-29.0	-22.9	0
13	-24.4	0	0
14	-38.7	0	0
15	-64.0	0	0
16	-79.3	0	0
17	-94.5	0	0
18	-109.8	0	0
111	-48.8	0	1.0
121	-29.0	0	1.0
131	0.0	0	1.0
141	+29.0	0	1.0
151	+48.8	0	1.0
112	-48.8	0	3.0
122	-29.0	0	3.0
132	0.0	0	3.0
142	+29.0	0	3.0
152	+48.8	0	3.0
113	-48.8	0	6.1
123	-29.0	0	6.1
133	0.0	0	6.1
143	+29.0	0	6.1
153	+48.8	0	6.1
114	-48.8	0	13.6
124	-29.0	0	13.6
134	0.0	0	13.6
144	+29.0	0	13.6
154	+48.8	0	13.6

*Base of Tower 3 is (0,0,0).

†Zero height equals 1.0 m.

Field Study Temperature Structure

Tower 2 is approximately 11 m south of the eastbound lanes and Tower 4 is approximately 11m north of the westbound lanes. A cross-roadway temperature gradient, ΔT_{horiz}, is approximated by taking the difference in temperature between Tower 2 and Tower 4 for identical sampling heights. Dabbert plots the ΔT_{horiz} as a function of crosswind speed for the 2.0, 3.8, and 7.5 m elevations. As expected, the temperature gradients generally decreased as a function of elevation. Dabberdt observes, "the cross-roadway temperature gradient was quite large: at 2 m, maximum values from –1.5 to 2.5 ^{0}C were obtained across the 57 m tower separation of the two towers at the roadway edges; at 3.8 m, the difference ranged from –0.75 to 1.5 ^{0}C; while at 7.5 m, it was still moderately large (from –0.4 to 0.75 ^{0}C). The difference was small for low wind speeds and increased with higher cross-road wind speeds" (Dabberdt et al. 1981).

To determine if cross-road temperature differences were due to "waste heat, differences in the thermal characteristics of the roadway and adjacent soil, or mixing of the atmospheric surface layer" Dabberdt performed a regression analysis of ΔT_{horiz} versus the groups presented in Table 4-3 (Dabberdt et al. 1981).

Table 4-3. Variables that Dabberdt correlated with ΔT_{horiz} in the FHWA study.

Group	Description
(1) TTI (upwind)	The total turbulence intensity at 2 m on the tower farthest upwind of the roadway. TTI is a good indicator of the degree of mechanical mixing in the ambient atmosphere.
(2) u_{road}	The cross-roadway wind speed component.
(3) TTI * u_{road}	When reference is made to Gaussian line-source dispersion concepts, this product is analogous to the dispersion term given by the transport wind and diffusion coefficient.
(4) Total vehicle volume	This term is approximately proportional to the waste heat emission rate for cruising automobiles.
(5) Volume Speed Sum	The product of vehicle volume and speed summed over all six lanes of the roadway. Since the energy output does have some speed dependence, this term also represents an approximation of the heat released by the roadway vehicles.
(6) Groups (5) / (3)	Scaling factor for the dispersion of heat from roadway vehicles, similar to the Gaussian line source dispersion formulation.

Dabberdt found that the "cross-road wind speed component has the highest and most consistent correlation with ΔT_{horiz}" and that "ambient TTI is virtually uncorrelated, while the traffic variables alone are poorly and inconsistently correlated … in no case do any of the five other independent variables show a higher correlation than u_{road} alone". The positive correlation of ΔT_{horiz} and u_{road} is a bit counter-intuitive. It suggests that as cross winds increase downwind temperatures increase. This is the opposite of what one would expect if inert tracers were being measured rather than temperature. With tracers, one generally assumes that downwind concentrations will reduce as wind speeds increase. Dabberdt theorizes that the positive correlation may be due to "the vertical mixing induced by thermal instabilities from vehicle heat emissions and vehicle-induced mechanical mixing dominate under light wind conditions, thereby effectively dispersing vehicle thermal emissions more than under higher wind conditions when more "conventional" dispersion (i.e., mechanical mixing) dominates" (Dabberdt et al. 1981).

The ΔT_{horiz} scatter plots do not show a bimodal distribution based on stability. In fact "downwind temperatures are virtually always higher than upwind temperatures at

each of the three heights" (Dabberdt et al. 1981). In effect, this rules out the possibility that the increased mixing of a stable or unstable temperature profile is the primary reason that cross road temperature gradients are formed.

Based on estimated heat flux data, Dabberdt concludes that vehicle heat emissions are "sufficient to create an unstable state over the roadway … even for most periods of stable ambient conditions (except when traffic volumes are very low)" (Dabberdt et al. 1981). To confirm this hypothesis, Dabberdt plotted the cumulative frequency distributions of the vertical temperature differences (2 – 3.8 m, 3.8 – 7.5 m, and 7.5 – 14.2 m) for both the towers 11 m from the roadway. This plot is reproduced here as Figure 4-3. It is clear that "the decrease in stability downwind of the roadway is apparent at all levels, although it is most pronounced near the surface" (Dabberdt et al. 1981).

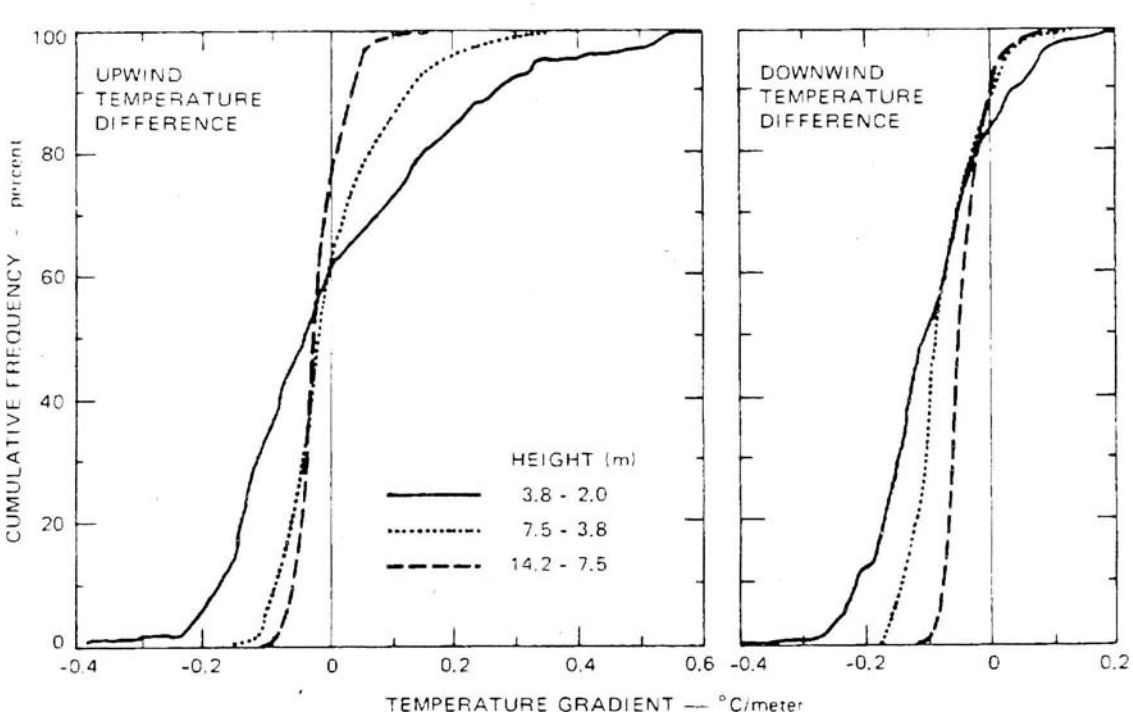

Figure 4-3. Cumulative frequency distributions of vertical temperature gradients for the at-grade roadway dispersion study conducted by Dabberdt, source (Dabberdt et al. 1981).

Field Study Turbulence Structure

Dabberdt explored the role that vehicle effects may have on dispersion near a roadway by comparing the change in total turbulent intensity, ΔTTI_{horiz}, from the upwind tower to the median and downwind towers. A scatter plot of ΔTTI_{horiz} versus the cross-roadway wind angle (θ_{road}) for the upwind and downwind towers demonstrated significant scatter at all four elevations for which TTI was measured (2.0 m, 3.8 m, 7.5 m, 14.2 m). This suggests that upwind versus downwind TTI is either not a function of cross wind angle, or is some combined function of cross wind angle and other independent parameters "such as vehicle speed and volume, wind/roadway orientation, and stability. The gradient is somewhat larger at the lower level, although not significantly. Values range from +0.5 to –0.5 m s^{-1} with the largest scatter at the lower levels" (Dabberdt et al. 1981). A regression analysis between ΔTTI_{horiz} and a variety of meteorological and traffic variables "shows that the up/downwind gradient of turbulence intensity at 2 m is consistently well correlated with only one parameter, the cross-road temperature gradient; the averaged r is about 0.53. This further suggests that the thermal vehicle emissions are the cause of the large cross-road temperature gradients observed" (Dabberdt et al. 1981).

Comparison of the upwind minus the median tower shows that ΔTTI_{horiz} for the lower sensors (2.0 m and 3.8 m) have similar distributions and exhibit large scatter from 0.0 to –1.3 s^{-1}. At 7.5 m the ΔTTI_{horiz} drops by approximately a factor of two and the upwind tower occasionally has a slightly greater turbulent intensity than the median. Based on these results Dabberdt notes "data from the median tower do suggest, however, that a uniformly well-mixed layer is present on the road up to a height of at least 4 m, and then damps out significantly by 7.5 m … [and] at all levels there is still no apparent dependence on wind/roadway angle. But since the median tower is located between traffic lanes, it is probably dominated by traffic features, thus minimizing any dependence on ambient wind direction" (Dabberdt et al. 1981). Since the median strip did not have a 3-component anemometer, ΔTTI_{horiz} calculations could not be made at the 14.2 m elevation.

Field Study Tracer Data Analysis

Since the Santa Clara study used differing tracers for the east versus westbound traffic, the significance of roadway emissions from one link being remixed by a downwind link could be explored. To facilitate the comparison of tracer data it is convenient to define σ_z as follows:

$$\sigma_z = \frac{Q\sqrt{2/\pi}}{u_{road}\chi} \tag{4-1}$$

where Q is the tracer release rate (in g m^{-1} s^{-1}), χ is the tracer concentration (in g m^{-3}) and u_{road} is the reference wind speed measured at approximately 11 m from the downwind edge of the most downwind link at an elevation of 3.8 m. The σ_z value was calculated only when the wind speed was greater than 1 m/s and the wind direction was not within 20^0 of parallel. This selection process resulted in a set of 19 one-hour samples.

Dabberdt stresses that "the use of the Gaussian line source formulation is not intended to imply that the two-dimensional pollutant distribution near the roadway is adequately described by Gaussian concepts. Rather, the surface level diffusion coefficient so derived is used as a scaling parameter of atmospheric mixing" (Dabberdt et al. 1981). The grouping of Q/χ in the σ_z scaling parameter is quite logical because one would expect downwind concentrations to scale with source strength. The inverse dependence of σ_z upon u_{road} is also intuitive, however, it is not clear that a representative wind speed for the complex meteorological field that develops in the near field of a roadway exists.

The separation of the east- and westbound center lanes is approximately 20 m with a 7.5 m median separating each link. The average σ_z scaling parameters at a downwind fetch of 40 m are "5.5 and 4.9 m for the downwind and upwind lanes, respectively. The average difference in coefficients normalized by the downwind coefficient was 7%" (Dabberdt et al. 1981). A variety of statistical tests including analysis-of-variance, student t-test, and a rank difference test were used to analyze the statistical difference between the σ_z values calculated for both links. Results from these analyses demonstrate that differences between σ_z values for the two links were not

significant, which suggests that enhanced dispersion from the downwind lanes is also statistically insignificant.

Summary and Discussion of Dabberdt's Findings

Based on the meteorological and tracer data collected during the at-grade field test, the following observations stand out:

- "Turbulence levels in the median and downwind of the roadway are consistently higher (by a factor up to 3.5) than the upwind ambient values.

- Cross-roadway turbulence differences showed no correlations with either traffic or ambient meteorological factors.

- The difference in turbulence levels between upwind and median locations is not correlated with vehicle speed, volume, or occupancy and is only fairly well correlated with wind speed.

- While the cross-roadway turbulence difference gradually decreases with height, the upwind-median difference is similar at 2 m and 3.8 m and then falls off sharply at 7.5 m.

- While turbulence levels are greatly increased by the roadway, they are not correlated with traffic parameters. This suggests that either the turbulence generation mechanism is insensitive to the traffic volume and speed variations over the ranges observed or that the other effects need to be considered; in fact, both concepts may be true" (Dabberdt et al. 1981).

- The tracer dispersion data does not show statistical evidences that dispersion of pollutants over two separated links leads to increased dispersion. This supports the hypothesis of traffic-insensitivity of tracer dispersion over a broad range of highway traffic flow conditions (Dabberdt et al. 1981).

- For relatively smooth terrain no correlation between downwind concentrations and traffic density were discovered.

- Surprisingly, one-way traffic resulted in above roadway concentrations on average 18% greater than two-way traffic for smooth terrain and high vehicle density.

- Wind tunnel studies demonstrated that receptor concentrations above the roadway were not affected by changing the vehicle speed from 12.5 to 50 mph. Similarly,

downwind concentrations were only slightly affected by changing vehicle speed and resulted in downwind concentrations decreasing by approximately 10%.

GM Study

The GM study was conducted in the mid 1970's and is one of the most controlled roadway dispersion studies ever conducted. The GM dataset was made public and was analyzed by a variety of researchers. In addition, the GM dataset has been used to calibrate many roadway dispersion models. In this section, a brief description of how the GM study was conducted, a review of the instrumentation used in the study, and previously published analyses of the experimental findings will be presented.

Overview of the GM Sampling Effort

The motivation for conducting the GM dispersion experiment initially grew out of concerns that the use of catalytic converters may result in significant concentrations of sulfuric acid near a roadway as Wilson explains below:

> "To meet federal and state emission standards, automobile manufacturers have incorporated catalytic converters in their exhaust systems to reduce hydrocarbons and carbon monoxide emissions to acceptable levels. However, gasoline contains trace amounts of sulfur (typically 0.03% by weight), which is converted to SO_2 during the combustion process. A portion of the SO_2 is subsequently oxidized to SO_3 by the catalytic converter, and ultimately, sulfuric acid aerosols result from the reaction of the SO_3 with water vapor. Several reports in the literature have documented this process and have identified the emission products during dynamometer operation. However, there was inadequate information on emissions during actual highway operation. Information was needed on the particulate sulfur emission rate, its chemical and physical properties, and its dispersion in the atmosphere near the highway" (Wilson et al. 1977).

A detailed review of how the GM study was conducted was published in a report titled "Results of the General Motors Sulfate Dispersion Experiment" (Cadle 1976). Additional details of EPA chemical analyses were published by Wilson (Wilson et al. 1977). Various reviews of the GM data collection abound in the literature, but one of the most succinct and informative was done by Benson (Benson 1980). His review of the GM study is included below to familiarize the reader with the salient features of the study.

> The General Motors (GM) Sulfate Experiment was conducted at the GM Milford, Michigan, proving grounds straightaway track during the month of October, 1975. The track is 5 kilometers long and is surrounded by lightly wooded, rolling hills. Three hundred and fifty two [catalyst equipped] cars, including 8 vehicles emitting tracer gas, were driven at constant speeds of 80 km/hr around the track. This simulated a traffic flow of 5,462 vehicles per hour along a four lane freeway with a median width of approximately 12 meters.

> Monitoring probes were stationed at 2 upwind locations and 5 downwind locations out to a distance of 113 meters from the track centerline. In addition, a monitoring location was situated in the track median. The westerly, median and closest 3 easterly locations were equipped with tower mounted sampling probes at elevations (z) of 0.5, 3.5, and 9.5 meters above the ground. The two additional more distant downwind probes were positioned at z=0.5 meters. Wind speed and direction measurements were made at each probe location using Gill UVW anemometers. Temperature profiles were recorded at the two outermost towers, 43 meters from the track centerline. The use of sulfur hexafluoride (SF_6) as a tracer gas in 8 of the vehicles eliminated interference from background pollutant levels. SF_6 is a highly inert gas found in only insignificant amounts in ambient air.
>
> Data from over 50 half hour test runs was compiled. Most of these were conducted during early morning hours to take advantage of the stable atmospheric conditions prevalent then. The cars were grouped into 32 single lane packs of 11 cars each and distributed over the track so that two packs from each direction passed the sampling area simultaneously at approximately 30 second intervals.
>
> The experimental procedure in the GM study was carefully controlled, resulting in one of the most reliable highway air quality databases yet compiled. The only shortcoming in the experiment was the lack of variability in the traffic parameters of speed, volume and occupancy" (Benson 1980).

Detailed GM Site Maps and Instrumentation Locations

Figure 4-4 depicts the roadway and tower locations for the GM experiment. The exact tower location coordinates are shown in Table 4-4. The nominal tower instrument elevations for each tower are shown in Figure 4-5; the exact elevations are listed in Table 4-5.

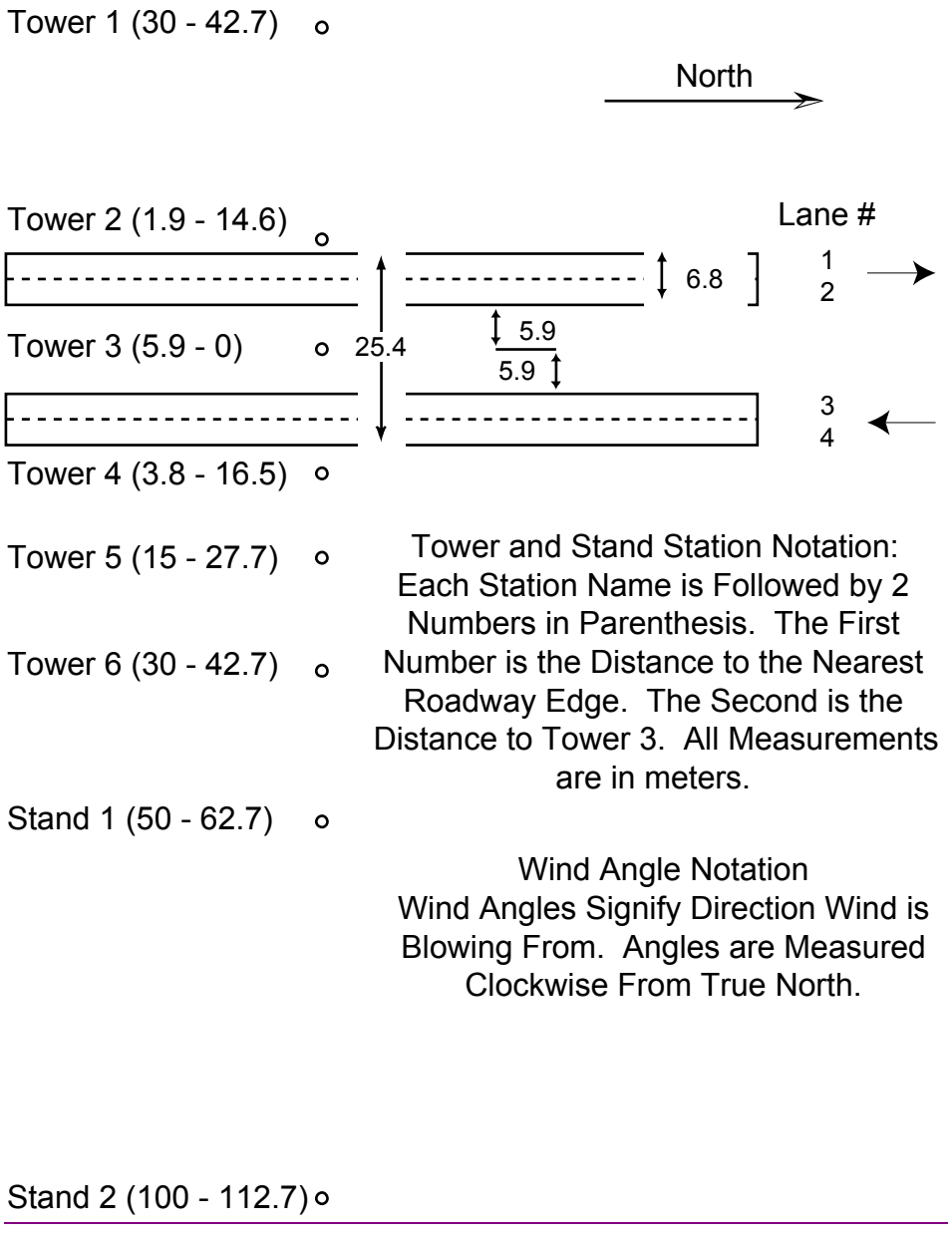

Figure 4-4. GM study site map.

Table 4-4. Sampling tower coordinates for the GM dispersion study. Note: the median tower is defined as the origin.

Tower #	X Coordinate	Y Coordinate
1	-42.7	-13.3
2	-14.6	-4.5
3	0	0
4	16.5	5.1
5	27.7	8.6
6	42.7	13.3
7	62.7	19.5
8	112.7	35.0

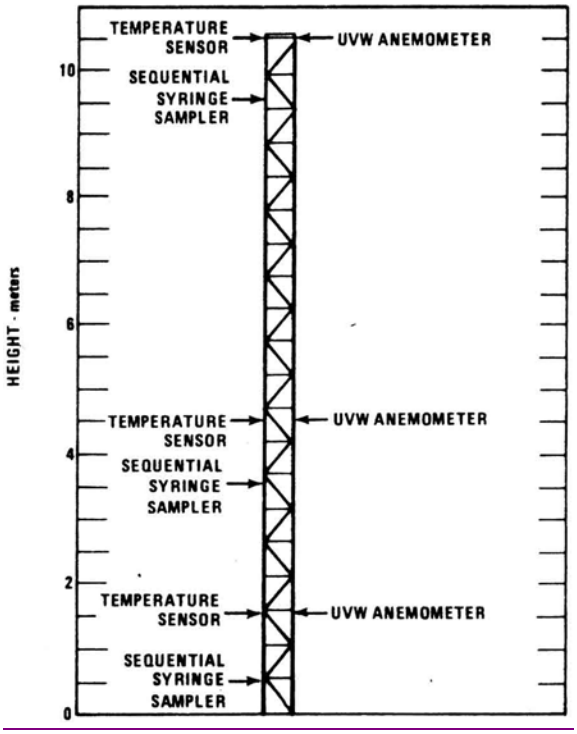

Figure 4-5. Nominal instrument elevation for each BM sampling tower, source (Eskridge and Hunt 1979).

Table 4-5. Exact elevation of GM sampling equipment (in meters).

Tower #	Sampler Index	SO4	SF6	UVW	Temperature
1	3	0.46	0.51	1.52	1.22
1	2	3.51	3.51	4.37	4.24
1	1	9.55	9.58	10.52	10.19
2	3	0.56	0.56	1.6	
2	2	3.63	3.63	4.42	
2	1	9.5	9.5	10.44	
3	3	0.56	0.56	1.45	
3	2	2.8	3.05	4.35	
3	1	9.58	9.58	10.37	
4	3	0.51	0.51	1.47	
4	2	3.58	3.61	4.37	
4	1	9.96	9.63	10.42	
5	3	0.56	0.56	1.47	
5	2	3.51	3.48	4.35	
5	1	9.55	9.5	10.42	
6	3	0.58	0.58	1.52	1.22
6	2	3.61	3.84	4.55	4.4
6	1	9.58	9.6	10.49	10.37
7	3	0.51	0.56	1.52	
8	3	0.51	0.56	1.42	

Wind, Temperature, and Concentration Field Measurements Collected in the GM Study

The following subsections list observations of the wind, temperature, wake, and concentration fields measured during the GM study as they appear in a number of reports and journals articles (Cadle et al. 1977; Cadle 1976; Chock 1977a; Chock 1977b; Chock 1980a; Chock 1980b; Wilson et al. 1977). Chock selected sensors at an elevation of 4.5 m located 30 m upwind of the roadway as representative of ambient wind speed and direction. Chock made his stability class estimations by calculating Richardson numbersbased on the 1.5 and 4.5 m wind and temperature sensors. In all 62, 30-minute sampling events resulted in data of sufficient quality to be included in the calibration data set. Tables 4-6 and 4-7 provide brief summaries of wind speeds and headings recorded during the GM sample periods. Table 4-6 contains sampling periods based on the 4.5 m wind heading and is identical in form to a table published by Cadle (Cadle et al. 1977). Table 4-7 is normalized so that all wind headings vary between 0 and 90 degrees, with 0 representing a parallel wind and 90 a wind blowing perpendicular to the road. Table 4-8 lists the sample period index, time stamp, 4.5 m wind direction, 4.5 m wind speed, absolute temperature, pressure, and estimated stability class for each time period. The stability class and sigma theta values are based on calculations made by Benson in the development of the CALINE3 model.

Table 4-6. Number of GM sample periods with similar wind direction, wind speed, and stability. Based on (Cadle et al. 1977).

Wind Speed, m/sec	Stability	Wind Direction				
		0^0-30^0 180^0-210^0	30^0-60^0 210^0-240^0	60^0-120^0 240^0-300^0	120^0-150^0 300^0-330^0	150^0-180^0 330^0-360^0
0-1	S	1	2	4	1	0
	U	0	0	1	0	1
>1-3	S	9	5	4	0	1
	U	9	4	9	1	5
>3	S	1	0	0	0	2
	U	0	1	0	0	1

Note: S = stable, U = unstable (including neutral).

Table 4-7. Number of GM sample periods with similar normalized wind direction, wind speed, and stability. A wind direction of 0^0 represents a parallel wind whereas a wind direction of 90^0 is perpendicular to the roadway. Day 272 has been removed because of equipment uncertainty.

Wind Speed, m/sec	Stability	Wind Direction			
		0^0-15^0	15^0-30^0	30^0-75^0	75^0-90^0
0-1	S	1	0	4	2
	U	1	0	0	1
1-3	S	7	4	10	0
	U	4	8	12	3
$\geq$3	S	2	0	0	0
	U	2	0	1	0

Note: S = stable, U = unstable (including neutral).

Table 4-8. Meteorological conditions for each GM tracer sampling period with valid tracer data.

Run Index	Time Stamp	Wind Direction	Wind Speed (m/s)	Stability Class	σ_θ	Temperature (K)	Pressure (mm Hg)
1	274140958	291	2.87	4	20	283.7	734
2	274143957	292	2.56	3	24	284.2	734
3	274150957	291	2.81	2	23	284.7	734
4	274153956	292	2.98	2	22	284.1	734
5	275080959	321	1.07	6	29	274.4	740
6	275083959	335	1.56	6	27	275.0	741
7	275090959	341	2.18	2	19	275.7	741
8	275093958	345	2.44	2	19	276.5	741
9	276081459	209	2.31	6	13	275.9	744
10	276084459	214	2.15	6	16	276.8	744
11	276091459	227	2.65	2	17	278.5	744
12	276094459	236	3.07	2	18	280.1	744
13	279080959	251	1.00	6	14	283.5	734
14	279084000	247	0.97	6	16	283.6	734
15	279090959	253	1.45	3	19	284.9	734
16	279093959	250	1.82	2	19	286.4	735
17	281080504	36	1.82	6	14	281.9	738
18	281083504	29	1.21	6	23	282.4	738
19	281090504	78	0.94	6	34	284.4	738
20	281093504	94	2.05	4	13	285.2	738
21	283081959	254	1.24	5	20	284.6	736
22	283085000	263	0.95	3	18	284.4	736
23	283092000	242	1.12	3	32	284.4	736
24	283095000	220	1.29	2	28	284.1	736
25	286081501	187	2.29	6	14	285.2	735
26	286084501	195	2.44	5	16	285.8	735
27	286091501	202	2.65	4	13	286.2	735
28	286094501	202	2.86	3	15	287.4	735
29	290080958	68	2.17	6	13	278.8	737
30	290083958	58	2.13	6	13	278.8	737
31	290090958	62	2.17	6	16	279.1	737

Table 4-8 Continued. Meteorological conditions for each GM tracer sampling period with valid tracer data.

Run Index	Time Stamp	Wind Direction	Wind Speed (m/s)	Stability Class	σ_θ	Temperature (K)	Pressure (mm Hg)
32	290093957	56	2.46	4	14	279.5	737
33	293103458	272	2.00	4	14	282.0	730
34	293110458	271	2.10	3	16	282.6	730
35	294080502	230	1.59	6	18	283.7	727
36	294083502	235	1.52	6	21	283.7	727
37	294090501	210	1.13	3	18	283.8	727
38	294093501	219	1.38	2	25	284.7	728
39	295080958	51	0.45	6	46	277.7	730
40	295083958	75	0.62	6	30	278.0	730
41	295090958	49	0.62	6	28	279.2	730
42	295093958	8	0.35	6	31	281.1	730
43	296080500	181	2.92	6	9	285.1	731
44	296083459	183	2.99	6	10	284.7	731
45	296090459	184	3.01	4	12	285.1	732
46	296093458	187	2.50	4	14	285.8	732
47	297080458	182	2.49	6	10	285.8	735
48	297083458	183	2.24	6	12	285.7	735
49	297090458	177	3.04	6	10	285.9	735
50	297093458	179	3.55	5	11	286.5	735
51	300080000	194	1.77	6	14	277.4	736
52	300083000	203	2.33	3	13	278.7	736
53	300090000	200	2.38	3	14	279.6	736
54	300093000	201	2.23	2	20	280.9	736
55	302080456	346	1.83	6	15	277.5	742
56	302083456	352	2.57	4	14	277.9	742
57	302090457	352	2.89	3	15	278.8	742
58	302093457	354	3.12	3	16	279.6	743
59	303080957	321	0.91	6	27	271.2	747
60	303083957	351	0.99	2	17	271.7	747
61	303090957	11	1.47	2	17	272.7	747
62	303093956	17	1.76	2	18	274.2	747

Near Roadway Wind Fields

"At 10.5 m above the ground, the velocity defects observed at all towers were small and randomly fluctuating about zero. Which shows that the traffic effect was minimal at this level. At the lower two levels [1.5 m & 4.5 m], on the other hand, the traffic effect was evident"(Chock 1980b). "There was no large variation of the crossroad wind component from one side of the road to the other, while the corresponding parallel wind component changed substantially at the bottom two levels. The parallel component of the median wind followed the direction of the upwind lanes" (Chock 1977a). "The turbulent kinetic energy generated from the traffic was transported at least 15 m downwind before being substantially dissipated. When the crossroad wind was high (> 2 m/s), the influence of vehicle packs passing at 29-second intervals was observed at 50 m downwind. The vertical dispersion of the turbulence energy extended to at least 4.5 m at 15 m downwind" (Chock 1977a).

"When the crossroad wind component was greater than about 1 m/sec, the wind at the upwind roadside tower was not modified by the traffic … at crossroad winds of less than 1 m/s, the bottom level wind at the same position was modified considerably … this indicates that the traffic wake creates an outward flux of momentum with an effective velocity of somewhat less than 1 m/sec" (Chock 1977a).

"The wind at the bottom level tended to move upward as it approached the roadway, and downward as it left the roadway. This is expected as the vehicles present an obstruction to the wind flow" (Chock 1977a). This phenomenon is consistent with the shelterbelt effect described by Dabberdt (Dabberdt et al. 1981). "At very low wind speed (< 1 m/sec), a significant upward motion (~> 0.15 m/sec) was observed at the median, which was not accompanied by a significant downward motion. Under these conditions, the buoyancy effects were expected to be most pronounced as the thermal plume would rise substantially before being advected and mixed downwind. The upward motion usually extended to the middle level of the tower" (Chock 1977a). "At wind speeds greater than 1 m/sec the vertical motion was small, being less than 0.1 m/sec" (Chock 1977a).

Lastly, Chock determined that "the roughness length at the test site was about three cm, which is typical of a long grass field. This was established from wind profile

measurements under essentially neutral conditions, assuming a homogeneous surface layer"(Chock 1977b).

The Temperature Field and Stability

"For all three levels [1.5, 4.5, 10.5 m], the downwind temperature was higher than the upwind temperature during the traffic runs …which indicates that heat was generated from the traffic (exhaust heat, engine heat, and friction heat) and transported downwind" (Chock 1977a). "Temperature differences were comparable for the lowest two levels, primarily due to the initial mixing by the traffic wake, which may extend up to a height of 4.5 m, 15 m downwind from the roadway" (Chock 1977a). Chock found that SF_6 and temperature gradients across the roadway correlate quite well. This suggests that the time scale for the buoyancy effect is large compared to mechanical mixing and, unless the cross-link wind component is near zero, the waste heat from traffic disperses like a passive tracer.

"It is worth noting that in terms of the Richardson numbers determined from the top and middle levels, the atmosphere downwind was more unstable than that upwind regardless of the ambient stability (upwind). This was due to higher heat input at the middle level than at the top level downwind from the roadway. For the lowest two levels, on the other hand, the downwind air need not be more unstable than the upwind air. In fact, there was a tendency to approach neutrality on the downwind side, indicating the influence of forced mixing due to the traffic wake in the lowest two levels" (Chock 1977a). Chock indicates that downwind of the roadway, "Ri [i.e. the Richardson number] at low levels tends to approach neutrality so that the upwind Ri may not be relevant in this region" (Chock 1977a).

Multiple measurements and analyses "indicate the importance of the high dilution effect due to the mechanical turbulence generated by the traffic. These dilution effects would tend to obscure the stability dependence of the dispersion" (Chock 1977b). For instance, Chock plots a comparison of vertical dispersion parameters as a function of stability in Figure 4-6. By way of comparison, dispersion parameters from the HIWAY model (discussed in a subsequent section) are shown. The HIWAY curves are a simple linear rollback from the classic Turner dispersion curves. "Note that the initial sigmas

are all comparable, whereas at 100 m the values derived from the experiment fall in between those of EPA's Class B and Class C. For the first 50 m there is little distinction among different stabilities. This is not surprising in view of the fact that downwind from the road, mechanical mixing dominates the mixing induced by stability considerations. In fact, the temperature data indicate that there is a tendency to approach neutral stability downwind from the road as one would expect from mechanical mixing"(Chock 1977b).

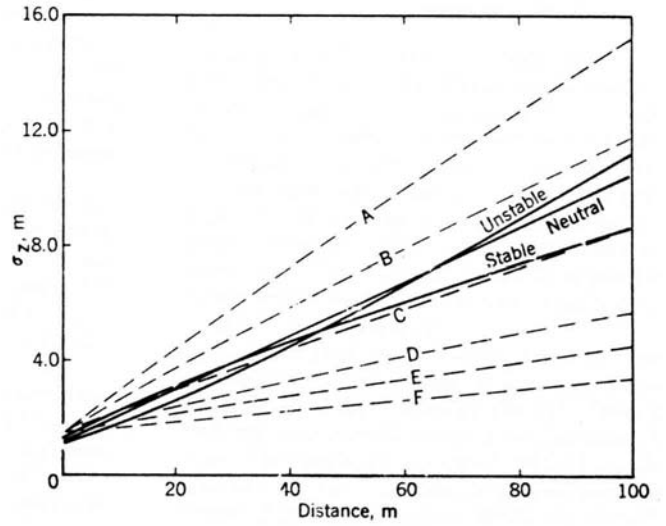

Figure 4-6. Comparison of GM Gaussian dispersion curves (solid lines) derived from curve-fitting GM tracer data versus HIWAY curves (simple extrapolations of the classic Turner curves). Note how the GM curves are essentially independent of stability near the roadway, source (Chock 1977b).

Concentration Field and Vehicle Wake Effects

The intense mechanical mixing near a roadway is expected to rapidly disperse pollutants close to the vehicles. Chock notes "it is expected that the expansion of the plume near the road is due primarily to mechanical mixing created by the traffic wake. However, the buoyancy effect due to the heated exhaust is also expected to play an important role. This is particularly true at distances further downwind" (Chock 1977a).

Consistent with the observation that the wind field upwind of a roadway is not influenced by the roadway when there is a significant cross-wind component, Chock observes that "the measurements show substantial upwind dispersion at crossroad wind speeds of less than 1 m/sec even when the wind is perpendicular to the road. Apparently,

the traffic wake is only mildly deflected by the low wind speed. At wind speeds greater than 1 m/sec, there is essentially no upwind dispersion."(Chock 1977b)

The GM data suggest that the direction of the wind with respect to the roadway orientation will significantly influence tracer fields as well. "When the wind is opposing the upwind traffic direction, intense shear occurs in the region upwind from the road. This also results in substantial upwind concentrations which may reduce concentrations in the median and downwind."(Chock 1977b)

Summary of GM Study Findings

A wealth of observations and analyses have been conducted with the GM data set. A subset of the findings that are salient to this study are presented below.

- At low wind speeds (less than 1 m/s), buoyancy of vehicle exhaust is measurable and may be significant for determining downwind concentrations near a roadway. At greater wind speeds, mechanical mixing dominates the diffusion of roadway pollutants.

- Roadway turbulence is clearly measurable up to an elevation of 4.5 m, 15 m downwind of a roadway and results in perturbations in the wind and temperature field.

- Roadway mixing does not appear to significantly influence wind and temperature fields at elevations greater than approximately 10.5 meters near a roadway.

- The orientation of the roadway with respect to the ambient wind direction appears to be important. If the wind and the traffic directions are opposite, pollutant mixing appears to be enhanced.

- The wake field near a roadway appears to travel at approximately 1 m/s. This can result in significant upwind pollutant concentrations during periods of low cross-road winds and will result in lower downwind concentrations downwind.

- The stability class downwind of a roadway is significantly different from its upwind counterpart. Analyses of Richardson numbers indicate that there is a trend toward neutrality downwind of a roadway and that vertical dispersion of pollutants in the near field are relatively independent of upwind stability class.

Gronskei Study

A study designed by Gronskei concludes that "vertical diffusion of exhaust gases tends to be larger from cars driving with high speed than from cars driving with lower speed" (Gronskei 1988). In the Gronskei studies, "two cars emitting different tracer components (SF_6 and $CBrF_3$) were driven one after the other with different speeds" (Gronskei 1988). Tracer gases were profiled at 10, 30, and 70 m downwind of the observed roadway, however, the article does not specify from what elevations samples are obtained.

The experimental procedure was essentially to let a fast car and a slow car emitting differing tracer gases pass by a sampling station. The cars were within 150 m and according to Gronskei, the vehicle wakes did not overlap. The roadway that the study was conducted on was not closed to the public and had an average vehicle flow rate of approximately 180 to 240 VPH.

Based on the published data, the average absolute percentage difference in the vertical standard deviation between the fast and slow moving vehicles was less than 30%. Given that the vehicle flow-rate was quite low, it is unclear if the trends Gronskei identified would still be present under more reasonable highway traffic loadings. It is also unclear if the presence of non-controlled traffic biased the data.

In a follow up paper by Eskridge and Petersen (Eskridge et al. 1991), Eskridge indicated that Gronskei's findings were consistent with their theoretical findings that a wake field behind a vehicle is speed dependant. Eskridge indicated "that it is expected from theoretical considerations that the effect of vehicle speed on pollutant concentrations will be more significant during stable atmospheric conditions, because in neutral and unstable conditions the vehicle-wake turbulence is quickly masked by the ambient turbulence" (Eskridge et al. 1991). However, Eskridge's analysis of the NYC data showed that for normal speed ranges "the predicted effect of speed on concentrations will be difficult to discern from the Long Island Expressway (LIE) data" and that "we cannot assess the influence of traffic speed on roadside concentration using the LIE data set for stable atmospheric conditions" (Eskridge et al. 1991).

UCD Dispersion Study

"A series of twelve intensively monitored 1-hour carbon monoxide (CO) dispersion studies were conducted near Davis, California in the winter of 1996. The experimental equipment included 12 CO sampling ports at elevations up to 50 m, three sonic anemometers, a tethersonde station, aircraft measurements of wind and temperature profile aloft, and a variety of conventional meteorological equipment. The study was designed to explore the role of vehicular exhaust buoyancy during worst-case meteorological conditions, i.e., low winds oriented in near parallel alignment with the road during a surface-based nocturnal inversion" (Held et al. 2001). During the study period ideal meteorological conditions were not experienced making a buoyancy analysis difficult. However, "From the study, field estimates of the CO emission factor (EF) from a California vehicle fleet using two different methods were computed. The analysis suggests that the CT-EMFAC/EMFAC emission factors currently used to conduct federal conformity modeling significantly over-predict CO emissions for high speed, free flowing traffic on California highways" (Held et al. 2001).

Interested readers are referred to the California Department of Transportation (CALTRANS) to obtain a compact disk with experimental raw data and a report titled "Observations and Model Simulations of Carbon Monoxide Dispersion" which summarizes experimental findings (Held et al. 1998). In addition, a Masters of Science thesis titled "Simulations of Carbon Monoxide Emissions from Vehicles over a Highway Using ARPS" by Edward Tai explores the use of a fully compressible non-hydrostatic fluid dynamics model to simulate pollutant transport based on the UCD data set. To obtain a copy of the thesis, please contact Tai's advisor Dr. John Carroll (jjcarroll@ucdavis.edu).

Summary of Literature Review Findings

A variety of experiments have been conducted to aid in our understanding of how pollutants are dispersed from a roadway. Many of these studies provide conflicting results, suggesting that there is still considerable uncertainty in our current knowledge of the physics of dispersion.

Early dispersion studies conducted by Drivas and Shair demonstrated that since Gaussian models do not account for wind shear, they do not adequately predict

concentration measurements downwind of a quasi-instantaneous line source. Furthermore, Drivas and Shair observed that "the semi-emperical diffusion equation, using the power-law velocity and eddy diffusivity profiles, works quite well in predicting dispersion from an urban ground-level cross-wind line source" (Drivas and Shair 1974). One must keep in mind that their experiments were not limited to the near field region (<100 m), and that Drivas and Shair's findings may not be applicable immediately downwind of a roadway.

Results from the NYC study indicate that at the roadway edge, vehicle effects were insignificant at an elevation of 16 m for parallel winds and 8 m for perpendicular winds. The FHWA study supports the NYC results and Dabberdt notes that at an elevation of 7.5 m, vehicular generated turbulence sharply attenuates and Chock concludes that at 10.5 m, wind and temperature perturbations were insignificant. This is not to say that the concentration of pollutants is zero at these elevations, rather, it indicates that near-field turbulence from the roadway will not significantly influence pollutant dispersion at this height. GM results indicate that vehicle effects are significant at least 15 m downwind and noticeable up to 30 m downwind of a roadway. Based on the wind component spectra, the range of frequencies affected by roadway activities range between 0.1 and 1 Hz with a distinct peak at 0.25 Hz. These data suggest that the characteristic eddy sizes produced by vehicles are approximately 4 to 8 meters in dimension.

The studies reviewed here indicate that in the immediate vicinity of a roadway, pollutant transport is dominated by the mechanical and thermal turbulence generated from vehicles and that ambient stability is largely insignificant. This conclusion was found independently in the NYC, GM, and FHWA study using a variety of metrics and techniques. This finding greatly simplifies the modeling of near roadway diffusion with simplistic dispersion equations because it effectively eliminates the need to consider ambient stability effects.

The literature indicates that there are conflicting theories as to the importance of exhaust buoyancy. Based on first principles, when the wind speed approaches zero one would expect some form of free-convection above the roadway. Both Chock and Dabberdt indicate that at low cross-wind speeds the experimental results are consistent

with plume rise. However, in a separate study, Rao indicates that no sign of organized convective motion could be attributed to vehicle waste heat.

Detailed wind tunnel experiments were conduced by Dabberdt to determine the relationships between vehicle speed, density, direction and near-field pollutant dispersion. Many of the results from this study were counterintuitive. For instance, downwind concentrations are lower when four lanes of traffic are moving in the same direction rather than two lanes traveling in opposite directions. One would expect that the head-on vehicle wake field would result in increased turbulent mixing. However, experimental results indicate that single direction flow has adequate turbulent intensity to completely mix the pollutants and additional turbulence does not significantly enhance mixing. Based on dual tracer releases, downwind concentration profiles for pollutants that are remixed by a downwind link are not significantly different than the profiles if the downwind link was not present. This further indicates that the intense turbulence over a roadway is localized and suitably intense to completely mix pollutants above a roadway. For smooth terrain, FHWA results indicate that vehicle speed and density have little impact (less than 10%) on downwind concentrations over the range of values tested. However, Gronskei concluded that vehicle speed can affect downwind concentrations by as much as 30 %. However, Gronskei's experiment was not as carefully controlled as Dabberdt's, and it is not clear if vehicle speed is indeed that significant.

Results from the GM study indicate that increased turbulence from the roadway has an effective propagation speed of approximately 1 m/s and is detectable at least 2 m upwind of a roadway. Therefore, one would expect non-zero concentrations upwind of a roadway and lower downwind concentrations if the cross-roadway wind component were less than 1 m/s. Both the GM and NYC studies indicate that the vehicle drag effect significantly altered the wind component parallel to the roadway. Since the studies reviewed here were essentially 2-D, given the symmetry of a line source, it is difficult to determine what the effects of altering the parallel wind component would have on pollutant transport. As a hypothetical example, near an intersection, an along roadway acceleration could result in concentration peaks that were not immediately downwind (based on ambient wind direction) of a roadway.

Chapter 5. Review of Contemporary Roadway Dispersion Models

Introduction

The literature abounds with techniques and models to estimate pollutant concentrations near roadways. These models vary in complexity from simple nomograms to complex fluid dynamics simulations. In this chapter, a review of selected modeling techniques will be introduced. Heavy emphasis will be placed on the CALINE models because they are currently approved as EPA regulatory models. In addition, a review of model complexity and parameterization will be discussed.

Early Dispersion Modeling Efforts

It is important to understand that most of the early roadway dispersion models and studies "grew out of the large body of knowledge … on plume dispersion from stationary sources at downwind distances of 100 meters and greater" (Benson 1980). Many of the earliest models estimated "near source dispersion … without rigorous study of the dynamics of the mixing processes at the source" (Benson 1980). For instance, the report titled "Mathematical Approach to Estimating Highway Impact on Air Quality" by the FHWA used initial estimates of horizontal and vertical Gaussian dispersion parameters based on "visual observations of smoke releases from a single vehicle" (Benson 1980).

In addition, many early papers focused on recasting classic dispersion equations so that they were more amenable to roadway dispersion analysis. For instance, Calder showed mathematically that one could use an infinite line source dispersion equation developed for perpendicular wind even if the wind was actually oblique (Calder 1973). His paper focused on coordinate transformations and existing dispersion equation formulations.

In the early 1970's several journal articles and reports were published exploring appropriate σ_y and σ_z estimations near the downwind edge of a roadway. The original Gaussian dispersion parameters were based on measurements made between 100 and 1000 m downwind of a point source. Prior to the existence of detailed data sets, roadway dispersion model estimates of σ_y's and σ_z's within 100 m of a roadway were quite simplistic. For example, the EPA model HIWAY extrapolated the 100 m sigmas to a zero fetch distance with initial values of σ_y= 3 m and σ_z= 1.5 m. These early attempts to

model roadway pollution prior to calibration data sets often resulted in dramatic over and under predictions.

With the availability of more detailed data sets such as the GM study, more elaborate modeling techniques became feasible. However, the paradigm of using Gaussian-based models for regulatory purposes had already been firmly entrenched and many of the studies conducted in light of these new data sets were primarily focused on introducing new formulations of the Gaussian dispersion parameters.

Early Gaussian and Non-Gaussian Dispersion Models as Reviewed by Sistla

Sistla conducted a review of eight roadway dispersion models based on the NYC tracer data (Sistla et al. 1979). Four of the models were non-Gaussian numerical models (MROAD2, DANARD, RAGLAND, and ROADS) and four were Gaussian type models (HIWAY, CALINE-2, AIRPOL-4, GM). Of the eight models, HIWAY was probably used most extensively because at one time it was an EPA approved model. However, most of the models reviewed by Sistla are now considered obsolete and would probably not be used for either regulatory or research purposes. They are included here for completeness and to introduce the reader to the wide variety of modeling approaches that have already been considered for roadway dispersion modeling.

Of the eight models, Sistla concludes that "the GM model [overall] performed [the] best" and "comparison of parallel wind cases indicated that the GM model predictions are markedly better than predictions of the other models" (Sistla et al. 1979). The observed versus predicted scatter plots lead Sistla to comment that "the scatter around the one-to-one line is quite small for [the] GM model compared to the HIWAY model" (Sistla et al. 1979). And, in general "the numerical models in all cases did no better than the Gaussian models" and the numerical models tended to consistently make serious over predictions (Sistla et al. 1979). In a separate analysis conducted by Sistla and Rao, it is observed that "although the GM model provides by far a better simulation than any of the models tested here, it is skewed toward under prediction" (Rao et al. 1980).

MROAD I (Kirsch and Mason 1975)

"This is a Eulerian two-dimensional grid model which numerically solves the mass conservation equation. The size of the grid can be specified by the user. The model allows for the existence of several line sources (all assumed to be perpendicular to the plane in the model) including elevated roadways. There is also a provision to include topography adjacent to the roadway. Mixing of pollutants is assumed to be uniform to 3.3 m above each roadbed. Wind profiles are described as a function of atmospheric stability, but can be specified by the user. The model can accept wind direction and speed for up to eight locations. The final wind field is based on the solution of a potential field and is fitted to the measured velocities via a least-squares fit" (Sistla et al. 1979).

DANARD (Danard 1972)

"This is a two-dimensional Eulerian model which solves the mass conservation equation according to the numerical methods outlined by Dufort and Frankel (Dufort and Frankel 1953). The grid is fixed in the horizontal, extending from –150 m to +150 m from the center of the roadway. The vertical grid is confined to 10 cells between the surface (assumed flat) and the mixing height. The pollutants are assumed to be mixed uniformly within the 3 m layer above the highway, but the user can specify the diffusivity value desired over the highway (Danard suggests a value of 20 m^2s^{-1}). The user must also specify the diffusivities (K_x, K_z) at the 10m height. Model inputs include a wind speed value, V, at the 10 m height and a cross-road component, u, at the same level. If the mixing height is greater than 10 m, the model requires additional wind measurements at higher levels" (Sistla et al. 1979).

RAGLAND (Ragland and Peirce 1975)

"The model of Ragland and Pierce solves the continuity of mass equation

$$u\frac{\partial c}{\partial x}-\frac{\partial}{\partial y}\left(K_y\frac{\partial c}{\partial y}\right)-\frac{\partial}{\partial x_3}\left(K_z\frac{\partial c}{\partial z}\right)=0 \qquad (5\text{-}1)$$

where u = u(z) is the wind speed in the x direction (downwind) as a function of height and c is the pollutant concentration. The eddy diffusivities are defined for neutral stability as

$$K_z = kzu_* \quad for \quad z \le 100\,m \qquad (5\text{-}2)$$

where k is the von Karman constant (0.4) and u_*, is the friction velocity defined in terms of geostrophic drag coefficient and geostrophic wind speed.

The model predicts concentrations for oblique and perpendicular cases by ignoring lateral diffusion and computing an effective advective wind speed equal to u(z) sin θ, where θ is the wind-road angle. In the parallel case the model solves the equation in three-dimensions including lateral diffusion" (Sistla et al. 1979).

ROADS (Pitter 1976)

"ROADS is a two dimensional Eulerian conservation of mass model. It computes the average stability class and generates a vertical profile of crossroad wind speed for each observation. The winds at a reference level are then averaged to obtain a reference cross-road wind speed. The horizontal crossroad wind speeds are then computed for all grid points on the basis of the reference wind speed and the vertical profile. Vertical velocities generated due to the presence of terrain features are also computed. The vertical velocities, which decay with height, are then specified at each grid point. The horizontal velocity departures from the previously determined values also adjust with distance in a specified manner. These procedures will generate a realistic pattern of vertical and horizontal crossroad velocities responding to terrain irregularities. The model determines the steady-state concentrations of pollutants by numerically solving the equations governing atmospheric advection and diffusion and chemical reactions. In each time step, the pollutants are first advected and diffused horizontally then advected and diffused vertically, and finally allowed to react to modify the pollutant mix. Lax-Wendroff finite difference scheme is used to numerically solve the advection-diffusion equation" (Sistla et al. 1979).

HIWAY (Zimmerman and Thompson 1975)

"The HIWAY model uses a steady state Gaussian equation to predict air pollution concentrations at receptor locations adjacent to a highway in relatively flat terrain. The concentration from a line source is given by

$$C = \frac{Q}{u}\int_0^D f\, dl \qquad (5\text{-}3)$$

where Q is the emission rate per unit length, u is the wind speed. D is the length of the line source and f is the point source dispersion function. The dispersion parameters σ_y and σ_z in the Gaussian plume equation are specified at each downwind distance as a function of atmospheric stability and distance as defined bv Turner (Turner 1969)" (Sistla et al. 1979).

According to Rao and Keenan, "previous studies have indicated that the EPA-HIWAY model significantly overestimates the pollutant concentrations for stable atmospheric conditions, especially under parallel wind-road orientation angles with low wind speed. This overestimation is due to the fact that the model's dispersion parameters do not properly account for the traffic-induced turbulence near roadways." (Rao and Kienan 1980). Subsequent studies have shown that if alternative functional forms of σ_y and σ_z where selected based on calibration with the GM and NYC data set the HIWAY model results could be significantly improved (Rao and Kienan 1980). These observations led to the development of the HIWAY-2 Model.

CALINE-2 (Ward et al. 1977)

> "This model also is based on the Gaussian plume formulation together with concepts of a box model. The model assumes that the pollutants emitted are well mixed over the roadway and up to a fixed height. This region is referred to as the "mixing cell". The downwind concentrations from the roadway are determined by using both continuous line source and continuous point source equation. The model uses Pasquill dispersion parameter curves which are modified to handle downwind distances of less than 100m from the source" (Sistla et al. 1979).

AIRPOL-4 (Carpenter and Clemena 1975)

> "This model, based on Gaussian formulation, uses two Euclidean coordinate systems, namely the roadway and receptor coordinate systems. It can be used for a variety of roadway configurations. The model can predict pollutant levels for all wind speeds (>0),, for any sampling interval, and for all traffic speeds (>0). The dispersion parameters σ_y and σ_z are incorporated in the model following the procedure used in HIWAY by Zimmerman and Thompson (Zimmerman and Thompson 1975)" (Sistla et al. 1979).

GM (Chock, 1978)

Chock outlined the following deficiencies of the HIWAY model, "(1) inadequate dispersion parameters; (2) no treatment for plume rise; (3) tendency towards severe over prediction when the winds are parallel to the road; (4) applicability not extended to very low wind speeds; (5) neglect of asymmetry due to the wind direction relative to the traffic direction; and (6) inadequate treatment of dispersion upwind of the road" (Chock 1978b). In attempt to address items 1 – 4, the GM line source model was developed noting that addressing items 5 and 6 did "not justify the added complexity their correction would require" (Chock 1978b). Chock attempted to address all six apparent deficiencies of the HIWAY model in a separate model based on K theory.

> "This model also uses a Gaussian line source approach, but avoids the point source assumption (used in HIWAY) and calculates the concentrations using the equation

$$C = \frac{Q}{\sqrt{2\pi}\sigma_z u}\left\{\exp\left[-\frac{1}{2}\left(\frac{z-h_0}{\sigma_z}\right)^2\right] + \exp\left[-\frac{1}{2}\left(\frac{z-h_0}{\sigma_z}\right)^2\right]\right\} \quad (5\text{-}4)$$

> where Q is the emission rate per unit length, u is the effective cross-road wind speed, h_o is the plume height. The effect of lateral and vertical dispersion on the distribution of concentration is incorporated by specifying σ_z, as a function of both downwind distance and wind-road orientation angle. Chock suggests that σ_z, is of the form $\sigma_z = (a + bx)^c$ where a, b and c are functions of atmospheric stability which are determined empirically, and x is the distance from the source" (Sistla et al. 1979).

The DeTar Line Source Model

In the late 1970's DeTar derived a modified Gaussian line source model based on the GM data set which represented the vertical dispersion parameter, σ_z, as a function of travel time from the source to the receptor rather than a function of downwind fetch (DeTar 1979). DeTar concluded that σ_z was directly proportional to travel time.

As Benson observed, if σ_z is considered a function of travel time, as the cross-wind speed approaches zero, σ_z will become infinite (Benson 1980). If one considers σ_z as a function of distance, as when the wind speed approaches zero downwind concentrations become infinite. However, in the DeTar formulation, since both the wind speed and σ_z appear in the denominator of the Gaussian equation, the downwind concentration as wind speed approaches zero is indeterminate. Thus, DeTar's scheme is much more numerically stable than the conventional σ_z parameterization. However, even though DeTar's equation is mathematically well behaved as wind speeds approach zero, use of a continuous line source Gaussian formulation to predict dispersion under calm winds is inappropriate.

Although DeTar's model is not currently used today, aspects of his formulation were incorporated into subsequent models such as the CALINE series of models. Specifically, the CALINE formulation employs DeTar's premise that initial vertical dispersion should be a function of time traveled over a roadway rather than fetch distance. The DeTar model did not specifically address how the horizontal spreading parameter, σ_y, should be calculated, which limits its applicability for finite-line source modeling. In addition, the DeTar formulation assumes a uniform wind field and neglects shear flow effects.

Chock's Advection-Diffusion Model

In 1978 Chock published an advection diffusion model based on the GM dataset which predicted concentrations that "agree reasonably well with observations" (Chock 1978a). At the heart of the model is the determination of the eddy diffusivity tensor, K_{ij}, above the roadway. K_{ij} components were determined by "relating algebraically the gradients of first-order moments to second-order correlations" which requires that "the second-order correlations are in local equilibrium or in a local steady state with respect to their dynamic behavior and that the gradient transports of second-order correlations are

influenced only by the local values of other correlations" (Chock 1978a). Effectively this indicates that in order to algebraically relate second and third order closure approaches, K-theory must itself be valid. K-theory is known to be invalid in a variety of atmospheric conditions thus Chock's basic premise is admittedly suspect. Chock assumes that K_{ij} for a pollutant is identical to K_{ij} for potential temperature, which is only a reasonable assumption for neutral stability. Chocks felt that his method was preferable to an "elaborate parameterization" approach where the eddy diffusivity tensor was fit to observed concentrations (Chock 1978a).

Eskridge & Hunt Velocity Deficit Formulation and Models

In 1979 Eskridge and Hunt published a theory for determining the wake structure of a single vehicle moving through still air (Eskridge and Hunt 1979). Their technique was based on "a perturbation analysis which yields analytic expressions for the mean velocity deficit in the wake and the variance of the turbulent velocity components" (Eskridge and Hunt 1979). In their formulation, Eskridge and Hunt "exclude nonlinear interactions between the vortices and drag-induced wake which may well be of importance near the vehicle), we shall ignore the effect of Γ [Γ is defined as the circulation of a trailing vortex pattern on the side of a vehicle] and consider the vehicle as a point source of momentum (or angular momentum) loss" (Eskridge and Hunt 1979).

The single vehicle in still air analysis was extended to account for multiple vehicles moving in weak wind so that their theory could be compared with GM tracer data. Eskridge contends that if the vehicle speeds are much greater than the ambient wind, the still air approach can be adapted to weak winds with a simple coordinate transformation (Eskridge and Hunt 1979). Multiple vehicles are accounted for by a simple superposition of a single vehicle wake field. However, for the approach to be valid, the wake fields of one vehicle cannot significantly overlap the wake field of a trailing vehicle. Geometrically, non-overlapping wakes requires that vehicles are significantly spaced and that the angle between the mean horizontal wind and the vehicle must be near perpendicular. To compare their theory with the GM data, Eskridge and Hunt had to assume that the GM vehicles were equally spaced even though they were closely pack with significant wake overlap.

Unfortunately, Eskridge and Hunt's formulation did not agree well with the GM data set. Plots of predicted along-wind and vertical turbulent intensities, $\overline{u'^2}$ and $\overline{w'^2}$ show essentially no correlation with observed values. The lateral turbulent intensity, $\overline{v'^2}$, and lateral velocity deficit due to wake turbulence demonstrated reasonable agreement with observed values. The along-wind velocity deficit, *u*, one of the main focuses of the paper was not plotted or discussed. It is assumed that predicted values of *u* bore little resemblance with field data.

Based on their theoretical formulations, Eskridge and Hunt published a modified K-theory model to simulate roadway pollutant fields near roadways (Eskridge et al. 1979). Their model did not incorporate thermal effects such as exhaust buoyancy and concentration predictions were shown to be only slightly better than the EPA HIWAY model.

Eskridge and Thompson conducted a wind tunnel study to determine the wake field behind a block shaped model vehicle (Eskridge and Thompson 1982). In their study, a "specially-constructed wind tunnel with a moving floor [that] moved at the free stream air speed to produce a uniform, shear-free, approach flow … [simulating] an automobile traveling along a straight highway under calm atmospheric conditions" (Eskridge and Thompson 1982). Modifications to the original Eskridge and Hunt theoretical formulations resulted in moderately better agreement with observed data. However, "the observed strong shear near the surface was not explained completely by the theory … and the existence of a large shear near the surface is incompatible with the assumption of a constant eddy viscosity as made by Eskridge and Hunt" (Eskridge and Rao 1986).

Based on the Eskridge and Thompson work, a revised version of the model ROADWAY was developed, which incorporated the new Eskridge theory of vehicle wake. The modified ROADWAY model was moderately better than the existing model, however "the model does not attempt to incorporate wind direction variation [and] under these conditions, one expects the model to over-predict pollutant concentrations" (Eskridge and Rao 1986). The ROADWAY model, as described by Rao (Rao et al. 1986) is presented below.

> "The ROADWAY model solves a conservation of species equation via finite-difference approximations. The model assumes a surface layer describable by surface layer similarity theory with the superposition of the effects of vehicle wakes. The vehicle wakes affect the wind field and the turbulence fields, and it is assumed in the model that the effect is linear … A vehicle wake is a region of increased turbulence and decreased velocity relative to the vehicle. The intensity of the wake is a function of vehicle speed, downwind distance, and distance from the center of the wake. An average velocity and turbulence field is calculated across the highway based upon the number of vehicles, vehicle speeds, and ambient, atmospheric (upwind) conditions. Using the calculated velocity and turbulence fields, pollutant concentration predictions are made over, upwind and downwind of the highway."

The CALINE3 & 4 Models

The CALINE3 model is Gaussian-based and is currently the EPA regulatory model for dispersion of pollutants from a free-flowing roadway. In addition, the CALINE3 algorithms are the backbone of many intersection models. Basically, the CALINE3 and CALINE4 models divide "individual highway links into a series of elements from which incremental concentrations are computed and then summed to form a total concentration estimate for a particular receptor location" (Benson 1979).

The CALINE4 model uses a parameterization scheme quite similar to CALINE3 for pollutant dispersion. If a reference is made to CALINE without specification to either model specifically, then the reference holds for both models. The CALINE3 model will be fully reviewed in this chapter, if there are significant differences between CALINE3 and CALINE4 parameterizations they will be highlighted. Many of the inner workings of the CALINE algorithms are not specified in their respective user manuals (Benson 1979; Benson 1984). In this study an inspection of the CALINE3 source code was performed to gain further insight into how the CALINE models numerically simulate roadway geometry and dispersion.

Mixing Zone Concept and Modified Dispersion Parameters

At the heart of the CALINE model is the concept of a mixing zone above the roadway where the intense mechanical and thermal turbulence result in enhanced mixing of pollutants. Figure 5-1 from the CALINE3 manual provides a graphical description of the mixing zone. The mixing zone is defined as the traveled way of a roadway link plus a three-meter buffer zone on each edge of the traveled way (Note: this leads to a total buffered area size of six meters). Inspection of Figure 5-1 would lead one to believe that the CALINE model uniformly distributed emissions, traffic? across a roadway, which is

not the case. In reality, the CALINE model simulates emissions with a series of line sources that are not necessarily coincident with the coordinates of the roadway.

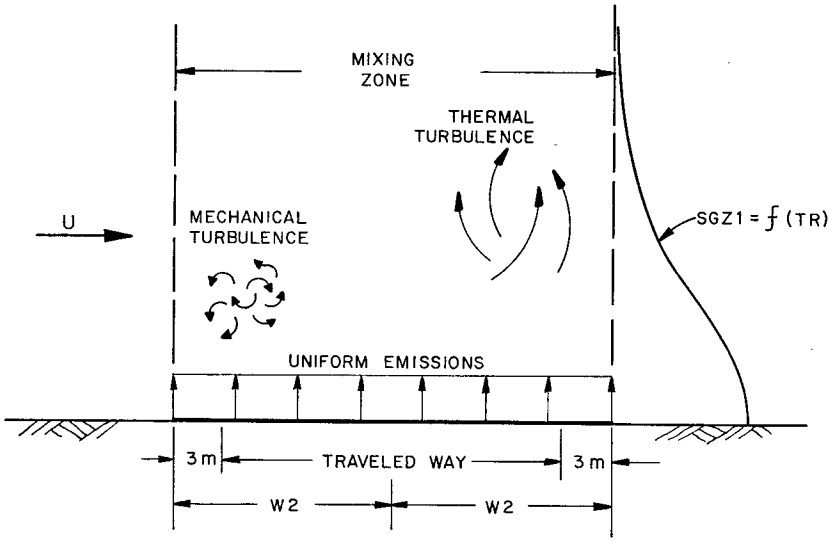

Figure 5-1. CALINE3 roadway mixing zone, source (Benson 1979).

The primary use of the mixing zone is the establishment of initial Gaussian dispersion parameters at a reference distance near the edge of a roadway. Since the Pasquill-Turner curves were based on far-field dispersion from passive releases, an alternative approach to determining the Gaussian dispersion parameters is necessary for near field dispersion from an active release.

CALINE3 uses Equations 5-5 and 5-6 whereas CALINE4 uses Equations 5-7 and 5-8 to determine the initial vertical spreading parameter, σ_z, at a roadway reference point. The CALINE σ_z relationships were based on curve fitting tracer data from the GM experiment. W_2 is one half of the width of the traveled way plus three meters, U (m/sec) is a wind speed determined at a representative elevation, and ϕ (PHI) is the angle that the horizontal wind makes with the roadway link. A ϕ near zero represents a parallel wind and a ϕ near 90 represents a perpendicular wind. TR (units of seconds) is defined as a residence time and SGZ1 (units of meters) is defined as the vertical mixing parameter at a reference point. For the CALINE3 model the reference point for SGZ1is W_2; in the CALINE4 model it is W_{MIX}. W_{MIX} is defined by Equation 5-9 and is shown graphically in Figure 5-2.

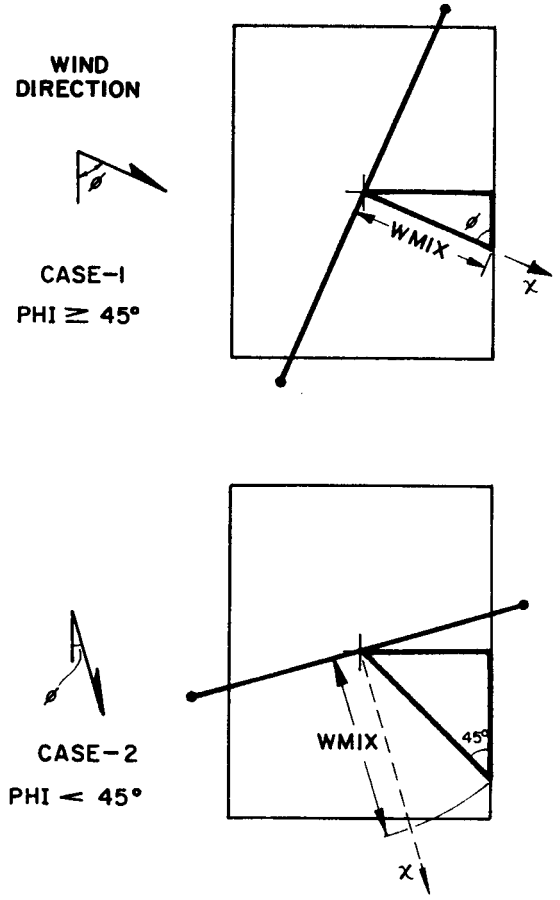

Figure 5-2. CALINE4 element geometry for determining WMIX (Benson 1984).

CALINE3 $SGZ1 = 1.8 + 0.11 * TR$ (5-5)

CALINE3 $TR = \frac{W_2}{U}$ (5-6)

CALINE4 $SGZ1 = 1.5 + 0.1 * TR$ (5-7)

CALINE4 $TR = \frac{W_2}{U\,Sin(\phi)} \quad PHI \geq 45^0$

$= \frac{W_2}{U\,Sin(45)} \quad PHI \leq 45^0$ (5-8)

CALINE4 $W_{MIX} = \frac{W_2}{Sin(\phi)} \quad PHI \geq 45^0$

$= \frac{W_2}{Sin(45)} \quad PHI \leq 45^0$ (5-9)

It should be made clear that the reference points W_2 or W_{MIX} are not coincident with the edge of the traveled way unless the wind direction is perpendicular to the road. These parameterizations are arbitrary definitions and are necessary when one is attempting to simulate a wind profile with significant shear with a model that assumes a constant wind speed over the entire domain.

TR does not represent a residence time that an air parcel would spend above a roadway in the CALINE3 model or in the CALINE4 formulation unless the wind angle with respect to the road is greater than 45^0. Benson notes that the definition of TR in this way is arbitrary. The situation is further complicated by allowing the user to specify the elevation at which the wind speed is considered representative.

Benson states that "the value of SGZ1 is considered by CALINE3 to be independent of surface roughness and atmospheric stability class. The user should note that SGZ1 accounts for all the enhanced dispersion over and immediately downwind of the roadway" (Benson 1979). The CALINE specification that vertical spreading of pollutants is independent of stability and is some function of roadway geometry is consistent with the findings in the literature review. The SGZ1 is based on an averaging time of 30 minutes, adjustments for differing averaging times (noted as ATIM in the figures) is accomplished by using a power law relationship.

CALINE3 and CALINE4 use different methods to determine the vertical mixing parameter downwind of a reference distance. In the CALINE3 model, the vertical mixing parameter is defined in Equation 5-10 for all positive fetches. The parameters α and β are determined by specifying σ_z at two reference points (note: the CALINE figures use the notation PZ or PY to represent these parameters). The first reference point is a fetch of W_2 with a σ_z=SGZ1. The second reference point is at a fetch of 10 km where σ_z is determined by the conventional Pasquill dispersion curve. Note that in the CALINE3 parameterization, as the fetch (i.e., x) approaches zero, σ_z approaches zero as well. The vertical dispersion parameter as a function of fetch for CALINE3 is shown in Figure 5-3.

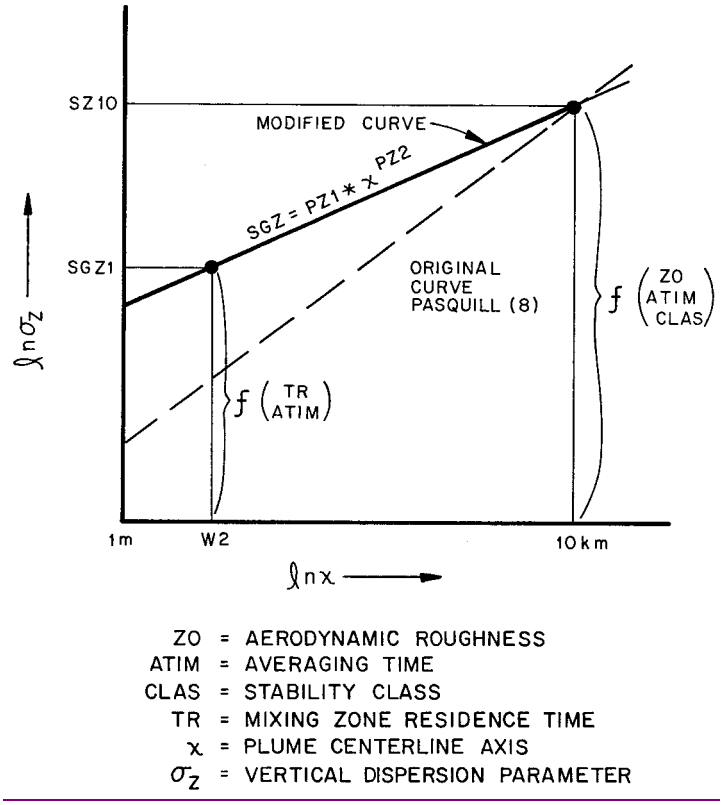

Figure 5-3. The CALINE3 vertical dispersion parameter, σ_z, as a function of downwind fetch distance (Benson 1979).

The CALINE4 scheme for estimating σ_z is presented in Equation 5-11 and shown graphically in Figure 5-4. In the CALINE4 parameterization there are a total of three reference points. The first reference point is W_2 in the CALINE3 model and for CALINE4 it is W_{MIX}, defined by Equation 5-7.. Note that in the CALINE4 formulation, σ_z is constant as x approaches zero, whereas in the CALINE3 formulation, σ_z is defined by a single function for all x and approaches zero at a zero fetch length. As a practical matter, since model guidance indicates that receptors are not to be sited closer than 3 m from the traveled way, the CALINE3 treatment of SGZ1 is inconsequential. Benson defines D_{REF} as a reference point 10 km downwind. D_{MIX} is defined as the lesser of the fetch distance over the mixing zone, the fetch such that $\sigma_y = 1.48 * W_2$, or W_{MIX}.

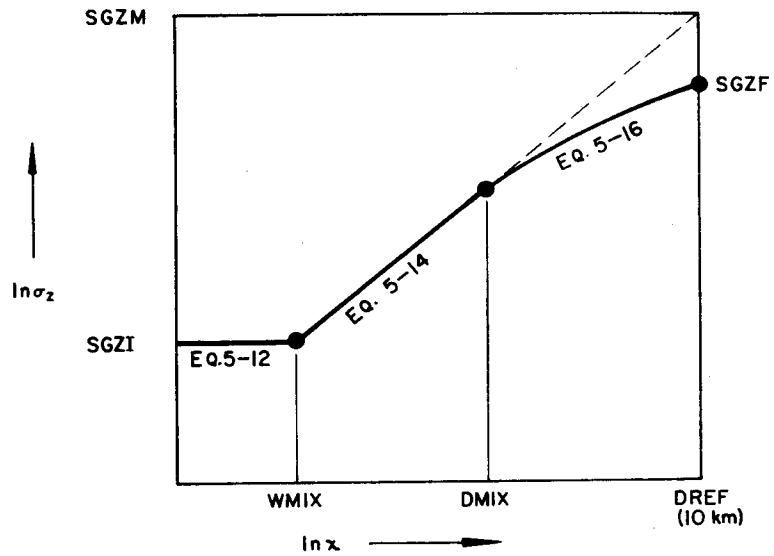

Figure 5-4. The CALINE4 vertical dispersion parameter, σ_z, as a function of downwind fetch distance (Benson 1979).

The fitting parameters used for Equation 5-11are quite involved and not explicitly grounded in physical arguments. For instance, CALINE4 uses a penalty system to correct σ_z for cases when it does not monotonically increase with fetch length. Only a brief outline of the parameter scheme is presented here. The determination of the CALINE4 α and β terms is similar to the CALINE3 approach with two notable exceptions. First, the first reference point is W_{MIX} and not W_2. Second, the stability class at 10 km (D_{REF}) downwind is slightly modified to account for vehicle waste heat effects. By assuming a heat loss factor, fuel economy, and energy content of gasoline, a heat flux due to emissions is calculated. Based on this calculation, an effective stability is determined for use at the 10 km reference point. Thus, vehicle buoyancy effects are incorporated by modifying the fitting parameters α and β by adjusting the σ_z at the 10 km reference point.

Obviously, the CALINE reference points W_{MIX}, D_{MIX}, D_{REF} are somewhat arbitrary and are artifacts of modeler preference. In addition, it is not expected that the vehicle buoyancy effect will have a significant impact on near field concentration estimates because the functional form of σ_z will be dominated by SGZ1 rather than a reference σ_z determined at 10 km downwind.

CALINE3 $\sigma_z = \alpha_1 x^{\beta_1}$ for $x > 0$ (5-10)

CALINE4 $\sigma_z = SGZ1$ for $0 < x < W_{MIX}$

$\sigma_z = \alpha_2 x^{\beta_2}$ for $W_{MIX} < x < D_{MIX}$

$$\sigma_z = \alpha_2 x^{\beta_2} \left(\frac{x}{D_{MIX}} \right)^{\gamma \ln\left(\frac{x}{D_{MIX}}\right)} \quad \text{for } x > D_{MIX} \qquad (5\text{-}11)$$

"The horizontal dispersion curves used by CALINE3 are identical to those used by Turner except for averaging time and surface roughness power law adjustments similar to those made for the vertical dispersion curves. The model makes no corrections to the initial horizontal dispersion near the roadway" (Benson 1979). A graphical depiction of σ_y for the CALINE3 model is presented in Figure 5-5. In the CALINE4 model σ_y proportional to the horizontal standard deviation, σ_θ, of the wind direction. The function form of σ_y is based on the method proposed by Draxler (Draxler 1976).

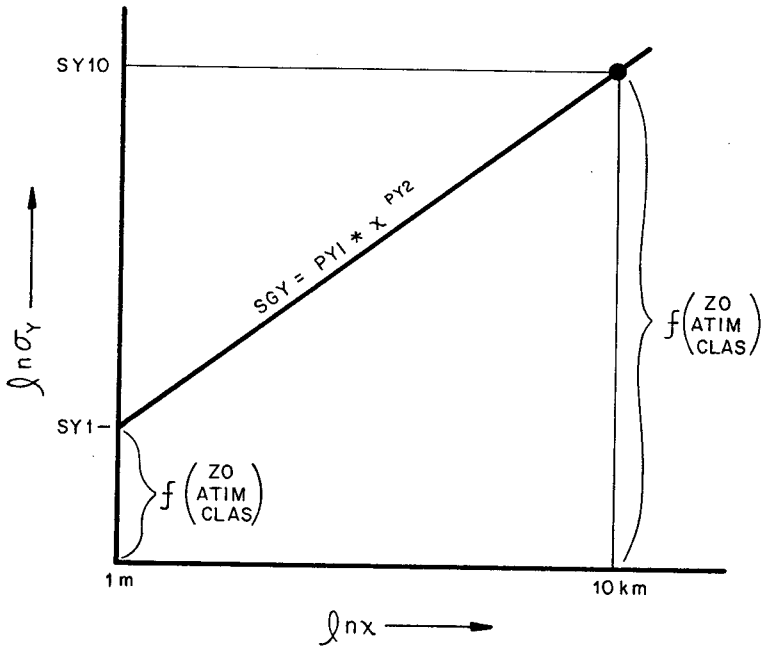

Figure 5-5. The CALINE3 horizontal dispersion parameter, σ_y, as a function of downwind fetch distance (Benson 1979).

CALINE Link Geometry

In the CALINE models, a roadway link is assigned an equivalent line source strength based on the product of a single vehicle emission factor (grams of pollutant per mile traveled) and vehicle flow rate (vehicles per hour). The CALINE models divide a roadway link into sub-links as shown in Figure 5-6. The first sub-link is square with each side length equal to W2 * 2 (i.e., the traveled way plus six meters). The lengths of subsequent sub-links are determined by Equations 5-12 through 5-15, with slightly differing algorithms for the CALINE3 and CALINE4 models. The sub-element width is W2 * 2 for all elements.

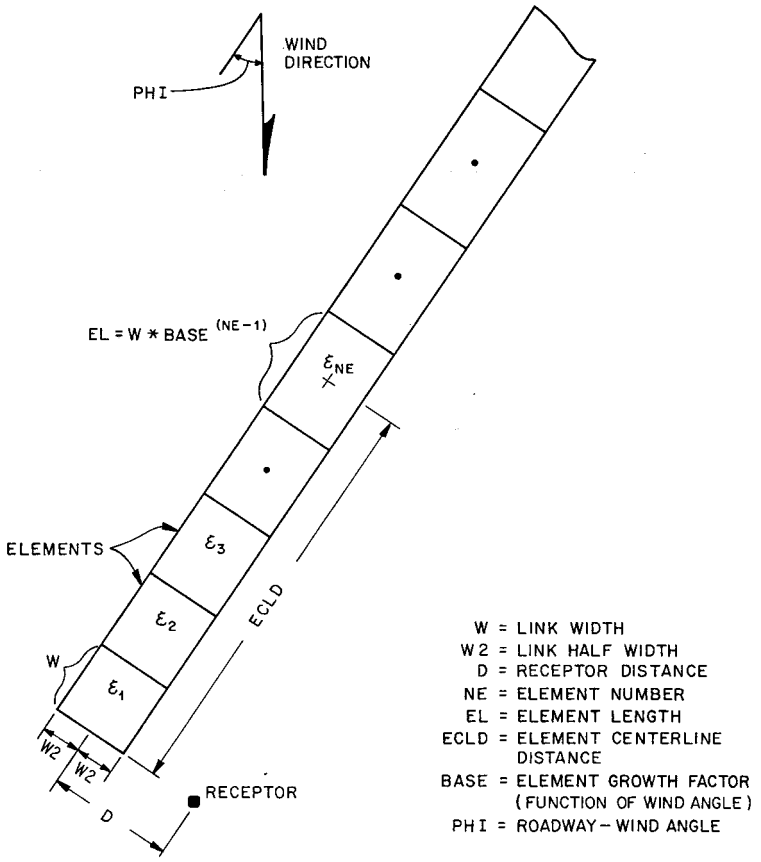

Figure 5-6. The CALINE sub-element series used to represent a roadway link (Benson 1979).

CALINE3 $EL = W * BASE^{(NE-1)}$ (5-12)

CALINE4 $EL = W * BASE^{NE}$ (5-13)

CALINE3 $BASE = \begin{cases} 1.1 & \phi < 20 \\ 1.5 & 20 \leq \phi < 50 \\ 2.0 & 50 \leq \phi < 70 \\ 4.0 & \phi \geq 70 \end{cases}$ (5-14)

CALINE4 $BASE = 1.1 + \frac{\phi^3}{2.5 * 10^5}$ (5-15)

Where:

EL – Sub-Element Length
W – Highway Width
NE – Element Number (Starting with 1)
BASE – Element Growth Factor

The location of the first sub-link is determined differently in CALINE4 than in CALINE3. CALINE3 determines the downwind edge of the first sub-link by the intersection of a line drawn perpendicular to the link, which intersects a downwind receptor. In the CALINE4 model, the centroid of the first sub-link (determined by the intersection of the link centerline and a line parallel with the wind direction) passes through the downwind receptor. If the wind angle is less than 45^0, CALINE4 will assume a wind angle of 45^0. Again, this is a somewhat arbitrary technique based on modeler preference.

The emissions for each sub-link are distributed on an axis that is centered on the midpoint of the sub-link and oriented perpendicular to the mean wind direction as shown in Figure 5-7. The length of each finite line source (FLS) is based on the wind direction, link width, and sub-link length. Based on examination of the CALINE source code, both models use Equation 5-16 to determine the FLS length. If the user specifies a wind angle/roadway link combination that results in a ϕ of zero or 90, the wind angle will be slightly perturbed so that Equation 5-16 is well behaved. A graphical depiction of terms used in Equation 5-16 is shown in Figure 5-8. Figure 5-9 is reproduced from the CALINE user manual and shows FLS locations and orientations for various roadway geometries and wind directions.

CALINE $$\text{FLSL} = \frac{W}{Cos(\phi)} + (EL - W\,Tan(\phi))Sin(\phi) \qquad (5\text{-}16)$$

Where:

EL – Length of the Sub-Element Along the Link Axis
W – Width of the Sub-Element
FLSL – Length of the Finite Line Source

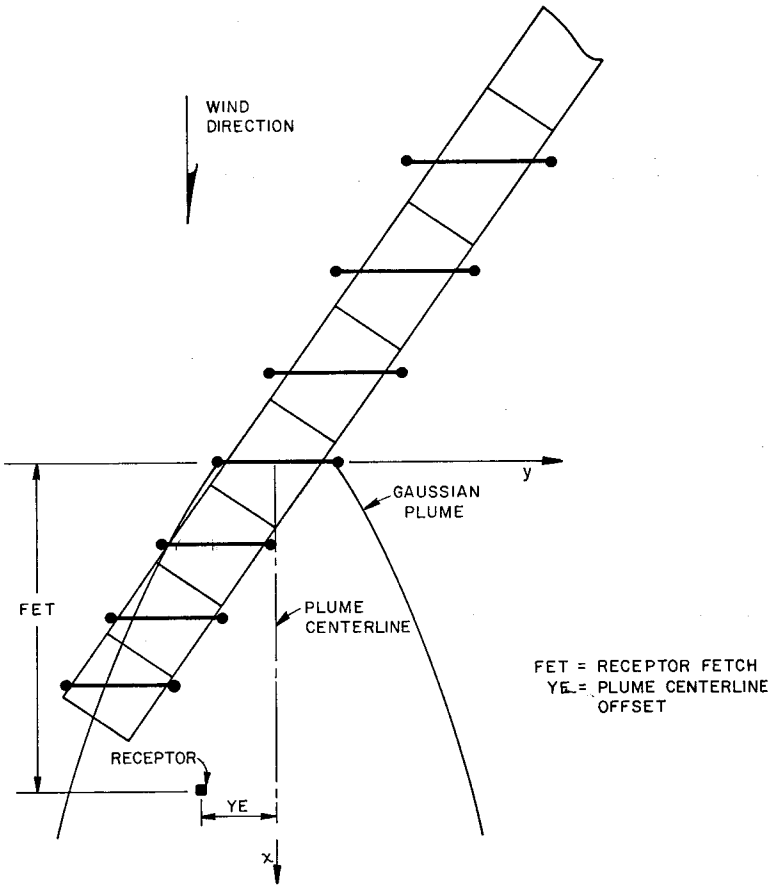

Figure 5-7. The CALINE finite line sources (FLS) perpendicular to the ambient wind direction representing emissions from each sub-element (Benson 1979).

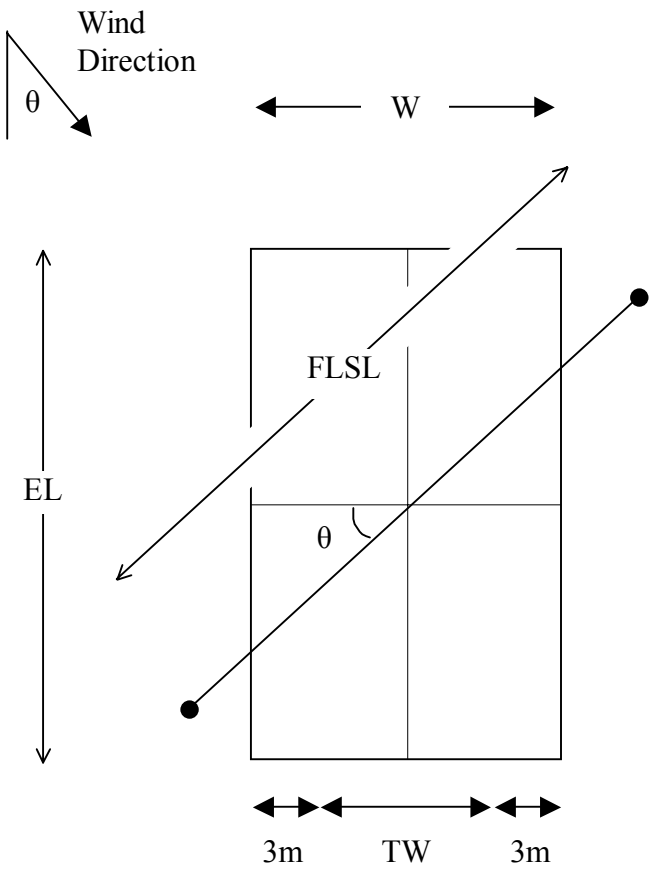

EL – Length of the Sub-Element Along the Link Axis
W – Width of the Sub-Element
TW – Width of Link's Traveled Way
FLSL – Length of the Finite Line Source

Figure 5-8. The CALINE finite line sources (FLS) geometry and notation.

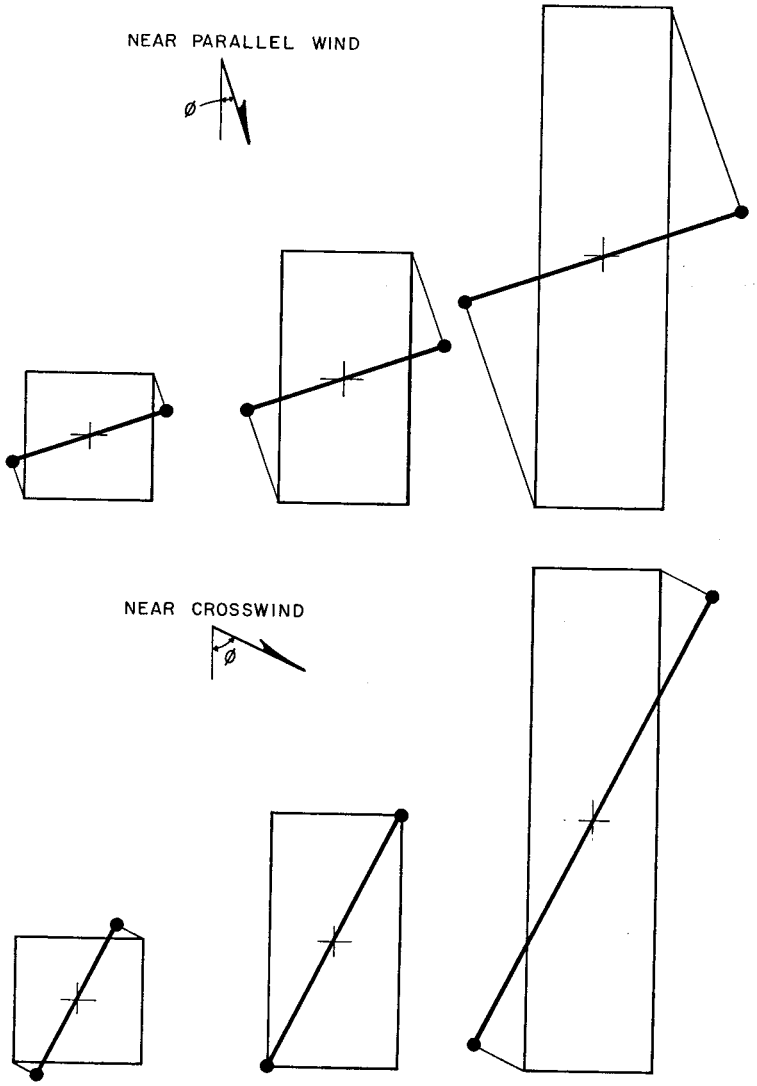

Figure 5-9. The CALINE FLS location for various sub-element sizes and wind angles (Benson 1979).

Figure 5-10 was created using the CALINE algorithms and shows the sub-element sizes, locations, and associated FLS's for a two lane roadway with a traveled way of seven meters. The wind direction for this figure is 60 degrees and the receptor is located 50 m from the link centerline. Similarly Figure 5-11 was created with a receptor located at the boundary of the CALINE mixing zone (i.e. 3 m from the nearest traveled way).

Inspection of these two figures demonstrates that as the receptor is moved closer to the roadway, modeling artifacts such as FLS length and orientation will have a

significant impact on concentration estimates. For instance, the FLS for the CALINE3 sub-element ε_{-1}, shown in Figure 5-11, is almost coincident with the receptor location.

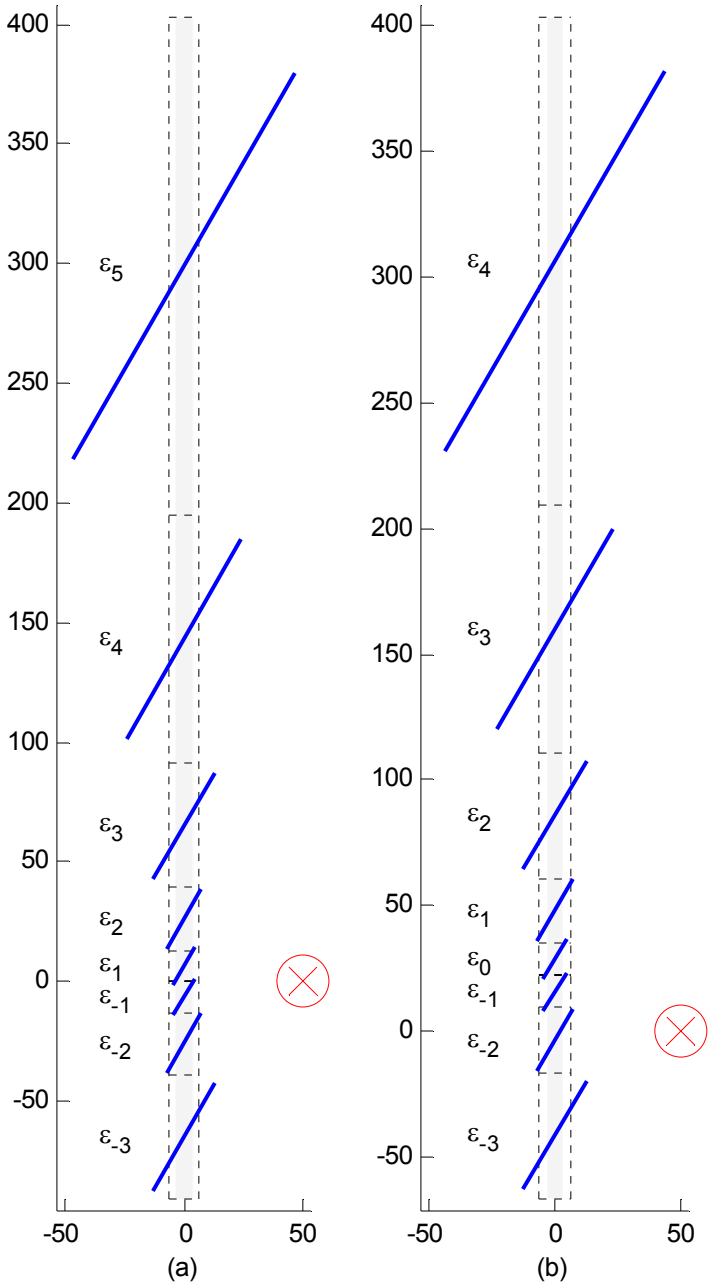

Figure 5-10. A graphical representation of the CALINE sub-element and finite line source approximation for a two lane roadway with a wind angle of 60 degrees and a receptor located 50 meters from the roadway centerline. The light gray area outlines the roadway link's traveled way, the dashed lines are the sub-element boundaries (which are labeled with the same notation given in the CALINE user manuals), the diagonal lines are FLS's used to represent emissions from each sub-element. The receptor is centered at the circled cross hairs. Figure a (b) is based on the CALINE3 (CALINE4) algorithms.

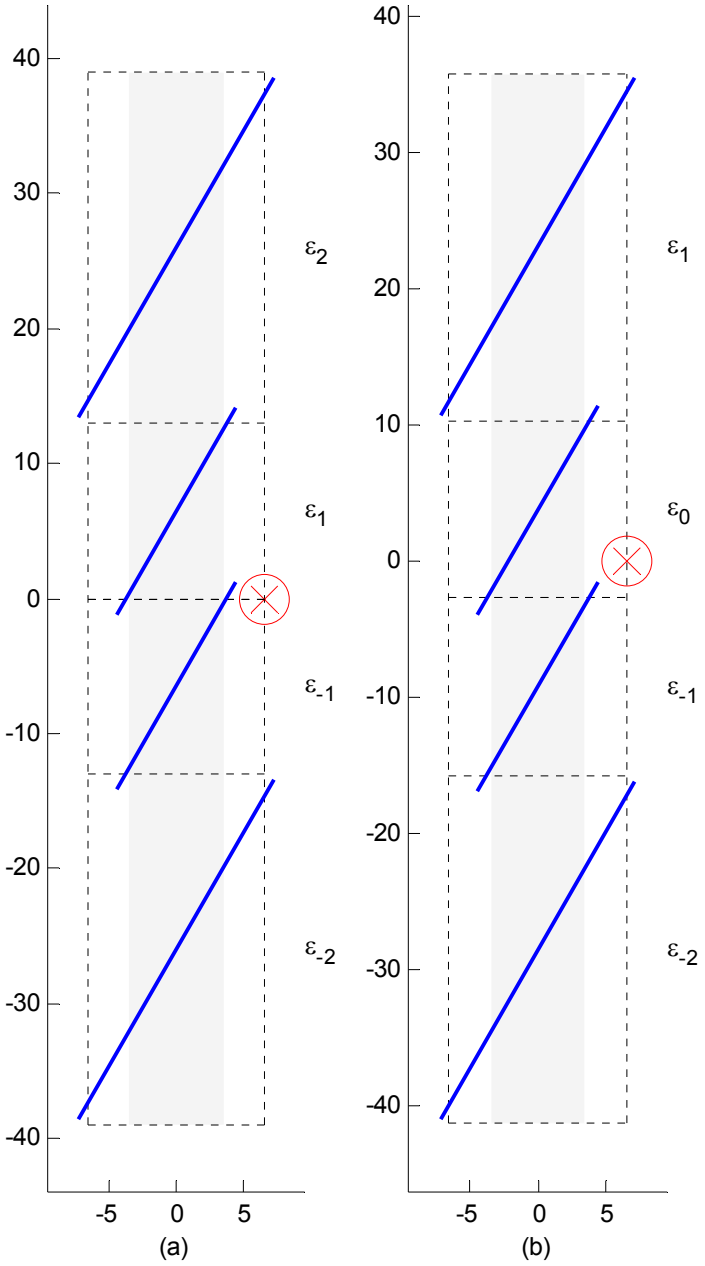

Figure 5-11. A graphical representation of the CALINE sub-element and finite line source approximation for a two lane roadway with a wind angle of 60 degrees and a receptor located 3 meters from a link's traveled way. The light gray area outlines the roadway link's traveled way, the dashed lines are the sub-element boundaries (which are labeled with the same notation given in the CALINE user manuals), the diagonal lines are FLS's used to represent emissions from each sub-element. The receptor is centered at the circled cross hairs. Figure a (b) is based on the CALINE3 (CALINE4) algorithms.

For each sub-element, the FLS is further divided into either five (CALINE3) or three (CALINE4) smaller FLS's (referred to here as sub-FLS) as shown in Figures 5-12 and 5-13. The length of the sub-FLS is determined by sub-element geometry and wind direction. The emission strength of each sub-FLS is weighted in an attempt to have higher emissions over the roadway. The weighting algorithms are slightly different in CALINE3 versus CALINE4. In the CALINE3 model the center sub-FLS has a weight of unity. The remaining four sub-FLS's are of equal lengths, the outermost sub-FLS's have a weight of 0.25 and the two innermost sub-FLS's have a weight of 0.75. The weighting scheme used in the CALINE4 model is somewhat more complex and its exact mechanisms are not essential for this analysis. Nevertheless, modeling algorithms such as these are not physically intuitive and may result in unpredictable near field model predictions.

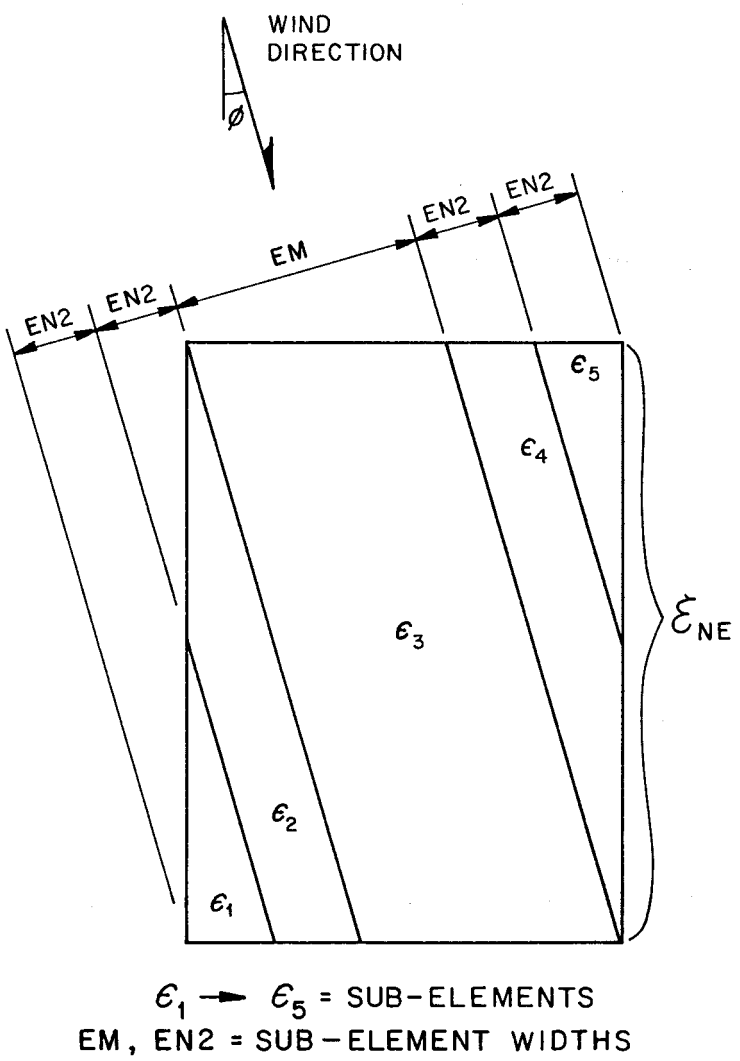

Figure 5-12. The CALINE3 sub-FLS element locations (Benson 1979).

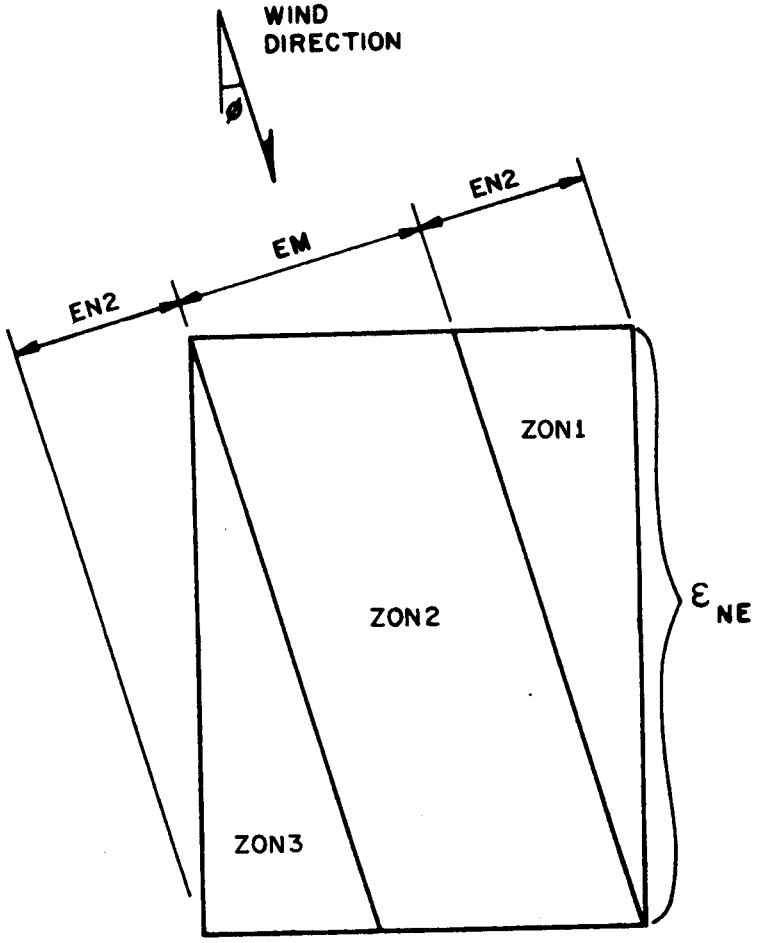

Figure 5-13. The CALINE4 sub-FLS element locations (Benson 1984).

Trends in Modern Roadway Dispersion Modeling Literature

Modeling pollutant fields near signalized intersections and street canyons appears to be the primary focus of recent roadway pollutant modeling literature. A street canyon is a roadway that is bounded by large impermeable structures such as buildings. Pollutant transport near canyons is quite complex and is strongly dependant on building geometry.

Street canyon simulations have been carried out with higher order closure techniques such as the κ-ε approach used by Albergel and Jasmin (Albergel and Jasmin 1998) and large eddy simulation (LES) techniques by Graf. (Graf et al. 1990). Simplistic nomograms techniques have also been developed for use in Europe by Buckland (Buckland and Middleton 1999). Between the extremes of nomograms and LES, a variety of recent publications have addressed street canyon pollutant fields including

(Berkowicz 1997; Buckland 1998; Chabni et al. 1998; Chan et al. 1995; Dabberdt and Hoydysh 1991; DePaul and M. 1986; Hargreaves and Baker 1997; Hassan and Crowther 1998a; Hassan and Crowther 1998b; Herbert et al. 1997; Hoydysh and Dabberdt 1988; Hunter et al. 1992; Johnson and Hunter 1995; Johnson and Hunter 1999; Kamenetsky and Vieru 1995; Kastner-Klein and Plate 1999; Koushki 1991; Lanzani and Tamponi 1995; Lee and Park 1994; Meroney et al. 1996; Nakamura and Oke 1988; Okamoto et al. 1996; Pavageau and Schatzmann 1999; Pearce and Baker 1997; Qin and Kot 1993; Rotach 1995; Yamartino and Wiegand 1986; Zoumakis 1995). Unfortunately, techniques used to model street canyons tend to be site specific and are difficult to extend to more generalized situations.

Another area of active research is modeling pollutant fields near signalized intersections. Determining the pollutant field near an intersection requires detailed knowledge of vehicle location and movement, modal emission characteristics, and atmospheric transport processes. In contrast to the street canyon literature, which primarily focuses on the kinematics of fluid flow with little emphasis on characterizing emissions, recent intersection analysis literature appears to focus more on characterizing vehicle location and emissions. Although there have been studies addressing the complex fluid dynamics within and near an intersection, such as the wind tunnel work done by Dabberdt and Hoydysh, many of the intersection models, such as CAL3QHC, TEXIN2, or FLINT use the dispersion algorithms developed for CALINE3 or a similar Gaussian type model (Cooper et al. 1997; Dabberdt et al. 1995; Hoydysh and Dabberdt 1994a; Hoydysh and Dabberdt 1994b). Most of the technical research pertaining to intersection modeling focuses on where pollutants are released, such as the novel queuing algorithms developed by Al-Deek (Al-Deek et al. 1996), or how to determine modal emission factors, such as the approach taken by Washington (Washington et al. 1998).

In the recent literature, three additional roadway dispersion studies were conducted by Matzoros, Baker, and Karim. In the Matzoros study, a model to simulate pollutant concentrations on an entire transportation network was developed (Matzoros and Vanvliet 1992a; Matzoros and Vanvliet 1992b). This model accounts for differing emissions for various vehicle operating modes and includes a novel queuing algorithm. In the Matzoros model, the dispersion algorithms used were Gaussian-based, and like

most new intersection models, greater emphasis is placed on emission factor and vehicle location issues than on developing new techniques to disperse roadway pollutants.

Baker (Baker 1996) introduced a roadway dispersion model that simulated roadway pollutant releases from a vehicle with a moving point source. Using this technique, the effect of vehicle speed could be directly incorporated into a Gaussian framework. Baker's dispersion algorithms used the theoretical velocity deficit equations developed by Eskridge et. al. for the near wake region (Eskridge et al. 1979; Eskridge and Hunt 1979; Eskridge et al. 1991; Eskridge et al. 1984; Eskridge and Rao 1983; Eskridge and Rao 1986; Eskridge and Thompson 1982). Baker used a Gaussian puff model for the far wake region. The moving point source approach appears promising but will be limited by the efficacy of the Eskridge model to accurately simulate near field velocity and turbulence perturbations near vehicles. Since Baker did not compare his model against a tracer study, such as the NYC or GM database, it is unclear if the model he derived is suitably robust for regulatory purposes.

Summary

Existing roadway dispersion models can be grouped into two basic categories, Gaussian and non-Gaussian models. In some respects, non-Gaussian models such as K-theory or higher order closure models, are more scientifically satisfying than Gaussian type models because they allow the modeler to parameterize mixing phenomenon in a physically meaningful and consistent manner. Chock's advection diffusion model and Eskridge's velocity deficit model are two higher order closure models presented in this chapter. In general, these models are quite complex to use and do not always predict concentrations better than their simplistic Gaussian counter parts. In addition, since the physics of roadway dispersion is not well understood, many of the higher order models effectively become complex curve-fitting models.

A variety of Gaussian type models such as the HIWAY and CALINE models were also introduced in this chapter. The strength of these models is their simplicity and robustness. Unlike the non-Gaussian numerical models, these models do not have convergence or numerical stability issues and can be run by regulatory personnel with relatively little training. The primary weakness of these models is the difficulty in directly incorporating important physical phenomena in a consistent and non-arbitrary

manner. One example of a simplifying assumption that is difficult to overcome is the Gaussian requirement of a uniform wind field. Chock notes that the determination of representative wind speed for calculations "is not obvious since the model assumes a constant wind speed (invariant with height), whereas the wind speed in the atmospheric surface layer increases with height. Turner suggested using the mean wind speed within 2 σ_z of the downwind distance. For transport distances between 0.1 and 1 km, the wind speed at a height of 10 m is generally used. For distances between 10 and 100 km, Pasquill recommended the mean between the geostrophic wind speed and the wind speed at a height of 10m. No suggestions were made for distances less than 100 m" (Chock 1977b).

No model is expected to work well in all situations. Furthermore, it is not clear if the dispersion models presented in this chapter accurately predict concentration fields for roadway configurations and meteorological conditions different from the calibration sets from which they were developed.

Chapter 6. Overview of the UCD 2001 Roadway Dispersion Model

Introduction

In this chapter a description of UCD 2001, a novel roadway dispersion model developed at the University of California, Davis will be presented. This chapter begins with an outline of the underlying paradigm of the UCD 2001 model. A discussion of the UCD 2001 code and input requirements follow. The UCD 2001 methodology for representing highway links with an array of point sources will also be covered in some detail. Lastly, a discussion of dispersion parameters required for the evaluation of the Huang point source dispersion equation is presented.

New Regulatory Model Paradigm

The UCD 2001 model is based on a simplified dispersion algorithm rather than a K-theory or higher order closure approach. This modeling approach was selected because a detailed understanding of the flux and covariance fields above and immediately next to a road are not fully understood. Using a K-theory or higher order closure model

to simulate a roadway may simply result in a complex curve-fitting algorithm, rather than provide additional insight into near-field roadway dispersion. Lastly, K-theory models require significant modeler expertise and computational resources, which may not be appropriate for regulatory screening purposes.

The UCD model uses the Huang algorithm, which is based on a power law approximation of both the wind and eddy diffusivity vertical profiles. Although a power law profile does not always agree with measurements, it is thought to be a better approximation than simply assuming constant wind and eddy diffusivity with height. A significant regulatory advantage of using power law approximations is that there is no ambiguity in specifying a representative wind speed. Since the Gaussian type models cannot account for wind shear, a modeler must select a representative wind speed based on model guidelines. However, with power law profiles, there is less interpretation on the part of the modeler and more consistency between users.

The new UCD model is based on a three-dimensional array of point sources rather than a ground-based line source. Since a point source does not have to be aligned with the wind in a special way, it eliminates the arbitrary link rotation that is necessary in the CALINE approach. UCD 2001 assumes a uniform mixing zone above the roadway that extends to 2.5m. Conceptually, the uniform placement of point sources above the road simulates the release of roadway pollutants as if they originated from a volume source. This approach is physically intuitive and leads to smoother concentration profiles above and near roadways.

The UCD 2001 model does not require ambient stability as an input. As previously noted, several independent researchers have concluded that dispersion in the near-field of a roadway is independent of ambient stability. Obviously, at some distance downwind, ambient stability will affect pollutant transport. However, since the UCD 2001 model is only intended for use within 100 m of a roadway, stability can be safely ignored.

UCD 2001 Programming Code Outline

UCD 2001 is written exclusively in the Java programming language. Java is an object-oriented language popularized by its use in internet applets in the late 1990's. The Java language was selected for the UCD 2001 model because it is platform independent,

therefore, the model code can run using virtually any operating system (e.g. PC compatible, Macintosh, and Unix).

A summary of the most significant classes in the UCD 2001 model are presented in Table 6-1. This list will be most beneficial to researchers interested in modifying the UCD 2001 code. Even if one does not anticipate altering the code, this table provides an overview of the essential components of the UCD 2001 model.

Table 6-1. Synopsis of selected UCD 2001 packages and classes.

Package or Class	Function
numerics.hyperbolics	This package provides routines to calculate gamma and modified Bessel functions. Routines are based on RISOE Computer Laboratory algorithms.
dispersion	This class facilitates the storage of meteorological parameters such as wind direction and eddy diffusivity constants.
link	An abstract class that defines the interface of all derived link objects. This is the super class of the highway_link class, additional link types such as intersection links can be derived from this class.
highway_link	A class derived from the link class used to simulate emissions from a highway or any other continuous flow roadway link.
highway_point_spacing	A class used to speed model performance by optimizing the number and placement of point sources used to represent a highway link.
huang	A container class that stores variables specific to each point source. This class is a member of the point class and simplifies and speeds the calculation of the dispersion equation derived by Huang.
point	A class representing a continuous point source of a pollutant.
point_vector	A utility class that allows the creation of a piecewise continuous array of point sources.
receptor	A class that stores the locations and estimated concentrations of pollutants released by nearby link sources.
UCD_2001	A class that drives the creation and interaction of all the other classes in the model.

UCD 2001 Coordinate System and Units

The UCD 2001 uses a three-dimensional Cartesian coordinate system. Positive x, y, z values are represented by the standard geometric convention. Angle measurements for wind speed use the standard meteorological convention. Wind angles represent the direction *from* which the wind is blowing in degrees measured clockwise from the positive Y axis. For example a wind heading of 90^0 indicates the wind is blowing from the positive x axis and a wind heading of 135^0 blows from the southeast quadrant. Unless otherwise stated, length measurements are in meters, emission factors are g/vehicle-mile-hour, and concentrations are in parts per million by volume (ppmv) or parts per trillion by volume (pptv).

User Input Variables

The UCD 2001 model requires the user to specify the roadway and receptor geometry, vehicle flow-rate and emissions information, and simplified meteorological estimates. The UCD 2001 model is still in development and would require a front-end for use by someone not familiar with computer programming. In its current form, the UCD 2001 model can receive information from, and direct output to, both text files and databases. Since the model dynamically allocates array sizes, an arbitrary number of links and receptors are possible, limited only by computer memory and storage. Table 6-2 summarizes UCD 2001 model inputs.

Table 6-2. User inputs required for the UCD 2001 roadway dispersion model.

Roadway and Receptor Geometry Inputs

- Beginning and end coordinates for each link centerline.
- Width of a link's traveled way.
- Receptor location coordinates

Vehicle and Emissions Inputs For A Highway Link

- Vehicle flow-rate in vehicles/hour for each link.
- Aggregate emission factor in grams/mile for each link.
- Molecular weight of the pollutant of interest (same)

Meteorological Inputs

- Elevation at which meteorological variables are measured or estimated.
- Average wind speed and direction.
- Estimated temperature and pressure. These variables are only used to convert concentrations to mixing ratios and do not have to be precise.

The UCD 2001 requires fewer input variables than most roadway dispersion models because metrological variables such as surface roughness and stability are not necessary. All other modeling parameters such as point array location and spacing are internal to the model and do not require user specification.

Point Source Array Generation for a Highway Link

A roadway link is internally represented by a three-dimensional array of point sources. Since the UCD 2001 model assigns a copy of each link to each receptor, the

density of the point array can be tailored to minimize computational time. The UCD 2001 code was designed to allow for programmatic flexibility in specifying how points are distributed on and above a roadway. In the most general sense, the UCD 2001 code allows for any piecewise continuous function of point locations above, lateral to, or along the fetch of a link. For instance, points can be exponentially spaced in the vertical direction so that there are more points near the road surface and point density would taper off with increasing elevation. Similarly, points placed along a roadway cross section could be non-linear to allow for a higher density of points near the center of the traveled way and a lower density near the link fringe. See Figure 6-1 for a pictorial representation of the cross and fetch directions of a highway link in plan view. If a link centerline is parallel to the y-axis, the cross-roadway axis is parallel to the x-axis and the fetch axis is parallel to the y-axis.

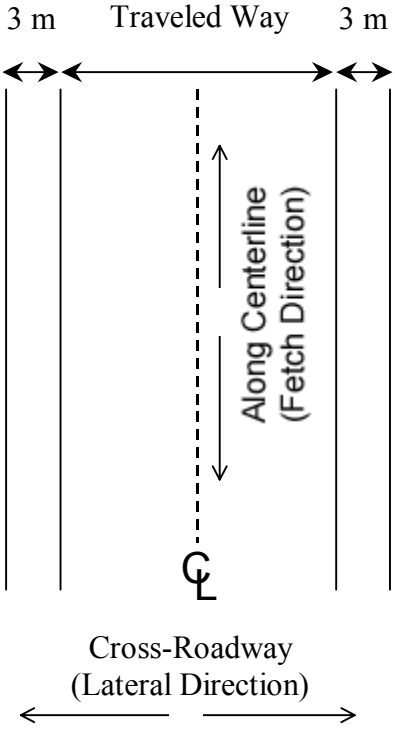

Figure 6-1. UCD 2001 link nomenclature and orientation in plan view.

Highway Point Source Locations

To determine point spacing for a highway link, the UCD 2001 model rotates the coordinate system so that the link centerline is aligned with the y-axis and the receptor is on the x-axis. The rotated link is then broken into several sub-links and each sub-link is assigned to a zone. Each zone has different point array densities, with point sources more densely spaced when a link is closer to a receptor. By assigning differing spacing schemes to zones, the computational time required to run the UCD 2001 code is significantly reduced while not significantly affecting precision. See Figure 6-2 for a schematic of how a link is parsed into sub-links and assigned to a zone. Table 6-3 lists the along-link length of each zone.

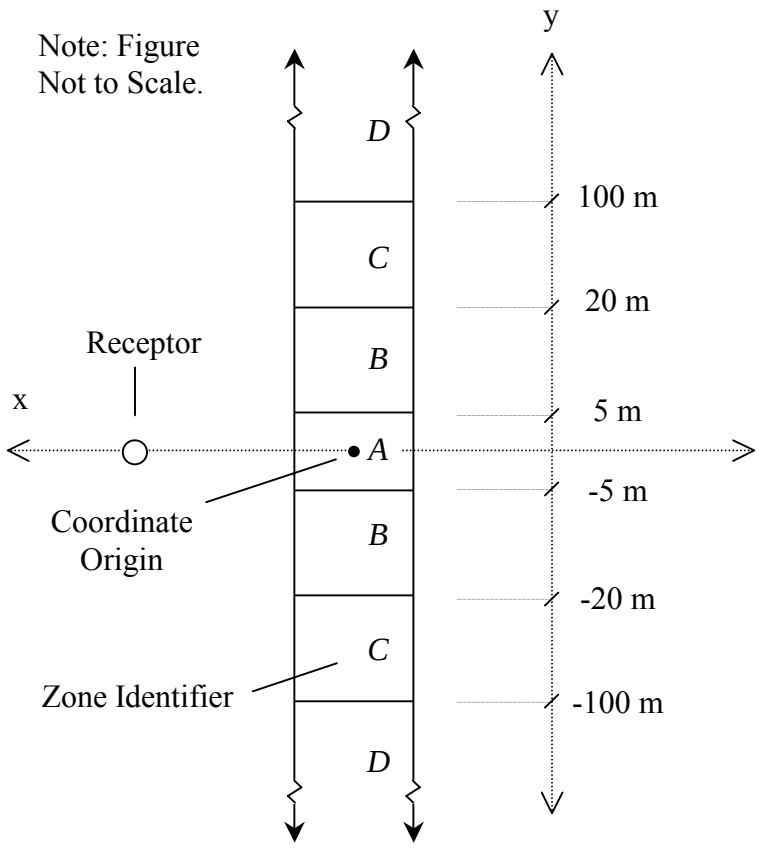

Figure 6-2. UCD 2001 highway link zone locations.

Table 6-3. Description and location of UCD 2001 highway link zones.

Zone	Description	Extent of Zone (m)
A	Ultra fine point source spacing for sub-links close to receptors.	ABS(y) < 5
B	Fine point source spacing.	5 < ABS(y) < 20
C	Normal point source spacing.	20 < ABS(y) < 100
D	Coarse spacing for sub-links far from a receptor.	ABS(y) > 100

Each zone is assigned a unique vertical, cross-link, and fetch spacing algorithm that fixes the point density above, lateral to, and along the link centerline, respectively. The UCD 2001 model uses a linear algorithm for point spacing, which results in a uniform spacing along any single orthogonal link direction. The point profiles along the principal axes of the link (i.e. along the vertical, cross-link, and fetch direction) correspond to an x, y, or z point location in the rotated link coordinate system. To determine the point source locations for a sub-link, the point profiles in the principal link axes are permuted to result in x, y, z Cartesian coordinates. Thus, the total number of points in a zone is the product of the length of each point profile. The point coordinates generated from this permutation are then mapped from the rotated coordinate system back to the actual coordinate system so that they are on or above the link they represent.

For example, if each point profile were only two members long with a fetch profile = (A,B), a cross-link profile = (D,E), and a vertical profile = (G,H) the coordinates (in the rotated coordinate system in x,y,z triplets) of the point sources assigned to this zone would be (A,D,G), (A,D,H), (A,E,G), (A,E,H), (B,D,G), (B,D,H), (B,E,G), (B,E,H). Table 6-4 lists the maximum distance between any two points along the vertical, lateral or fetch highway link axes.

Table 6-4. UCD 2001 point source spacing for each highway link zone.

Zone	Distance Between Point Sources along the Principal Axes of a Highway Link		
	Vertical	Lateral	Fetch
A	0.5	0.5	0.5
B	“	1.0	1.0
C	“	3.0	5.0
D	“	5.0	100.0

Vertical points are placed between the 0.0 and 2.5 m elevations, resulting in vertical point profile of [0.0, 0.5, 1.0, 1.5, 2.0, 2.5] for all zones. The number of lateral points varies for each zone and is based on lateral point spacing and effective link width. Effective link width is defined as the width of a highway link traveled way plus six meters. The additional six meters accounts for the lateral spread of pollutants due to the intense mechanical mixing associated with vehicular wakes. For instance if a link width was 6 m, the effective link width would be 12 m.

In general, the number of points required to span a distance x with a minimum spacing of y is one plus the integer component of y/x. For our 6 m wide example link, five points (12/3 + 1) equally spaced along the lateral axis would be required to ensure a point spacing of 3.0 m for zone C. The resulting lateral point profile for this example is [-6, -3, 0, 3, 6]. The cross-section point profile is at least one member long and always has a centroid of zero. For example, a 10 m wide link would have an effective width of 16 m and a zone D lateral profile of [–7.5, -2.5, 2.5, 7.5]. See Figures 6-3 and 6-4 for a pictorial representation of the lateral spacing for these two link examples.

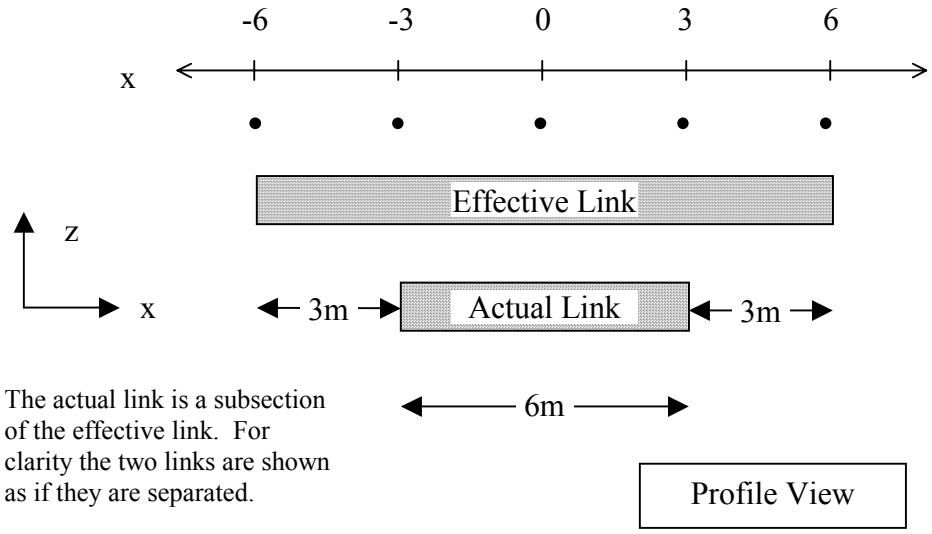

Figure 6-3. UCD 2001 lateral point spacing for a 6 m link in Zone C (3 m point spacing).

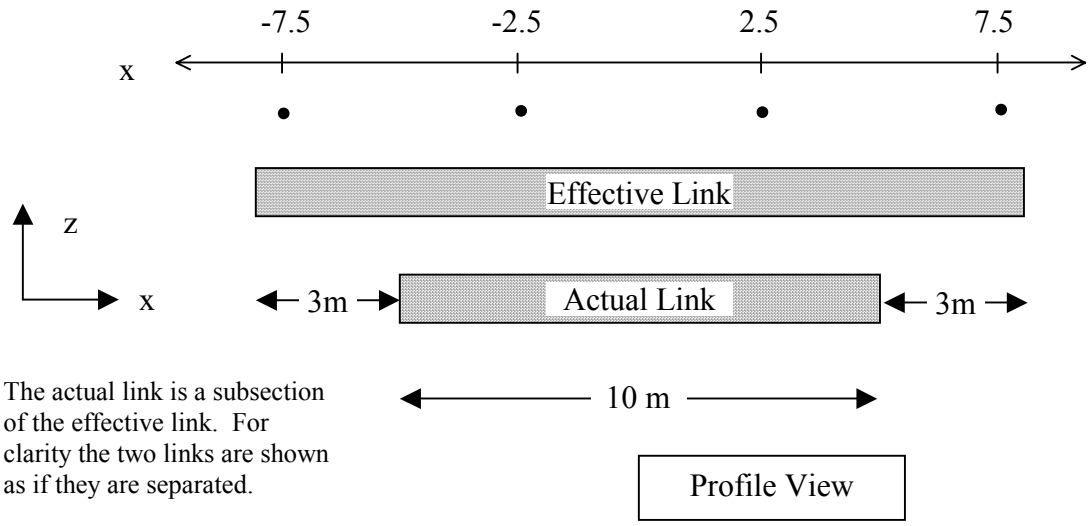

Figure 6-4. UCD 2001 lateral point spacing for a 10 m link in Zone D (5 m point spacing).

Fetch point profiles are also linear and span the length of a sub-link element. The fetch spacing for any particular sub-link may be modified so that the point profile endpoints are coincident with the sub-link endpoints. For instance, if a zone D sub-link had one endpoint at y = 100 m and the other endpoint at y = 850, the fetch point profile based on a 100.0 m spacing from Table 6-4 would be [125, 225, 325, 425, 525, 625, 725, 825] with a total of 8 points. To ensure that emissions from sub-link intersections are smooth, it is preferable to have fetch point profiles endpoints coincident with the sub-link endpoints. For this example, the spacing would be changed from 100.0 m to 93.75 m, resulting in a profile of [100, 193.75, 287.5, 381.25, 475, 568.75, 662.5,756.25, 850] with a total of 9 points as shown in Figure 6-5.

Left side. 9 points are placed based on a spacing of 93.75 m so that the end points are on the sub-link end points.

Right side. 8 points are placed based on a spacing of 100 m and are centered on the sub-link.

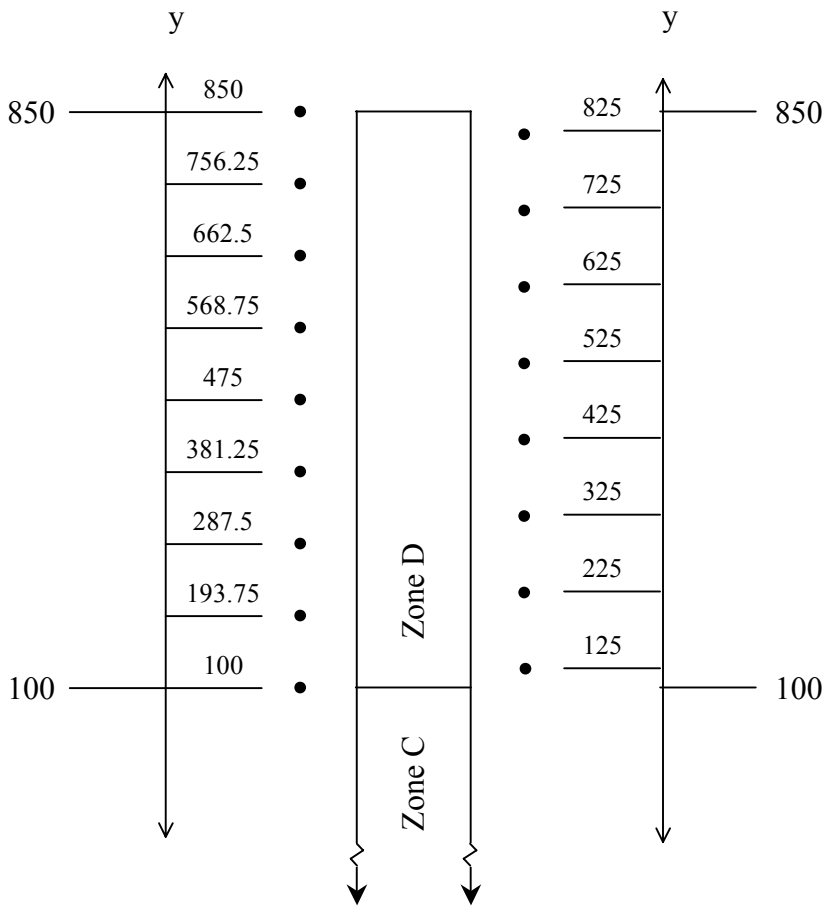

Figure 6-5. UCD 2001 fetch point spacing for a 750 m sub-link in Zone D (100 m point spacing). The UCD 2001 model will internally represent a link as shown on the left hand side to ensure that the end points are coincident with the end points of the sub-link.

Highway Link Point Source Emission Factors

The formula used to determine the emission factor of each point source is presented as Equation 6-1, its derivation is outlined in this section.

$$P_{EF} = \frac{L_{EF} \times \overline{S}_F}{L_{xz}} \quad (6\text{-}1)$$

Where:

P_{EF} is the single point emission factor [mass/time]
L_{EF} is the link emission factor [mass/time-length]
$\overline{S}_F$ is the average fetch spacing for a x-z lamina plane [length]
L_{xz} is the total number of points in a x-z lamina plane [unitless]

One can conceptualize the highway point placement as a series of point laminas oriented in the x-z plane spaced along the fetch (or y) link axis as shown in Figure 6-6. The total emission rate for each lamina is the product of the length of the sub-element the lamina represents and the highway-link emission factor. For a lamina that is not on the border of two zones, each lamina represents a length of roadway equal to the fetch spacing of the zone. For laminas placed on the border of two zones, each lamina represents the average of the two zones' spacings. The emissions from a single lamina at the end of a link are equal to the emissions from one half the link spacing of the zone that terminates the link.

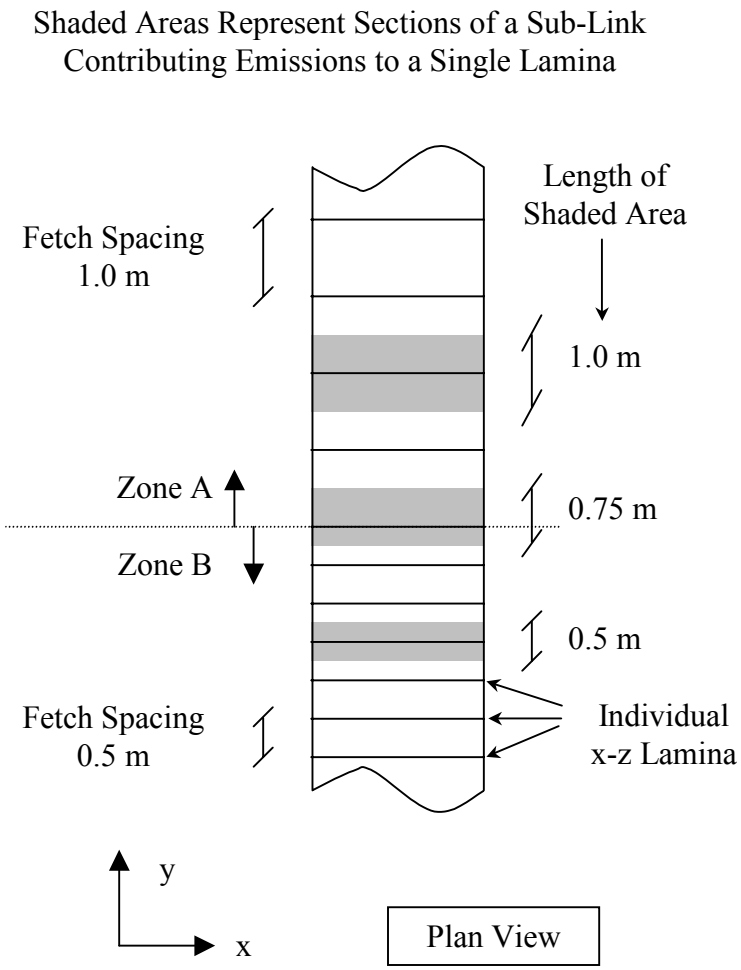

Figure 6-6. Relationship between fetch spacing and x-z lamina emissions for a UCD 2001 highway link.

The number of points in each highway link x-z lamina is the product of the size of the vertical and lateral point spacing profiles. For example, a zone B representation of a 3 m wide link would have a vertical spacing profile of [0.0, 0.5, 1.0, 1.5, 2.0, 2.5] and a lateral profile of [-4.5, -3.5, -2.5, -1.5, -0.5, 0.5, 1.5, 2.5, 3.5, 4.5]. A single x-z lamina is composed of 60 (6*10) points and is depicted in Figure 6-7. Since the UCD 2001 model assumes uniform mixing above the roadway, the emission factor for each point in a single x-z lamina is identical. Thus, the emission factor for each point source is the total emissions for a single lamina divided by the total number of points in each lamina.

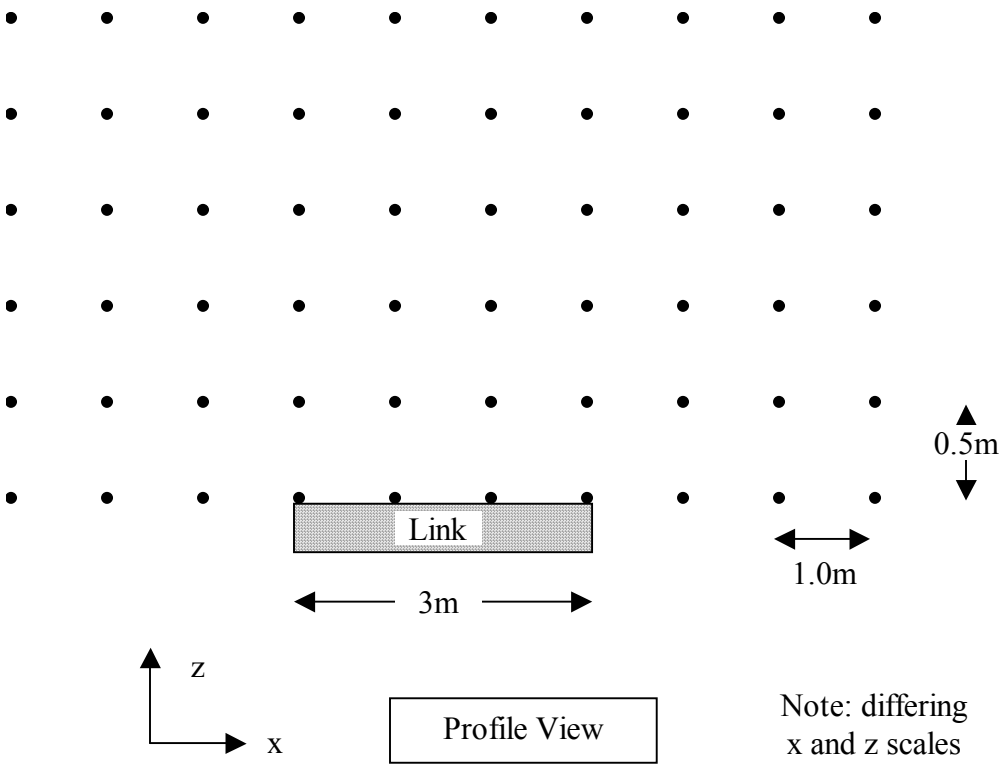

Figure 6-7. UCD 2001 zone B point source locations for a highway link with a 3 m traveled way.

Huang Dispersion Equation Coordinate System Requirements

The UCD 2001 model uses the Huang point source dispersion equation to estimate pollutant concentrations downwind of a continuous point source. This equation was presented in Chapter 2 and is restated as Equation 6-2 below for convenience. To evaluate Equation 6-2, five normalized coordinate lengths (x, y, y_s, z, and z_s) and a number of dispersion parameters must be specified. In this section, the determination of normalized coordinates will be discussed. The determination of dispersion parameters is discussed in the following chapter.

$$\overline{C} = \frac{Q}{\sigma_y \sqrt{2\pi}} \exp\left[-\frac{(y-y_s)^2}{2\sigma_y^2} \right] \frac{(zz_s)^{\left(\frac{1-n}{2}\right)}}{xb\alpha} \exp\left[-\frac{a\left(z^\alpha + z_s^\alpha\right)}{xb\alpha^2} \right] I_{-v}\left[\frac{2a(zz_s)^{\frac{\alpha}{2}}}{xb\alpha^2} \right] \qquad (6\text{-}2)$$

The coordinate system in Equation 6-2 requires that the average wind direction is aligned with the x-axis and that the point source is at x=0. The coordinate transformation required to convert receptor and point source coordinates to a form consistent with Equation 6-2 is graphically depicted in Figure 6-8 and described in Table 6-5.

Table 6-5. An outline of steps used by the UCD 2001 model to determine Huang dispersion parameters x, y, y_s, z, and z_s based on receptor location, point location, and wind direction.

1) Translate the Cartesian coordinate system so that the point source is on the plane defined by x=0, y=0. For instance if a point source is at coordinate (A, B, C) and the receptor is at coordinate (D, E, F) their new locations would be (0, 0, C) and (D-A, E-B, C), respectively.
2) Rotate the coordinate system so that the wind direction is aligned with the negative x-axis. Note: wind direction is the direction that the wind is blowing from.
3) After the coordinate transformation, y_s is zero, z_s is the elevation of the point source (which is C in the example above) and the coordinates of the receptor can be used as x, y, z in Equation 6-2.

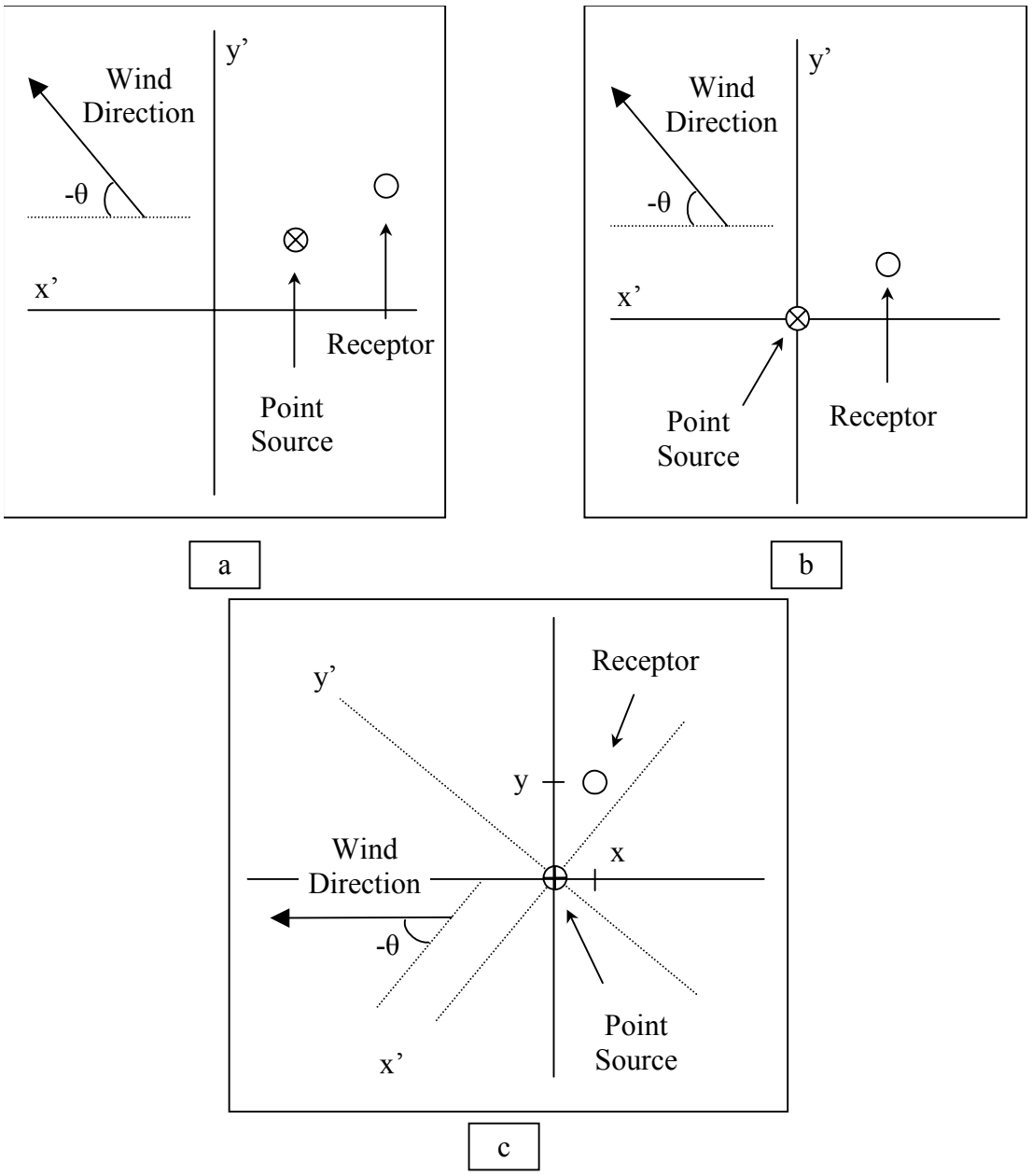

Figure 6-8. UCD 2001 coordinate rotation and translation scheme to determine Huang dispersion equation coordinates based on wind direction and receptor and point source locations. Pane (a) shows the actual point and receptor coordinates. Pane (b) is a new coordinate system with the point source located at x and y=0. Pane (c) is a new coordinate system where the wind direction is parallel with the x axis. In the pane (c) system, the x and y receptor coordinates correspond with fetch and off center-line distances for use in a dispersion equation.

Selection of CALINE and UCD 2001 Dispersion Model Parameters for the GM Database

To enable both the calibration and evaluation of the UCD 2001 model with the same database, the GM SF_6 tracer data set was split into two separate groups of measurements. The first group was used to empirically determine the parameters necessary to evaluate the Huang dispersion equation. The second group was used to evaluate model performance on an independent data set. In this chapter, the selection criteria for the Huang parameters and an evaluation of these terms will be presented. A complete analysis of modeled versus predicted SF_6 concentrations for both the UCD and CALINE models will be presented in the following chapter.

Model Input Data

The link and receptor locations used for CALINE and UCD 2001 simulations are depicted in Figure 4-4. The GM site was represented as two links oriented north-south, each with a width of 6.8 m. The UCD 2001 model internally adds 3 m to the side of each link whereas the link width had to be directly entered as 12.8 m into the CALINE input files. Each link extends 2500 m in each direction away from the sampling site to simulate an infinite link. The receptor coordinates are the SF_6 sampling port locations listed in Tables 4-4 and 4-5. Based on personal communication with Paul Benson, the developer of the CALINE models, it was determined that a roughness length of 250 cm and a representative wind speed elevation of 4.5 m were used to calibrate the CALINE models. Benson also made available his stability class determination, along with additional meteorological estimates, for each time period. It is assumed that the CALINE models will have the best performance when the input parameters are identical to their calibration values.

Both the CALINE3 and CALINE4 model user manuals indicate that a surface roughness between 3 and 400 cm should be used. Benson notes that z_0 should be within "the reasonable limits of power law approximation" (Benson 1979), or "15% of average canopy height"(Benson 1984). Chock, one of the principal investigators in the GM study, determined the surface roughness to be 3 cm for the GM study (Chock 1977b). Benson employed a canopy height estimate of 250 cm in calibrating his model. The

exact reason is unknown, but perhaps this was done to incorporate the presence of moving vehicles. However, since the CALINE user manuals indicate that the lowest recommended surface roughness was 3 cm, it is not clear whether one should use the measured, or pseudo surface roughness for a GM simulation. To avoid arbitrarily selecting a single surface roughness, the measured surface roughness and the CALINE calibration surface roughness are both evaluated.

Nominal GM Receptor Coordinates

The location of each sampling tower and the nominal elevation of each SF_6 sampling port are depicted in Figure 6-9. In this figure, each sampling port is assigned a receptor ID. The relative positioning of each receptor in this figure is geometrically similar to plots presented in this chapter and to data presented in the Appendix.

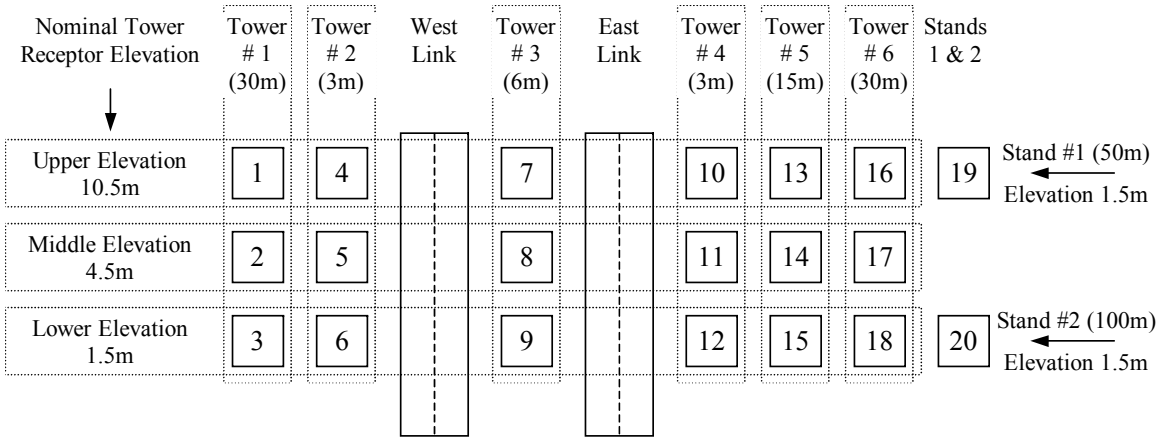

Note: if the receptor locations are referred to as normalized and the wind is from the east, the concentration data will be manipulated for certain figures so that wind is effectively from the west. To accomplish this normalization, stand 1, stand 2, and tower #5 concentrations are disregarded because they have no downwind equivalent. In addition, concentration data from towers #2 will be exchanged with tower #4, and tower #1 data will be exchanged with tower #6.

Figure 6-9. GM receptor location nomenclature. Each numbered box represents a receptor location and ID. Numbers in parenthesis are the nominal distance from a tower or stand to the edge of the nearest traveled way. Several figures in this chapter are oriented geometrically similar to the location of the receptor ID's shown in this figure.

Splitting the GM Data into Representative Sub-groups

The GM data set is comprised of 62, 30-minute sampling periods with reliable tracer and accompanying meteorological data. SF_6 concentrations were recorded at 20 fixed sampling ports for each time period. A valid SF_6 concentration was not reported for receptor 8 at time period 274153956, receptor 14 at time period 294083502, and receptor 10 at time period 296083459. Thus, the entire GM data set is comprised of 1237 SF_6 data points.

A summary of the meteorological conditions for each of the time periods was presented previously in Table 4-8. The 62 sampling runs were conducted on 16 separate days. On each sampling day except day 293, four 30-minute sampling runs were conducted over a 2-hour continuous time period. On day 293, only two 30-minute sampling runs were collected.

The 62 sample data set was parsed into two 31-member groups. Group 1 is comprised of the time periods in Table 4-8 with an odd index key and group 2 is populated with even key time periods. This method of data parsing ensures that each group contains one half of the sample periods from any given day. Meteorological conditions varied more significantly from day to day than from period to period over any given day. Thus, the grouping method results in meteorologically similar datasets.

It is also convenient to define two additional groupings of the GM dataset. Group 4 contains all 62 sample periods and group 3 is a 61 sample period sub-set of group 4 that excludes time period 295093958. The 4.5 m elevation wind speed and heading during time period 295093958 was 0.35 m/s and 8, respectively. The CALINE models severely overpredict SF_6 concentrations for this low, near-parallel wind speed event resulting in overestimations of 600% or more for certain receptors. The group 3 sample period allows one to evaluate both CALINE and UCD 2001 performance without considering this time period. It should be noted that the 295093958 time period has an odd time key and is therefore in the Group 1 data set as well. A summary of GM data groupings are presented in Table 6-6.

Table 6-6. GM dataset groupings used for dispersion model analysis.

Group Identifier	Group Description
Group 1	One-half of the GM dataset based on selecting the odd key values from Table 4-8. This group contains 31 30-minute sample periods.
Group 2	One-half of the GM dataset based on selecting the even key values from Table 4-8. This group contains 31 30-minute sample periods.
Group 3	All sample periods excluding time period 295093958. This group contains 61 30-minute sample periods.
Group 4	The full 62 member GM dataset.

Evaluation of UCD 2001 Dispersion Parameters

The Huang point source equation and supporting parameterizations are reproduced below for convenience. For greater clarity and consistency with the variable names in the UCD 2001 code, the restated equations have been slightly modified so that each symbol used to represent a parameter is unique. To numerically evaluate the Huang dispersion equation, estimates of the parameters a, b, c, d, e, n, p must be specified. Although it would be possible to empirically determine all seven Huang dispersion parameters based on the GM database, using dispersion parameters estimates from differing data sets is a more robust and unbiased approach to calibrating the UCD 2001 model. Note: the UCD 2001 model uses the MKS system for most measurements include the dispersion parameters.

$$\sigma_y = c + dx^e \tag{6-3}$$

$$K_z = bz^n \tag{6-4}$$

$$u = az^p \tag{6-5}$$

Consistent with literature findings, it is assumed that the meteorological fields downwind of the roadway are neutrally stratified. The Brookhaven National Laboratories

(BNL) estimate lateral standard deviation parameters for neutral stability to be 0.32 * $x^{0.78}$ (BNL as cited in (Huang 1979)). HIGHWAY, an EPA roadway dispersion model, estimates the initial lateral dispersion to be 3.0 m (Zimmerman and Thompson 1975). Based on these estimates the Huang parameters c, d, and e should be 3.0, 0.32, and 0.78 respectively.

A typical estimate of the wind profile power law exponent 'p', for neutral stability, is 0.25 (EPA 1995). The parameter 'a' is uniquely defined if the wind speed at an arbitrary elevation is known. Since UCD 2001 requires the specification of wind speed and direction at a reference elevation, parameter 'a' is determined at run-time. For calibration of the UCD 2001 model with the GM dataset the 4.5m wind speed was used. A variety of methods to estimate the eddy diffusivity parameters 'b' and 'n' appear in the literature. As discussed in Chapter 2, for neutral stability one could assume 'n' to be unity and 'b' to be u^*.

A preliminary study to determine how well the parameter estimation scheme listed above agreed with the GM data set was conducted. Results of this study suggested that all parameters based on existing literature showed good agreement with the dataset except the vertical eddy diffusivity constants. Approximately five thousand differing schemes to estimate 'b' and 'n' were considered and evaluated with the UCD 2001 model. In these simulations, both 'b' and 'n' were allowed to be functions of meteorological variables such as wind speed and the cross-link component of wind speed. Based on this analysis, it was determined that 'b' and 'n' should be assigned values of 0.28 and 0.81, respectively. Notice that 'b' and 'n' are not functions of ambient meteorological conditions, suggesting that the eddy diffusion downwind of a roadway is a function of roadway activity and not of ambient meteorology.

Although model performance could be enhanced by selecting more elaborate parameter estimation schemes, the simplistic approach used by the UCD 2001 model enhances model robustness and results in a more predictable response between model input and concentration estimates. An evaluation of UCD 2001 model performance for this parameter set will be presented in the following chapter.

Chapter 7. Evaluation of CALINE3, CALINE4, and the UCD 2001 Model Performance Using the GM SF_6 Tracer Database

Introduction

An evaluation of the UCD 2001, CALINE3, and CALINE4 models' ability to simulate the GM SF_6 database is presented in this chapter. The UCD 2001 model used one-half of the GM dataset for calibration (group 1) and used the remaining half of the dataset to evaluate model performance. The CALINE models were calibrated with the entire GM dataset.

This chapter introduces an error metric, based on the sum of squared difference between observed and predicted SF_6 concentrations, to evaluate both CALINE and UCD performance. This error metric is applied to all four data groupings allowing for side-by-side comparison of model performance with differing datasets.

Model Error and Perturbation Error Metrics

A variety of metrics to evaluate dispersion model error is available. For this analysis, error is defined as the squared difference between a single modeled and observed data point. Error for a group of data points is the simple arithmetic sum of the error associated with each single data point as shown in Equation 7-1. This 'squared-residual' approach was used because it weights higher concentration data points as more important than the low concentration data points. This in effect weights the near field concentration estimates as more significant than far field measurements. Given that near field estimates have more regulatory significance than far-field estimates for microscale modeling, the squared-residual approach is a natural and intuitive error metric for this data set.

$$E = \sum_{i}^{n} (O_i - P_i)^2 \qquad (7\text{-}1)$$

Where:

E is the error between an observed data set and one predicted by a dispersion model.
i is an index of a data point in a data set
n is the total number of points in a data set
O is observed dataset
P is the predicted dataset

For comparative purposes, it is convenient to determine the error between an observed dataset and a modified version of itself. Perturbed error (PE) is presented in Equation 7-2 and is defined as the sum of the squared residuals between an observed data set and a data set arrived at by increasing each member of the observed data by a certain percentage. For example, consider an observed data set γ comprised of only three members 10, 20, and 30. If we increase each member by 20% (i.e. $\alpha = 20$) we can arrive at a new three member data set λ with members 12, 24, and 36. The perturbed error for this example set is 56 ($[12-10]^2 + [24-20]^2 + [36-30]^2$).

If one compared observed concentrations that were taken over different time intervals, but downwind of a atmospheric boundary layer tracer release with similar meteorological conditions, there would still be variations in the observed data due to the stochastic nature of turbulent transport as discussed by Rao below.

> "[Since dispersion] models predict the ensemble means whereas any given observation reflects a single realization or an event from a population, it should be recognized that the model predictions will almost always differ from the corresponding observations, even if the models and the input data for the models are perfect. The bootstrap re-sampling procedure is used to quantify the variability in the observed concentrations due to the stochastic nature of the atmosphere. The results suggest that the variability in the observations due to the random nature of the atmosphere is about 30%. Therefore, if the predicted values are within 30% of the measured concentrations, the difference between model predictions and observations should not be considered to be significant. Thus a 'perfect' air quality model should predict to within 30 % of its corresponding observed concentrations."

The perturbed error index provides a method to relate naturally expected error with the error in dispersion model estimates. Given that two different observed data sets can naturally vary by 30% for similar meteorological conditions, it is unlikely that a predicted dataset can have an error less than a PE_{30}.

$$PE_{\alpha} = \sum_{i}^{n} \left\{ (1 + \frac{\alpha}{100}) \times O_i - O_i \right\}^2 \qquad (7\text{-}2)$$

Where:

PE is the error between an observed data set and a dataset arrived at by increasing each member of the observed data by a the percentage α.
α a percentage increase in the observed data set
i is an index of the data point in a data set
n is the total number of point in the data set
O is observed dataset

UCD 2001 and CALINE Model Performance Evaluation

Dispersion model performance is examined in this section with a variety of methods. First, model error tables based on the sum of the squared residual method are presented. This section is followed by an analysis of observed versus predicted scatter plots and histograms for each dispersion model. Third, each model's ability to reproduce the 40 highest observed concentrations is analyzed. Lastly, a decoupled analysis comparing observed and predicted concentrations ranked by magnitude, rather than by time and receptor locations, is outlined.

In addition to the analysis presented in this section, model predictions for each time period are presented in appendices A through E. The appendices are presented in tabular format and include descriptive statistics in addition to the raw predicted and observed data points.

Determination of Dispersion Model Error and Associated Perturbation Error Index for all four GM Dataset Groupings

Based on Equation 7-1, the model errors associated with UCD 2001 and CALINE simulations of the GM dataset are presented in Table 7-1. Tables 7-2, 7-3, 7-4, and 7-5 compare the inter-model error for each GM grouping. Figures 7-2 and 7-1 plot dispersion model error and PE as a function of α for both the group 3 and group 4 datasets. In these figures, the PE α that results in the same error as a model estimate is highlighted. Note: error calculations were based on the parts per trillion (ppt) SF_6 measurements.

Table 7-1. Comparison of UCD 2001 and CALINE model performance based on the GM SF6 database.

Model	Error, Sum of Squared Residuals (in millions)			
Group	1	2	3	4
Number of 30-minute Samples	31	31	61	62
CALINE3, z_0= 250 cm	863	154	242	1,017
CALINE3, z_0= 3 cm	1,085	268	418	1,353
CALINE4, z_0= 250 cm	677	122	190	800
CALINE4, z_0= 3 cm	868	199	308	1,068
UCD 2001	88	92	158	180

Table 7-2. Inter-model comparison of performance for group 1 of the GM dataset.

		Ratio of Model A to Model B Error (A/B) * 100%				
Model A Below ↓	Model B Right→	CALINE3 z_0(250cm)	CALINE3 z_0(3cm)	CALINE4 z_0(250cm)	CALINE4 z_0(3cm)	UCD 2001
	Error ↓→	863	1,085	677	868	88
CALINE3 z_0(250cm)	863	100%	80%	127%	99%	976%
CALINE3 z_0(3cm)	1,085	126%	100%	160%	125%	1228%
CALINE4 z_0(250cm)	677	78%	62%	100%	78%	766%
CALINE4 z_0(3cm)	868	101%	80%	128%	100%	982%
UCD 2001	88	10%	8%	13%	10%	100%

Table 7-3. Inter-model comparison of performance for group 2 of the GM dataset.

		Ratio of Model A to Model B Error (A/B) * 100%				
Model A Below ↓	Model B Right→	CALINE3 z_0(250cm)	CALINE3 z_0(3cm)	CALINE4 z_0(250cm)	CALINE4 z_0(3cm)	UCD 2001
	Error ↓→	154	268	122	199	92
CALINE3 z_0(250cm)	154	100%	58%	126%	77%	168%
CALINE3 z_0(3cm)	268	173%	100%	218%	134%	292%
CALINE4 z_0(250cm)	122	79%	46%	100%	61%	134%
CALINE4 z_0(3cm)	199	129%	75%	163%	100%	218%
UCD 2001	92	59%	34%	75%	46%	100%

Table 7-4. Inter-model comparison of performance for group 3 of the GM dataset.

		Ratio of Model A to Model B Error (A/B) * 100%				
Model A Below ↓	Model B Right→	CALINE3 z_0(250cm)	CALINE3 z_0(3cm)	CALINE4 z_0(250cm)	CALINE4 z_0(3cm)	UCD 2001
	Error ↓→	242	418	190	308	158
CALINE3 z_0(250cm)	242	100%	58%	128%	79%	154%
CALINE3 z_0(3cm)	418	173%	100%	220%	136%	265%
CALINE4 z_0(250cm)	190	78%	45%	100%	62%	121%
CALINE4 z_0(3cm)	308	127%	74%	162%	100%	195%
UCD 2001	158	65%	38%	83%	51%	100%

Table 7-5. Inter-model comparison of performance for group 4 of the GM dataset.

		Ratio of Model A to Model B Error (A/B) * 100%				
Model A Below ↓	Model B Right→	CALINE3 z_0(250cm)	CALINE3 z_0(3cm)	CALINE4 z_0(250cm)	CALINE4 z_0(3cm)	UCD 2001
CALINE3 z_0(250cm)	1,017	100%	75%	127%	95%	565%
CALINE3 z_0(3cm)	1,353	133%	100%	169%	127%	752%
CALINE4 z_0(250cm)	800	79%	59%	100%	75%	444%
CALINE4 z_0(3cm)	1,068	105%	79%	134%	100%	593%
UCD 2001	180	18%	13%	23%	17%	100%

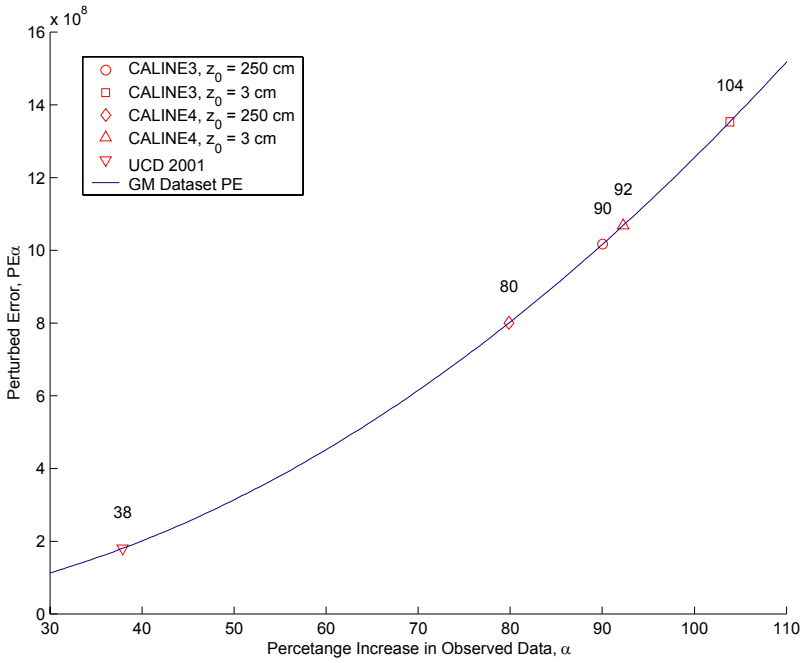

Figure 7-1. Plot of perturbed (PE) error versus α for the group 4 (total data set) GM dataset. Model error from the CALINE and UCD 2001 predictions are plotted on the GM PE curve so that model prediction error can be related to a PE index value.

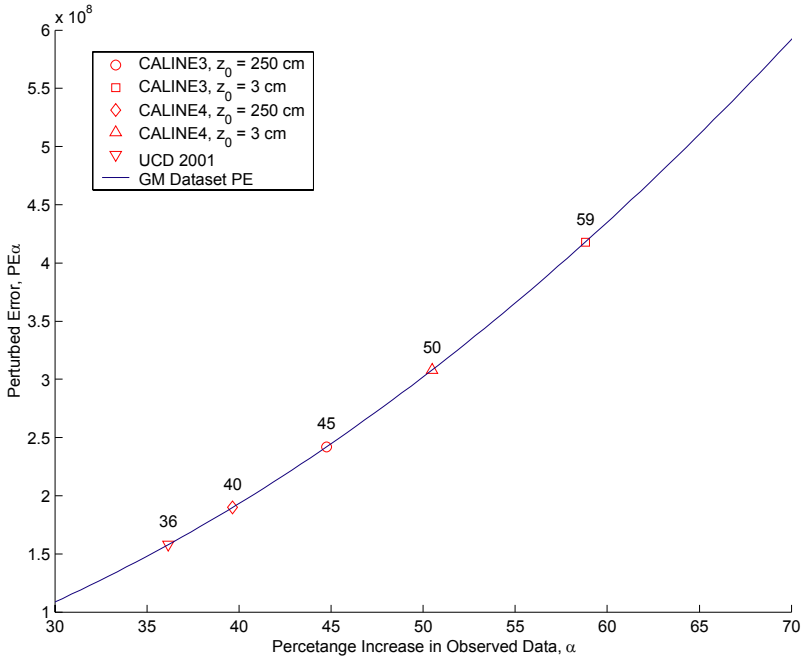

Figure 7-2. Plot of perturbed (PE) error versus α for the group 3 (total data set less sample 295093958) GM dataset. Model error from the CALINE and UCD 2001 predictions are plotted on the GM PE curve so that model prediction error can be related to a PE index value.

As indicated in Table 7-1, the UCD 2001 group 1 and group 2 errors (in millions) are 88 and 92 respectively. As previously mentioned, UCD 2001 parameter calibration was based on group 1 data, and group 2 data points were used to explore the efficacy of the UCD 2001 model to simulate an independent data-set. Since the UCD 2001 error for both group 1 and 2 were nearly identical, it suggests that the UCD 2001 model is effective in predicting pollutant concentrations for datasets other than the one used for calibration purposes.

The UCD 2001 error (in millions) is approximately 180, whereas the CALINE3 error was 1,353 (1,017) and the CALINE4 error was 1,068 (800). Certain CALINE performance indices are presented as two numbers, the first number is based on model simulations that use the measured surface roughness of 3 cm, the second number is in parenthesis and is based on a surface roughness of 250 cm. As shown in Figures 7-2, the α equivalents (i.e. the α corresponding to a perturbed error that is equal to a given modeled error) for the UCD 2001, CALINE3, and CALINE4 models are 38, 104 (90),

and 92 (80) respectively. The UCD 2001 α equivalent of 38 compares favorable with the theoretical α minimum of 30.

As shown in Table 7-5, the ratio of UCD 2001 to CALINE3 and CALINE4 group 4 error is 0.13 (0.18) and 0.17 (0.23), respectively. This corresponds to an error reduction of 87% (82%) and 83% (77%) when UCD 2001 is compared to CALINE3 and CALINE4, respectively. In other words, the UCD 2001 error is approximately one tenth to one fifth of the CALINE error, which corresponds to an error reduction of approximately 80 to 90 percent.

CALINE3, CALINE4, and UCD 2001 model predictions for time period 295093958 are presented in Figures 7-3, 7-4, and 7-5, respectively. The 4.5m wind speed for this time period was approximately 0.35 m/s and near parallel to the road. For this time period both CALINE3 and CALINE4 significantly over-predict pollutant concentrations, with overestimates exceeding 500% at several receptors. The UCD 2001 model also tended to over predict concentrations for this time period, however, the over-estimates were not as severe as their CALINE equivalents. Observed versus predicted scatter plots for time period 295093958 can be contrasted against those based on time period 274140958 where the 4.5m elevation wind speed was approximately 2.9 m/s with a heading of 291. UCD 2001 model predictions were near ideal during these time periods and give reference to the considerable scatter present in the 295093958 scatter plots. Time period 274140958 scatter plots for the UCD 2001, CALINE3, and CALINE4 models are presented as Figures 7-6, 7-7, and 7-8, respectively.

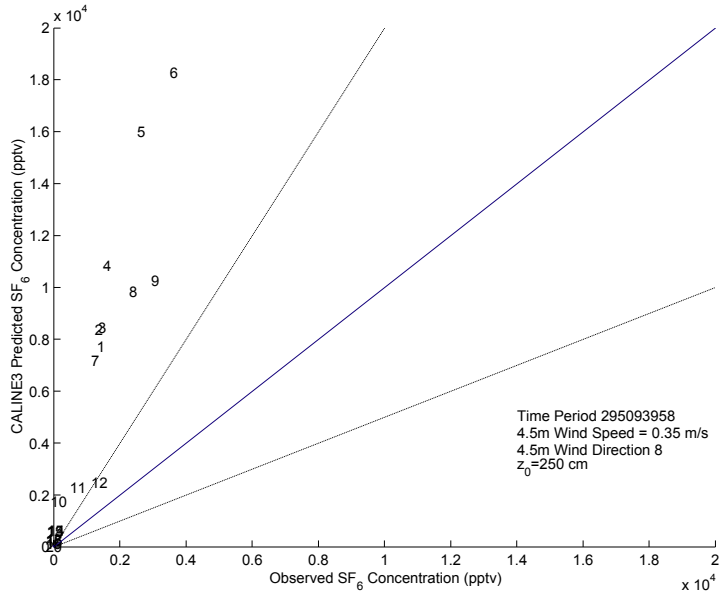

Figure 7-3. CALINE3 (z_0=250 cm) predicted versus observed SF_6 concentrations for time period 295093958. Each plot point corresponds to a receptor ID shown in Figure 6-9. The solid line is a 1:1 ratio and the dashed lines form an envelope between 1:2 and 2:1 ratios.

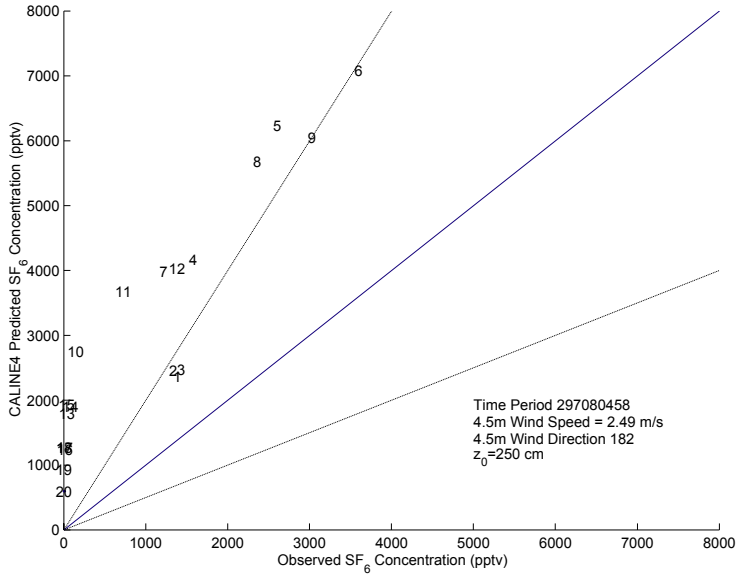

Figure 7-4. CALINE4 (z_0=250 cm) predicted versus observed SF_6 concentrations for time period 295093958. Each plot point corresponds to a receptor ID shown in Figure 6-9. The solid line is a 1:1 ratio and the dashed lines form an envelope between 1:2 and 2:1 ratios.

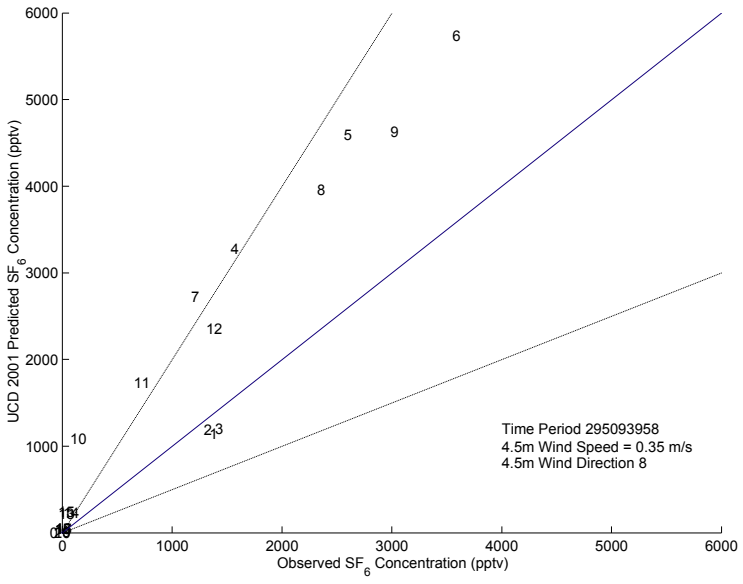

Figure 7-5. UCD 2001 predicted versus observed SF_6 concentrations for time period 295093958. Each plot point corresponds to a receptor ID shown in Figure 6-9. The solid line is a 1:1 ratio and the dashed lines form an envelope between 1:2 and 2:1 ratios.

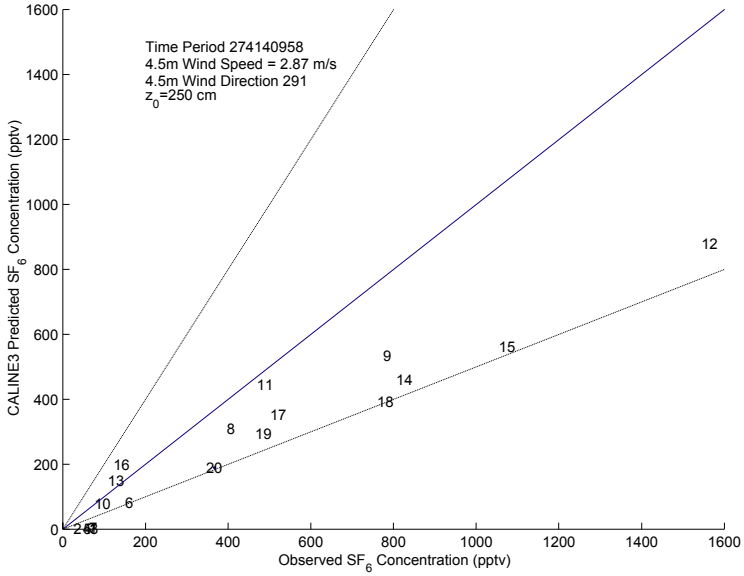

Figure 7-6. CALINE3 (z_0=250 cm) predicted versus observed SF_6 concentrations for time period 274140958. Each plot point corresponds to a receptor ID shown in Figure 6-9. The solid line is a 1:1 ratio and the dashed lines form an envelope between 1:2 and 2:1 ratios.

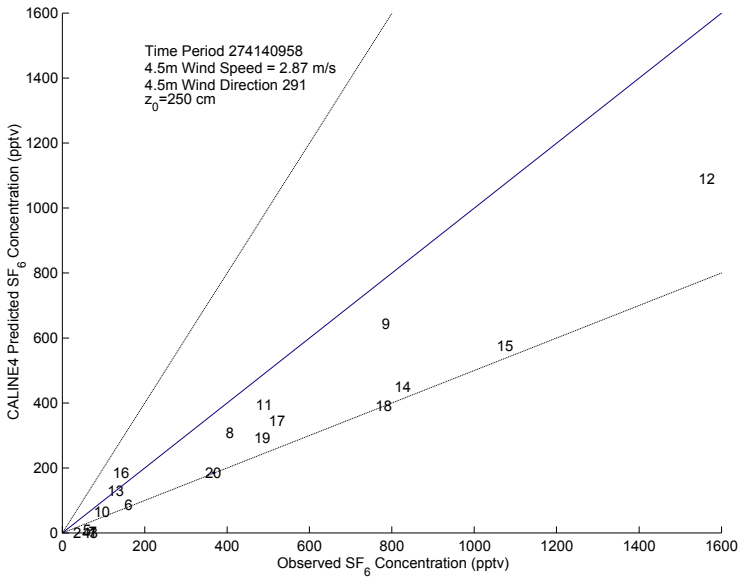

Figure 7-7. CALINE4 (z_0=250 cm) predicted versus observed SF_6 concentrations for time period 274140958. Each plot point corresponds to a receptor ID shown in Figure 6-9. The solid line is a 1:1 ratio and the dashed lines form an envelope between 1:2 and 2:1 ratios.

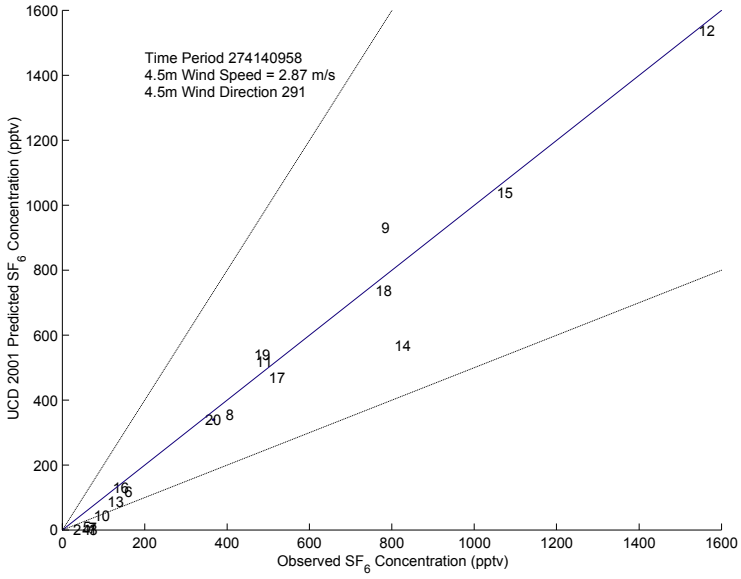

Figure 7-8. UCD 2001 predicted versus observed SF_6 concentrations for time period 274140958. Each plot point corresponds to a receptor ID shown in Figure 6-9. The solid line is a 1:1 ratio and the dashed lines form an envelope between 1:2 and 2:1 ratios.

If one only considers the group 3 data subset, the UCD 2001, CALINE3, and CALINE4 errors are 158, 418 (242), and 308 (190) , respectively. As shown in Figure 7-1, these error estimates have α equivalents of 36, 59 (45), and 50 (40), respectively. As indicated in Table 7-4, the ratio of UCD 2001 to CALINE3 and CALINE4 error is 0.38 (0.65) and 0.51 (0.83). Thus, even when time period 295093958 is excluded, the UCD 2001 significantly outperforms the CALINE series of model resulting in error reductions up to 62%.

Dispersion Model Scatter Plot and Histogram Analysis

The Equation 7-1 error residual method does not discriminate between positive and negative residuals. Therefore, a model may have a low error, but consistently under predict pollutant concentrations. To determine if the UCD 2001 and CALINE models tended to over or under predict, scatter plots and histograms were generated which isolate each receptor. The scatter plots appear in this thesis as Figures 7-9 through 7-13 and the histograms appear as 7-14 through 7-18. Each plot depicts the normalized receptor location described in Figure 6-9, which ensures that the left most receptor in the figure is upwind. Very low concentrations (less than 100 pptv) were not included in these figures because they distorted the histogram scales and made them difficult to interpret. Several of the time period 295093958 data points do not appear in the CALINE scatter plots because they exceed the figure's axis range.

The receptor with the highest concentration will most likely lead to a violation and is most significant for regulatory purposes. As expected, the tower approximately 3 m downwind and the median tower logged the highest observed SF_6 concentrations at the lowest sampling port (1.5m elevation). Predicted to observed histograms demonstrate that the UCD 2001 model tends to over predict downwind tower concentrations. The UCD 2001 model predictions result in 50 over predictions and only 12 under predictions at the 1.5m median tower. At the 3-m downwind tower there are 37 over predictions to 25 under predictions. Almost all of the 37 under predictions for these two receptors were in the 0.8 to 1.0 bin which indicates that most of the under predictions were within 20% of the observed concentrations. As shown in Figure 7-14, for the same two receptor locations, the CALINE3 model results in 90 under predictions and 34 over predictions.

Similarly, as shown in Figure 7-16, the CALINE4 model results in 91 under predictions and 33 over predictions. It should be noted that a significant portion of these under predictions were much less than 20% of the observed concentrations.

All three models tend to under predict pollutant concentrations upwind of the roadway. Inspection of the scatter plots shows that a large fraction of the predicted concentrations three meters upwind of the roadway were less than 50% of the observed SF6 concentration. However, given that upwind concentrations are significantly lower than downwind concentrations, the tendency for underestimation should have little regulatory significance.

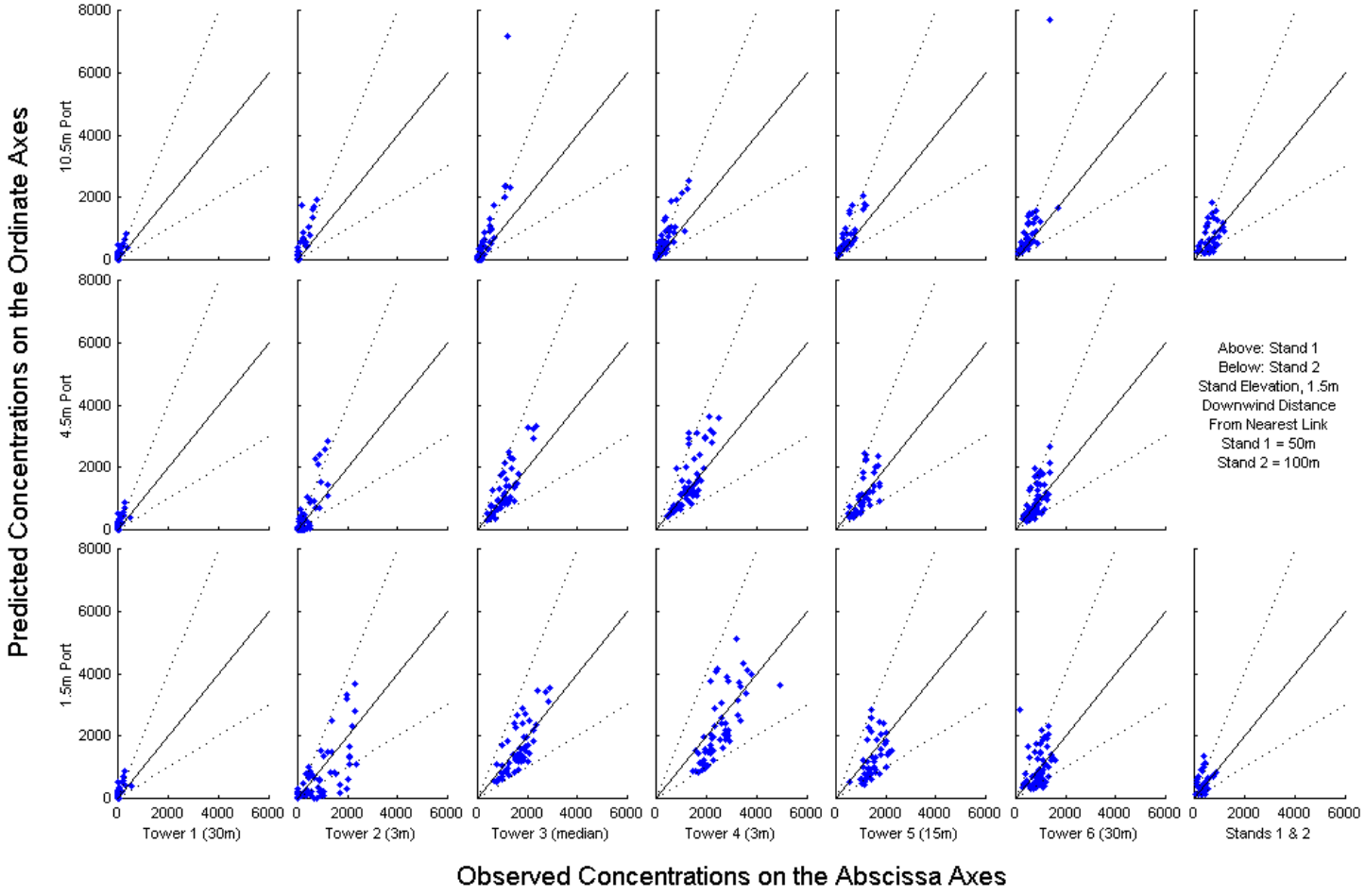

Figure 7-9. Scatter plots of CALINE3 (z_0=250 cm) predicted to observed concentrations ratios for each receptor location. SF_6 concentrations less than 100 pptv have been excluded. The solid line is a 1:1 ratio and the dashed lines form an envelope between 1:2 and 2:1 ratios. Each plot represents a single receptor using the normalized coordinate system described in Figure 6-9.

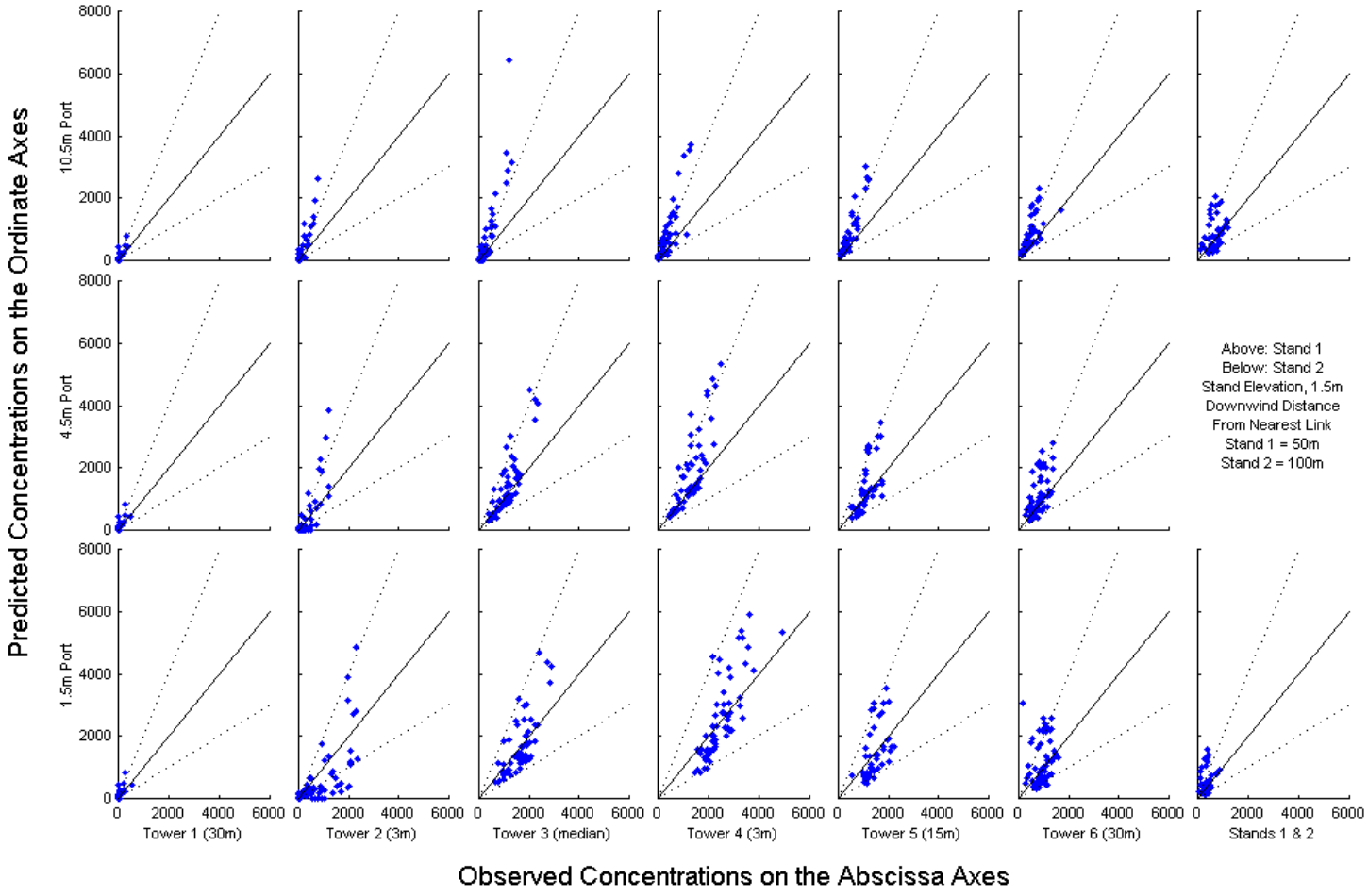

Figure 7-10. Scatter plots of CALINE3 (z_0=3 cm) predicted to observed concentrations ratios for each receptor location. SF_6 concentrations less than 100 pptv have been excluded. The solid line is a 1:1 ratio and the dashed lines form an envelope between 1:2 and 2:1 ratios. Each plot represents a single receptor using the normalized coordinate system described in Figure 6-9.

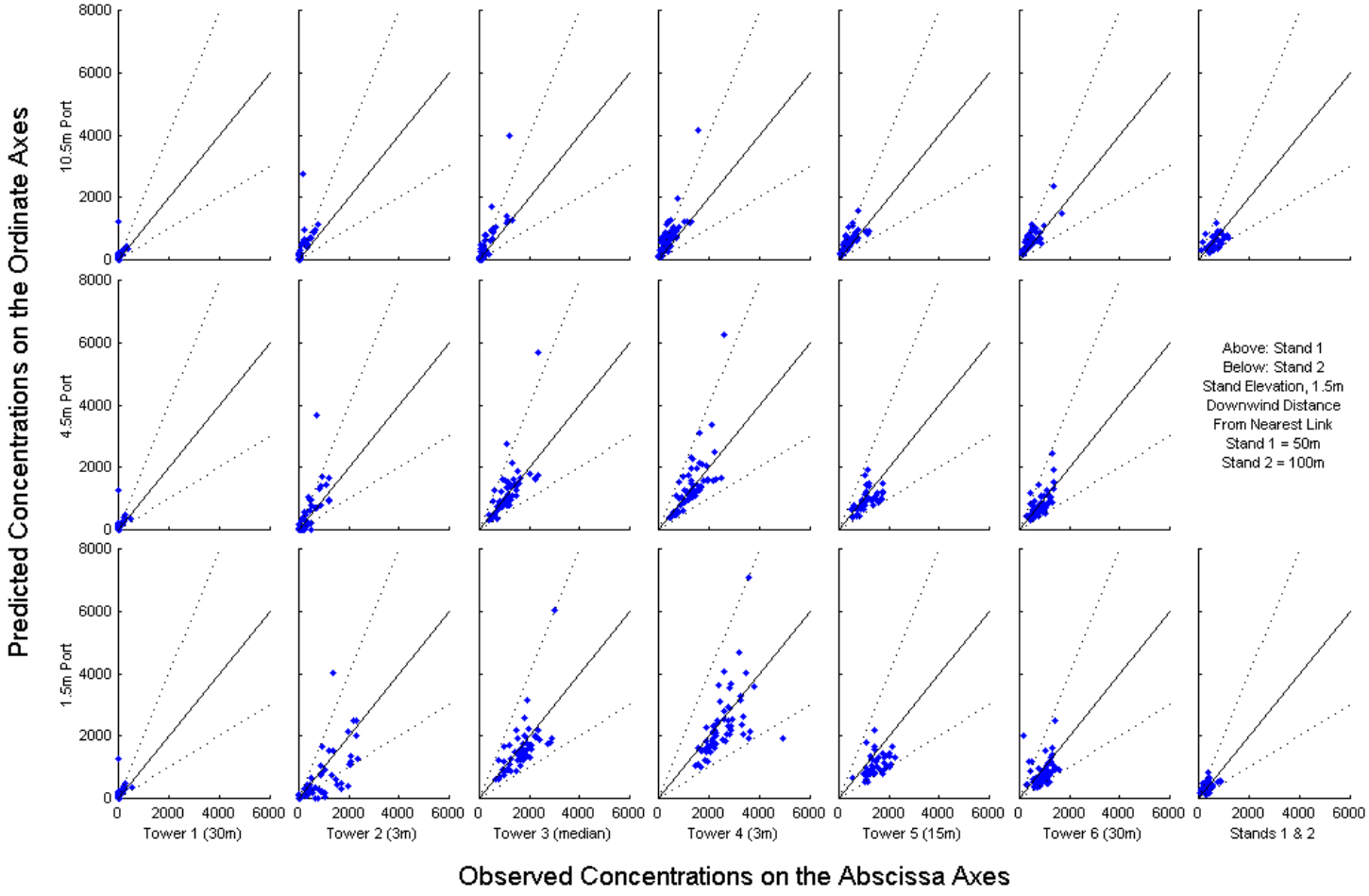

Figure 7-11. Scatter plots of CALINE4 (z_0=250 cm) predicted to observed concentrations ratios for each receptor location. SF_6 concentrations less than 100 pptv have been excluded. The solid line is a 1:1 ratio and the dashed lines form an envelope between 1:2 and 2:1 ratios. Each plot represents a single receptor using the normalized coordinate system described in Figure 6-9.

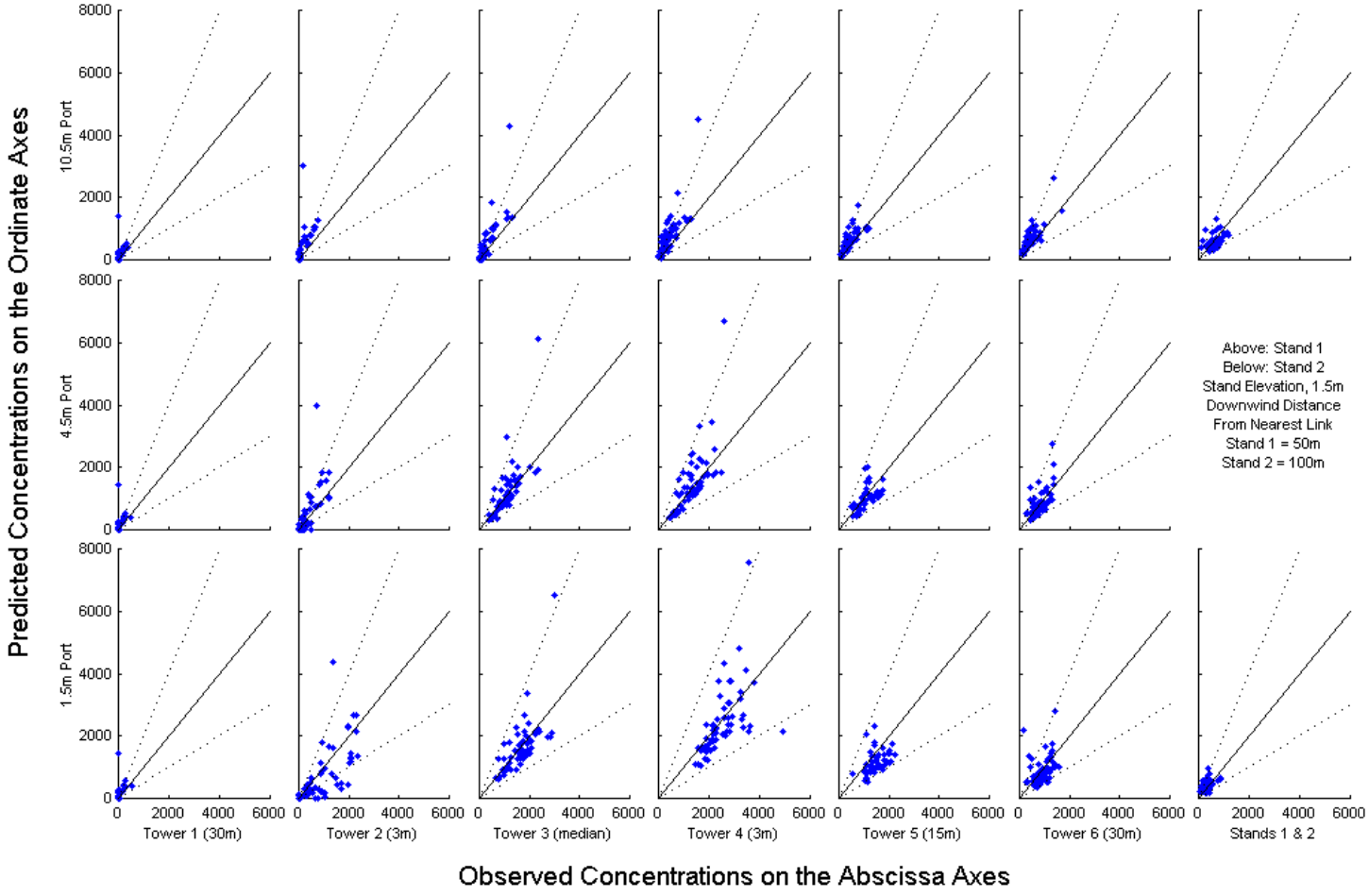

Figure 7-12. Scatter plots of CALINE4 (z_0=3 cm) predicted to observed concentrations ratios for each receptor location. SF_6 concentrations less than 100 pptv have been excluded. The solid line is a 1:1 ratio and the dashed lines form an envelope between 1:2 and 2:1 ratios. Each plot represents a single receptor using the normalized coordinate system described in Figure 6-9.

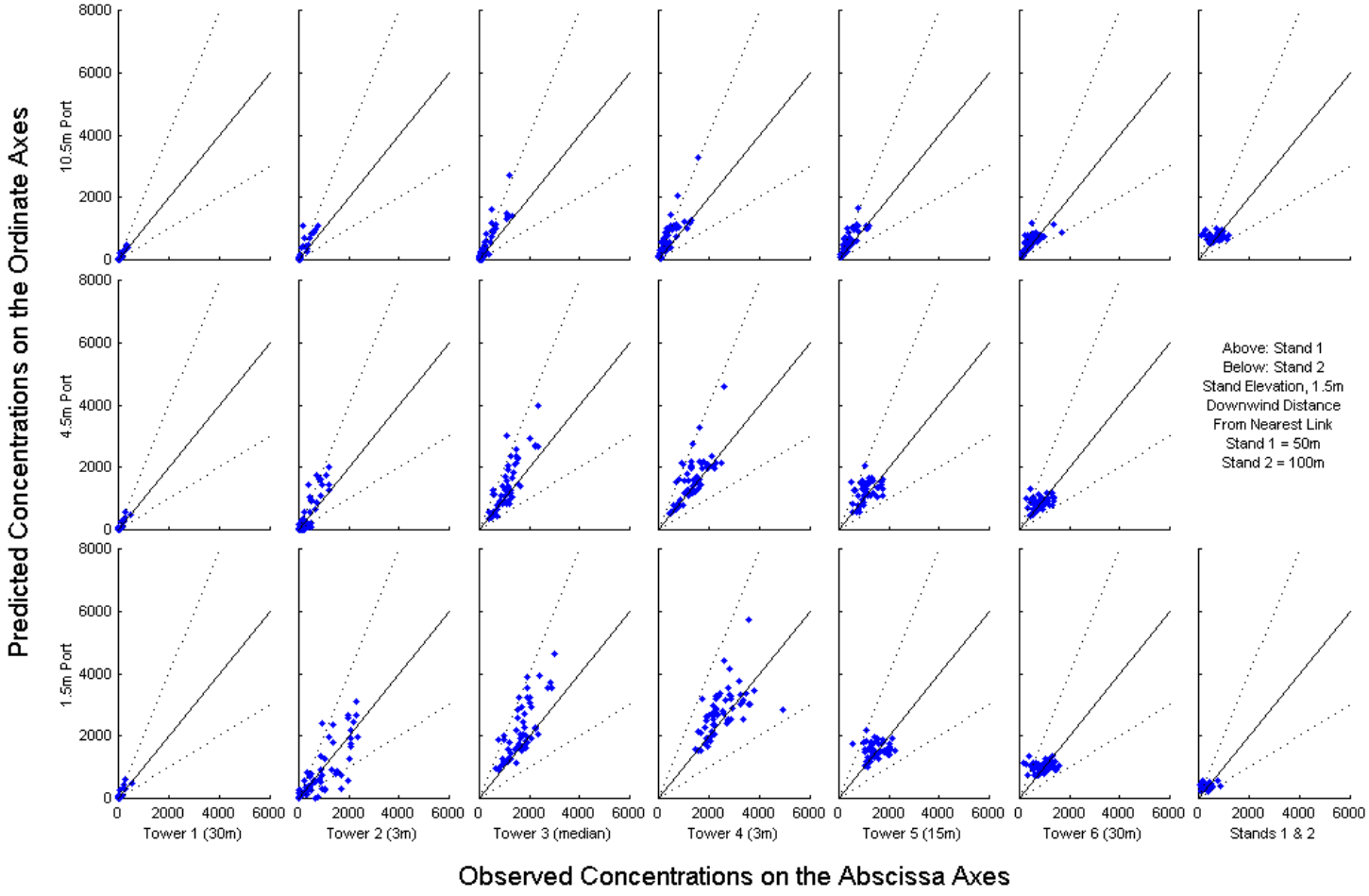

Figure 7-13. Scatter plots of UCD 2001 predicted to observed concentrations ratios for each receptor location. SF_6 concentrations less than 100 pptv have been excluded. The solid line is a 1:1 ratio and the dashed lines form an envelope between 1:2 and 2:1 ratios. Each plot represents a single receptor using the normalized coordinate system described in Figure 6-9.

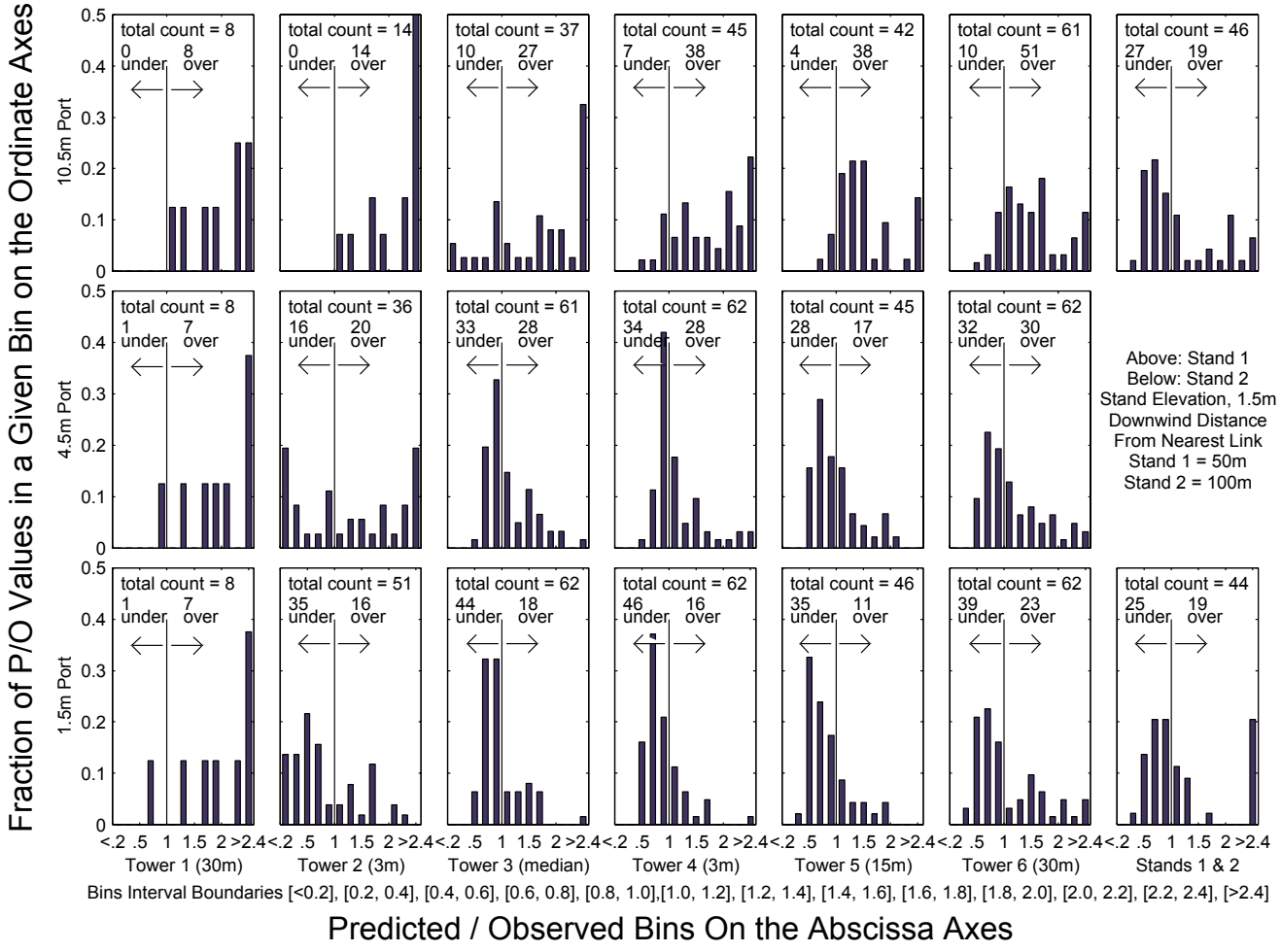

Figure 7-14. Histogram of CALINE3 (z_0=250 cm) predicted to observed concentrations ratios for each receptor location. SF_6 concentrations less than 100 pptv have been excluded. Each histogram represents a single receptor using the normalized coordinate system described in Figure 6-9.

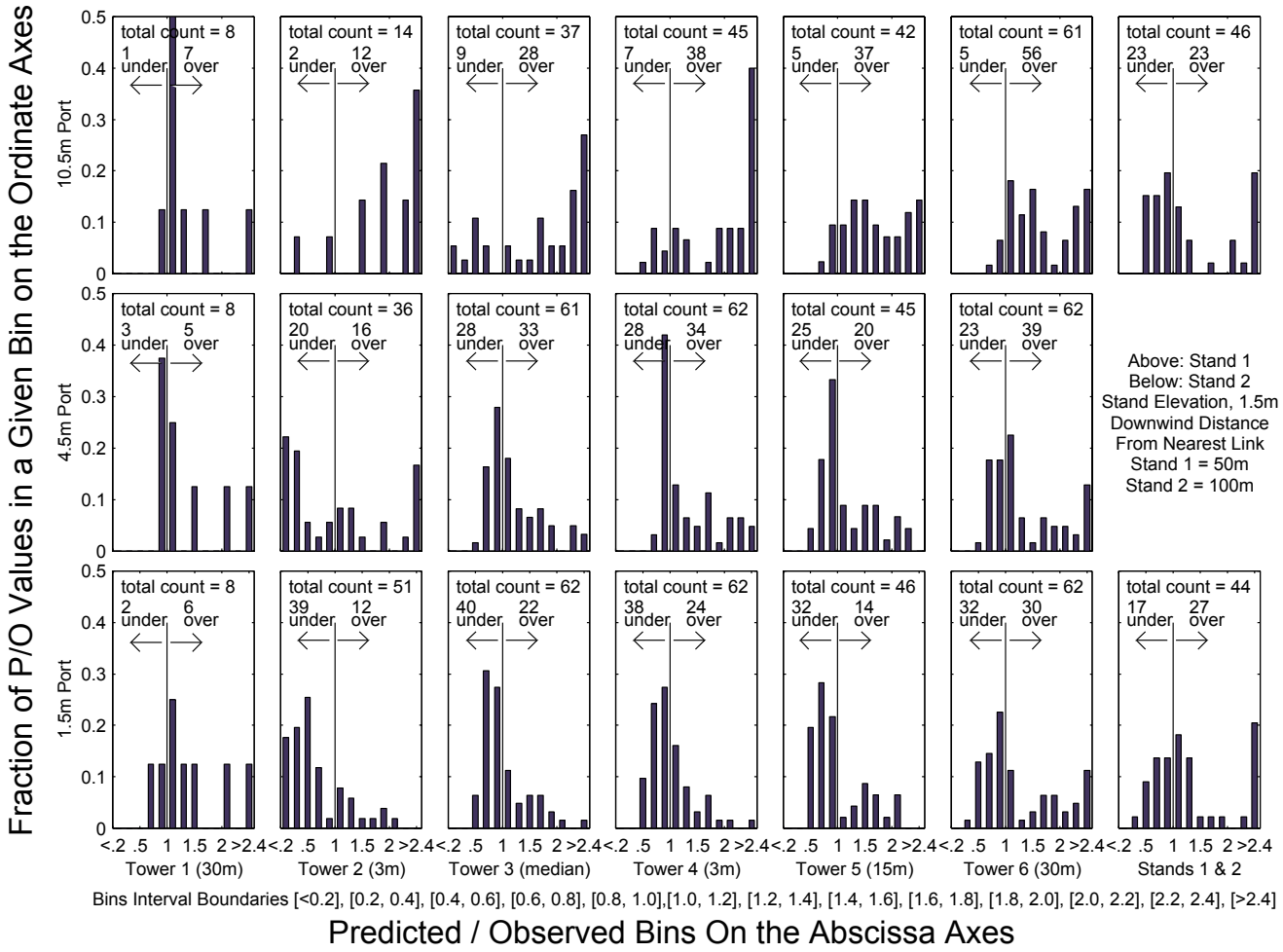

Figure 7-15. Histogram of CALINE3 (z_0=3 cm) predicted to observed concentrations ratios for each receptor location. SF_6 concentrations less than 100 pptv have been excluded. Each histogram represents a single receptor using the normalized coordinate system described in Figure 6-9.

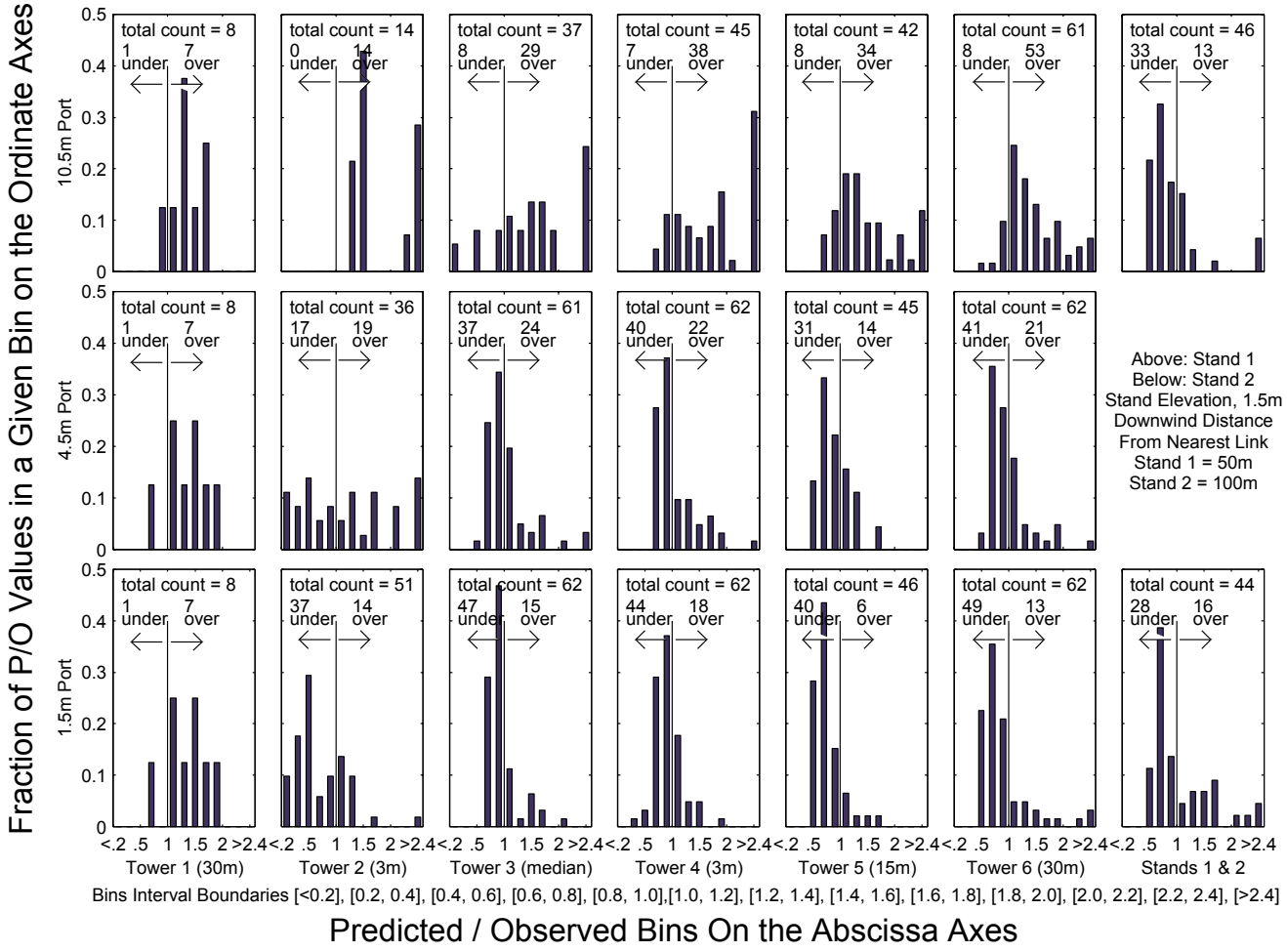

Figure 7-16. Histogram of CALINE4 (z_0=250 cm) predicted to observed concentrations ratios for each receptor location. SF_6 concentrations less than 100 pptv have been excluded. Each histogram represents a single receptor using the normalized coordinate system described in Figure 6-9.

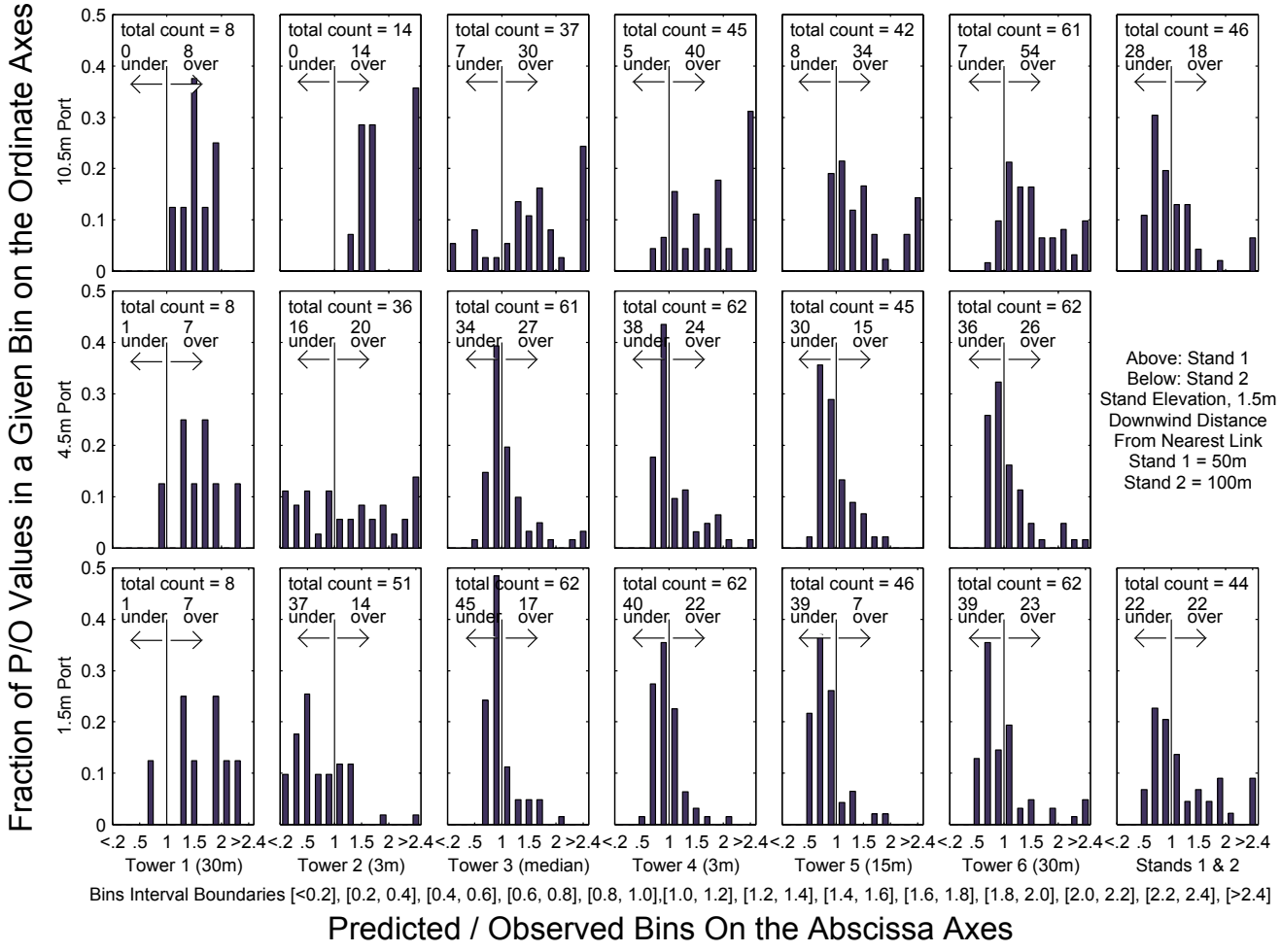

Figure 7-17. Histogram of CALINE4 (z_0=3 cm) predicted to observed concentrations ratios for each receptor location. SF_6 concentrations less than 100 pptv have been excluded. Each histogram represents a single receptor using the normalized coordinate system described in Figure 6-9.

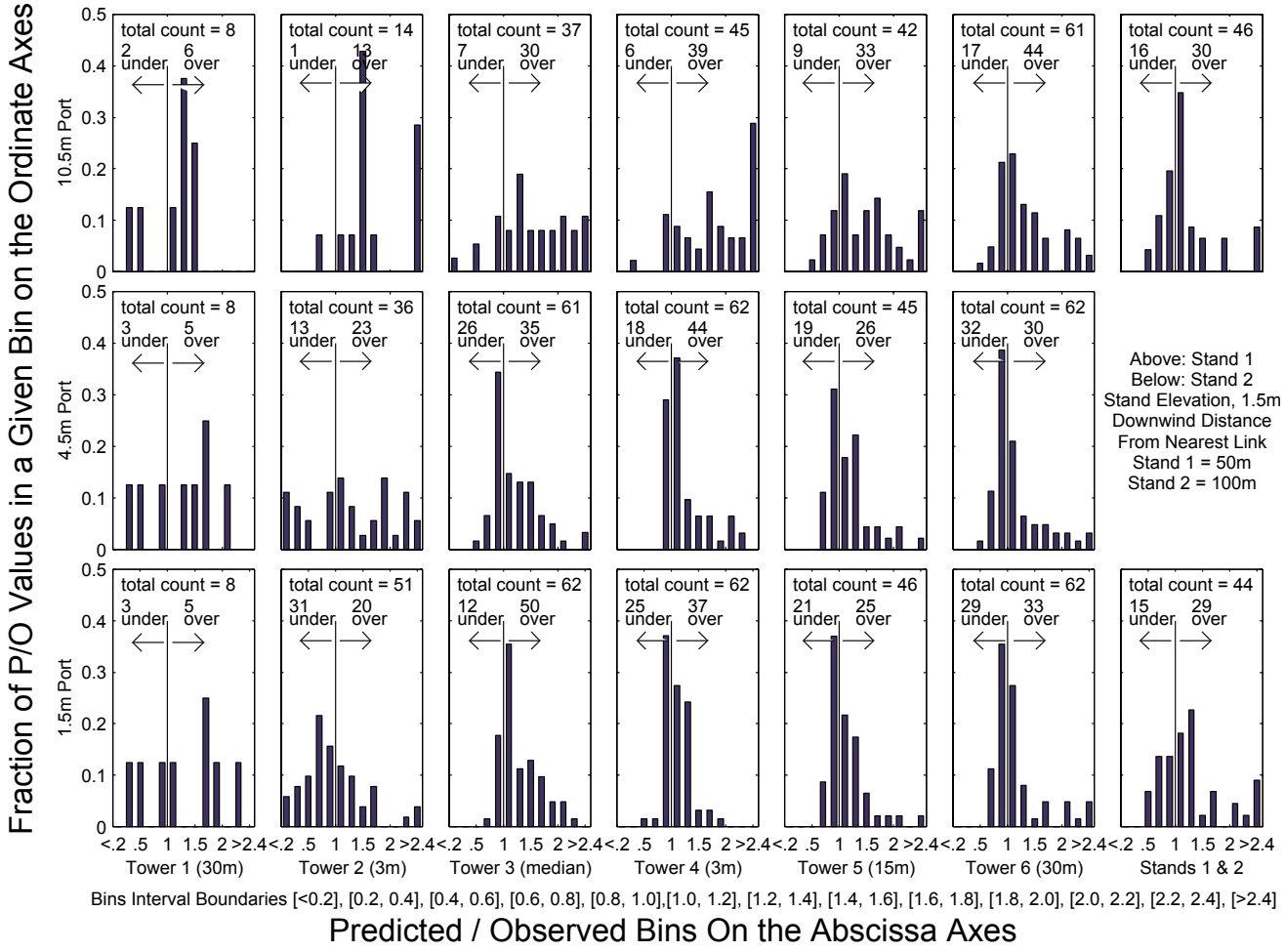

Figure 7-18. Histogram of UCD 2001 predicted to observed concentrations ratios for each receptor location. SF_6 concentrations less than 100 pptv have been excluded. Each histogram represents a single receptor using the normalized coordinate system described in Figure 6-9.

Analysis of the 40 Highest Observed Concentrations

A compilation of the 40 highest observed concentrations recorded during the GM experiment and the CALINE and UCD 2001 model predictions for these data points are listed in Table 7-6. Figure 7-19 presents the data in Table 7-6 in both scatter plot and histogram form. Four of the CALINE3 model simulations resulted in significant over predictions of SF_6 concentrations, with predicted to observed concentrations (P/O) ratios of 3.4, 4.2, 5.1, and 6.2. The CALINE4 model also over predicted the same four concentrations as the CALINE3 model, however, the P/O ratios for CALINE4 ranged from approximately 2 to 3. The CALINE4 model under estimates approximately 25 of the 40 greatest observed concentrations. Many of these under predictions are near or lower than the 0.5 P/O envelope.

All 40 of the UCD 2001 model predictions lie between a 1:2 and 2:1 observed to predicted envelope. The UCD 2001 model under predicts 17 data points and over predicts 23. However, 15 of the 17 under predictions were minor with a P/O ratio between 0.8 and 1.0. The remaining two UCD 2001 under predictions have P/O ratios of 0.76 and 0.58. The P/O ratio of 0.58 occurred at receptor 12 at time stamp 297080458 when the 4.5 m wind speed and direction were 2.49 m/s and 182 degrees, respectively. The observed versus predicted model concentrations for CALINE3, CALINE4, and UCD 2001 for time period 297080458 are presented as Figures 7-20, and 7-21, respectively.

As shown in Figure 7-22, the UCD 2001 model appears to adequately predict concentrations for all receptors except for receptor ID 12. Without additional data, it would be difficult to conclusively determine if receptor ID 12 for time period 297080458 is anomalous or represents a significant trend.

Table 7-6. The top 40 observed concentrations in the GM experiment. The observed concentration, ranked in descending order, and the CALINE3 (CL3), CALINE4 (CL4), and UCD 2001 model predictions for each time period are listed; CALINE model predictions were determined for a surface roughness of 3 cm and 250 cm. To the right of each model prediction is the predicted to observed ratio. In addition, the experimental timestamp, receptor ID, 4.5m wind direction (WD), 4.5m wind speed, and 4.5m cross-link component of the wind speed for each measurement are presented. This table is continued on the next page.

Rank	Time Stamp	Receptor ID	WS	WD	CWS	Observed Concentration	CL3 z_0=250	P/O	CL3 z_0=3	P/O	CL4 z_0=250	P/O	CL4 z_0=3	P/O	UCD 2001	P/O
1	297080458	12	2.49	182	-0.08	4922	3608	0.73	5313	1.08	1938	0.39	2136	0.43	2851	0.58
2	281083504	6	1.21	29	0.59	3770	3969	1.05	4105	1.09	3601	0.96	3734	0.99	3442	0.91
3	297083458	12	2.24	183	-0.12	3644	4092	1.12	5920	1.62	2126	0.58	2327	0.64	2998	0.82
4	295093958	6	0.35	8	0.05	3570	18291	5.12	20047	5.62	7084	1.98	7555	2.12	5732	1.61
5	296080500	12	2.92	181	-0.05	3543	3364	0.95	4844	1.37	1940	0.55	2155	0.61	3011	0.85
6	295090958	6	0.62	49	0.47	3477	4308	1.24	4327	1.24	4019	1.16	4108	1.18	3383	0.97
7	279084000	12	0.97	247	-0.89	3356	2497	0.74	2583	0.77	2627	0.78	2682	0.80	2552	0.76
8	296083459	12	2.99	183	-0.15	3327	3582	1.08	5176	1.56	2067	0.62	2274	0.68	3149	0.95
9	297090458	6	3.04	177	0.16	3302	3711	1.12	5362	1.62	2366	0.72	2553	0.77	3041	0.92
10	294090501	12	1.13	210	-0.56	3270	2682	0.82	2984	0.91	3285	1.00	3400	1.04	3332	1.02

Table 7-6 (Continued).

Rank	Time Stamp	Receptor ID	WS	WD	CWS	Observed Concentration	CL3 z0=250	P/O	CL3 z0=3	P/O	CL4 z0=250	P/O	CL4 z0=3	P/O	UCD 2001	P/O
11	281090504	6	0.94	78	0.92	3220	3135	0.97	3250	1.01	3156	0.98	3209	1.00	3034	0.94
12	295080958	6	0.45	51	0.35	3215	5127	1.59	5154	1.60	4658	1.45	4792	1.49	3750	1.17
13	295093958	9	0.35	8	0.05	3005	10256	3.41	10301	3.43	6051	2.01	6507	2.17	4623	1.54
14	294093501	12	1.38	219	-0.87	2915	1837	0.63	2174	0.75	2550	0.87	2628	0.90	2875	0.99
15	295083958	6	0.62	75	0.60	2870	3759	1.31	3894	1.36	3684	1.28	3747	1.31	3207	1.12
16	297083458	9	2.24	183	-0.12	2864	3530	1.23	4246	1.48	1902	0.66	2106	0.74	3525	1.23
17	294083502	12	1.52	235	-1.24	2857	2166	0.76	2207	0.77	2311	0.81	2366	0.83	2555	0.89
18	296093458	12	2.50	187	-0.30	2841	1995	0.70	2756	0.97	2182	0.77	2360	0.83	3279	1.15
19	276081459	12	2.31	209	-1.12	2831	2111	0.75	2185	0.77	2050	0.72	2124	0.75	2488	0.88
20	296083459	9	2.99	183	-0.15	2827	3087	1.09	3709	1.31	1774	0.63	1978	0.70	3704	1.31
21	302080456	12	1.83	346	-0.45	2824	3911	1.38	4217	1.49	2885	1.02	3061	1.08	3340	1.18
22	303090957	6	1.47	11	0.28	2784	2074	0.74	3046	1.09	3547	1.27	3746	1.35	4166	1.50
23	279080959	12	1.00	251	-0.95	2773	2425	0.87	2517	0.91	2512	0.91	2564	0.92	2513	0.91
24	294080502	12	1.59	230	-1.22	2757	2199	0.80	2282	0.83	2321	0.84	2378	0.86	2554	0.93
25	303093956	6	1.76	17	0.52	2739	1860	0.68	2604	0.95	2915	1.06	3049	1.11	3542	1.29

Table 7-6 (Continued).

Rank	Time Stamp	Receptor ID	WS	WD	CWS	Observed Concentration	CL3 z_0=250	P/O	CL3 z_0=3	P/O	CL4 z_0=250	P/O	CL4 z_0=3	P/O	UCD 2001	P/O
26	297080458	9	2.49	182	-0.08	2707	3390	1.25	4355	1.61	1763	0.65	1969	0.73	3526	1.30
27	276084459	12	2.15	214	-1.20	2690	2053	0.76	2014	0.75	2061	0.77	2129	0.79	2414	0.90
28	296090459	12	3.01	184	-0.21	2659	1620	0.61	2267	0.85	1830	0.69	2000	0.75	3165	1.19
29	275080959	12	1.07	321	-0.68	2608	3069	1.18	3036	1.16	2784	1.07	2883	1.11	2707	1.04
30	303083957	12	0.99	351	-0.16	2584	2418	0.94	3409	1.32	4045	1.57	4334	1.68	4394	1.70
31	295093958	5	0.35	8	0.05	2580	16019	6.21	17444	6.76	6232	2.42	6676	2.59	4590	1.78
32	281080504	6	1.82	36	1.07	2571	2593	1.01	2735	1.06	2534	0.99	2594	1.01	2692	1.05
33	297093458	6	3.55	179	0.06	2545	1863	0.73	2748	1.08	1887	0.74	2047	0.80	2782	1.09
34	297083458	11	2.24	183	-0.12	2460	3576	1.45	5332	2.17	1670	0.68	1849	0.75	2126	0.86
35	300080000	12	1.77	194	-0.43	2423	4142	1.71	4466	1.84	3097	1.28	3284	1.36	3372	1.39
36	303080957	12	0.91	321	-0.57	2393	4076	1.70	4033	1.69	3624	1.51	3748	1.57	3297	1.38
37	296080500	9	2.92	181	-0.05	2392	3462	1.45	4663	1.95	1896	0.79	2132	0.89	3930	1.64
38	302093457	6	3.12	354	-0.33	2368	1079	0.46	1253	0.53	1287	0.54	1372	0.58	1964	0.83
39	297083458	8	2.24	183	-0.12	2356	3340	1.42	4053	1.72	1731	0.73	1918	0.81	2675	1.14
40	295093958	8	0.35	8	0.05	2337	9839	4.21	9797	4.19	5672	2.43	6106	2.61	3957	1.69

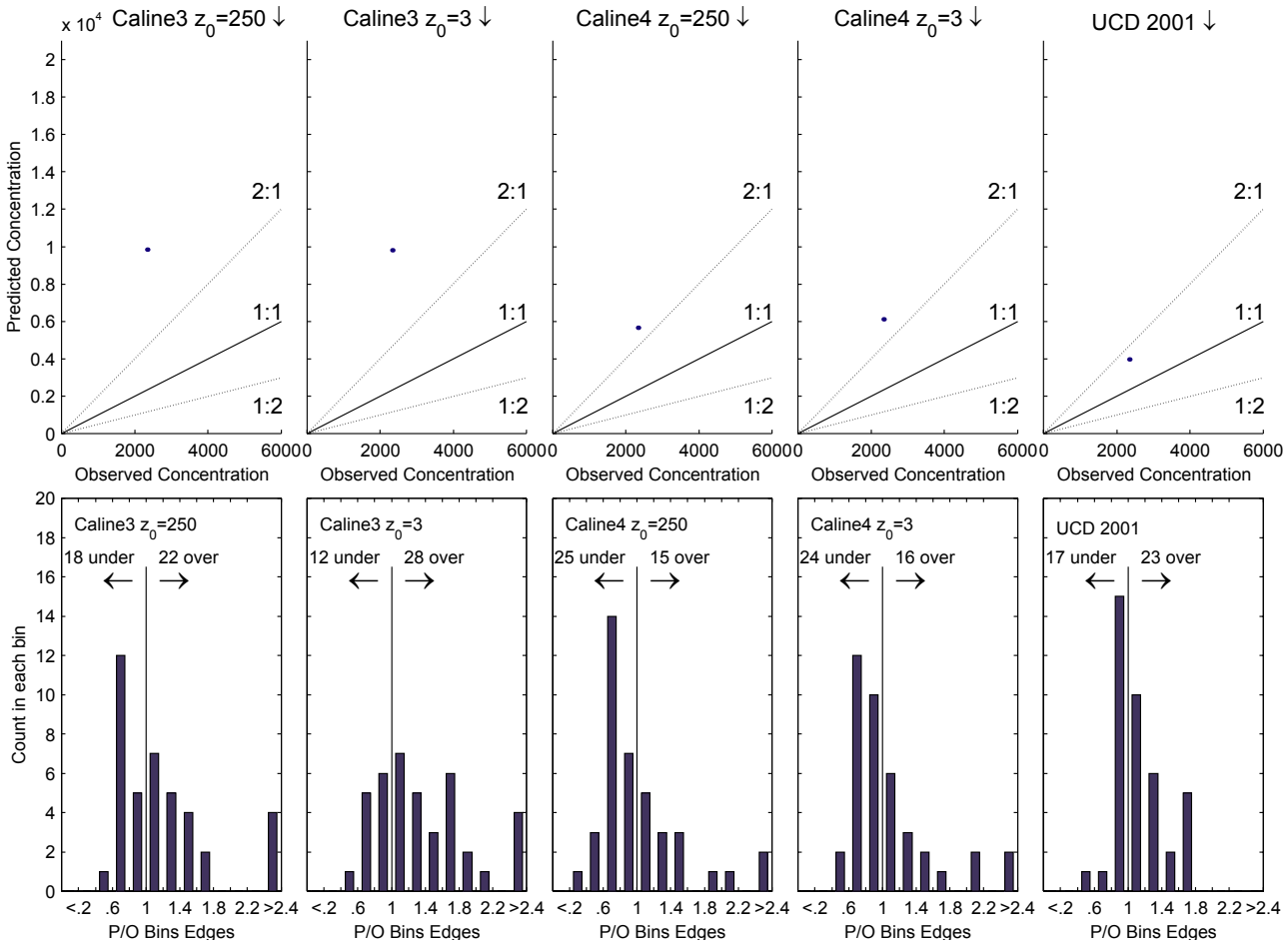

Figure 7-19. Comparison of model predictions of the 40 highest observed concentrations. The top figures are scatter plots of observed to predicted concentrations. The bottom plots are histograms of predicted to observed (P/O) ratios for each dispersion model binned by P/O value. P/O values greater than 1 are represent over-predictions, whereas P/O values less than 1 are under-predictions.

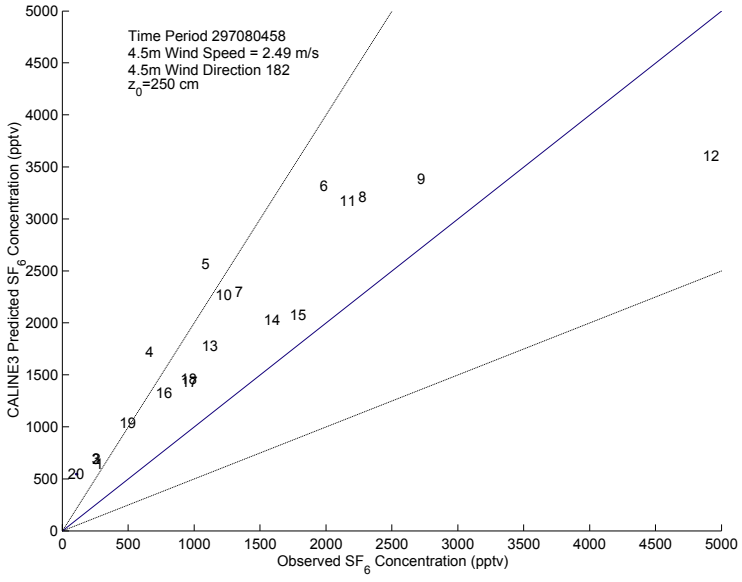

Figure 7-20. CALINE3 (z_0=250 cm) predicted versus observed SF_6 concentrations for time period 297080458. Each plot point corresponds to a receptor ID shown in Figure 6-9.

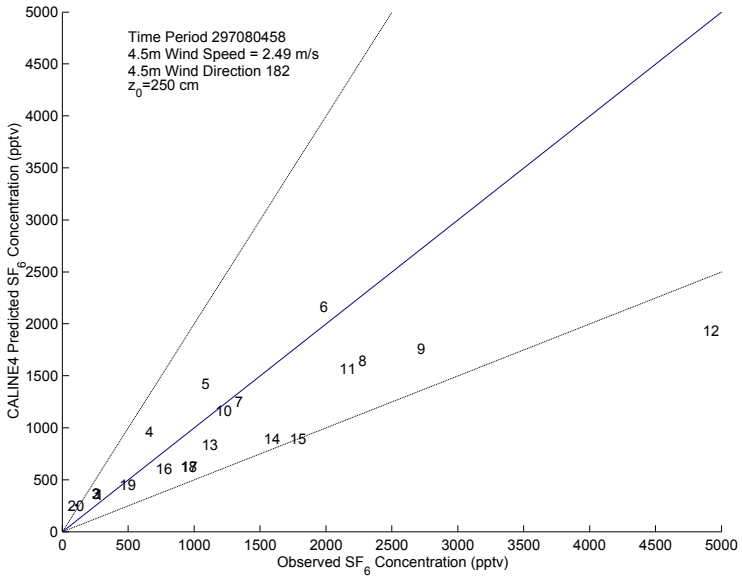

Figure 7-21. CALINE4 (z_0=250 cm) predicted versus observed SF_6 concentrations for time period 297080458. Each plot point corresponds to a receptor ID shown in Figure 6-9.

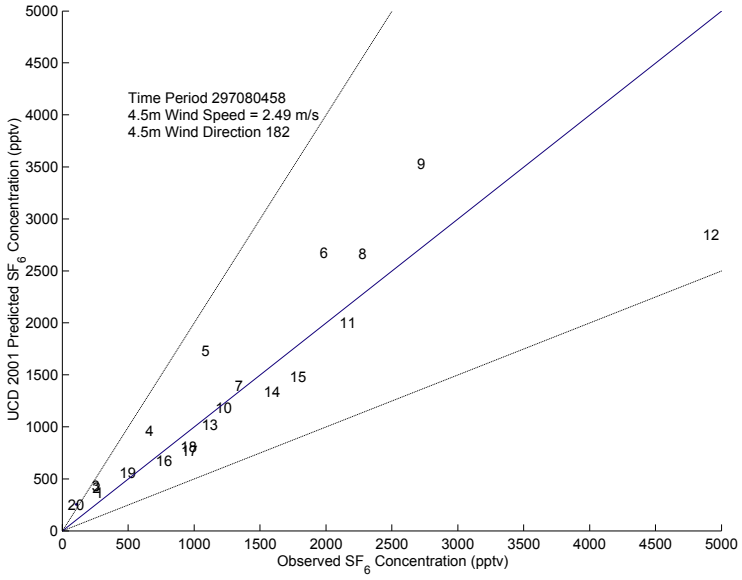

Figure 7-22. UCD 2001 predicted versus observed SF_6 concentrations for time period 297080458. Each plot point corresponds to a receptor ID shown in Figure 6-9.

Decoupled Concentration Analysis

A scatter plot of observed versus decoupled predicted concentrations is presented in Figure 7-23. In this plot, the observed and predicted concentrations are decoupled from their temporal and spatial location and are ordered by increasing magnitude. Although it is difficult to draw physical insight from this plot, decoupled analysis is routinely used to determine model robustness for regulatory analysis. Inspection of Figure 7-23 demonstrates that the CALINE3 model predicts concentrations significantly greater than the maximum observed concentration in the GM dataset. Both the CALINE4 and UCD 2001 model appear to close to the 1:1 observed versus predicted guideline.

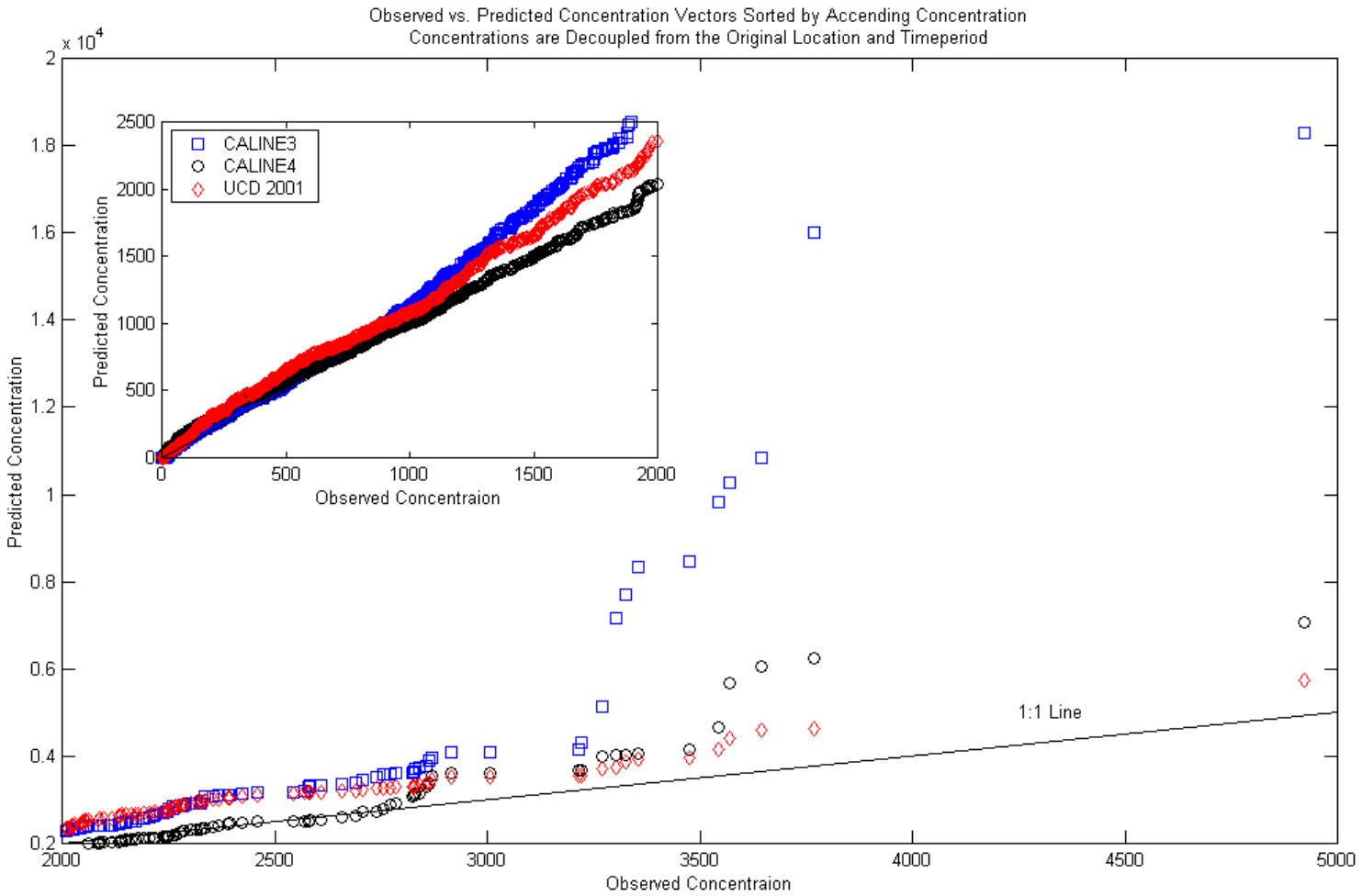

Figure 7-23. Observed GM SF_6 concentrations plotted against CALINE and UCD 2001 predicted concentrations. Concentrations are sorted by magnitude and are decoupled from their original time and location. Each vector contains approximately 1200 points.

Summary

The UCD 2001 model errors for the group 1 and 2 data sets are 88 and 92 (in millions), respectively. Since the errors associated with the calibration and independent datasets are nearly identical, it suggests that the UCD 2001 model is capable of effectively simulating datasets other than those used to calibrate the model.

Worst-case meteorological conditions are those that result in the highest observed pollutant concentrations. Based on experience gleaned from classical dispersion studies, it is assumed that low magnitude, near parallel wind conditions represent the worst case conditions for roadway dispersion modeling purposes. In this analysis, it was shown that UCD 2001 model is capable of simulating these worst-case conditions adequately, with substantially better performance than the CALINE models, although the UCD model tends to over predict receptor concentrations for these conditions.

When all 1237 SF_6 data points were considered, the UCD 2001 model results in a 80 to 90 percent reduction in error when compared to the CALINE simulations. If one excludes the low wind speed period that leads to serious CALINE over predictions, the UCD 2001 model still results in significant error reduction. For example, the UCD 2001 model has approximately 62 percent error reduction for the group 3 data set when compared to CALINE3 with an estimated surface roughness of 3 cm.

Based on an analysis of predicted to observed histograms and scatter plots, the UCD 2001 model resulted in fewer under predictions when compared to CALINE3 and CALINE4. Furthermore, when the UCD 2001 model under predicted, its under predictions were less severe than their CALINE equivalents.

Lastly, the UCD 2001 adequately reproduced all but one of the top 40 observed concentrations. In this top 40 analysis, all 40 data points were within 50% to 200% of the observed concentration, with most points centered on the 1:1 agreement line. Top 40 scatter plots for CALINE3 confirmed this models propensity to significantly over predicted pollutant concentrations for worst case meteorological conditions. Unlike CALINE3, CALINE4 did not tend to make severe over predictions. However, it did have a tendency to under predict top 40, with one data point below the 50% scatter plot envelope.

Chapter 8. Conclusion and Final Observations

Introduction

In this dissertation the regulatory underpinning, theoretical basis, and performance of the UCD 2001 roadway dispersion model were presented. In this chapter, a brief summary of findings and implications of this analysis will be presented.

Comments On UCD 2001 and CALINE Model Performance

The UCD 2001 model was shown to outperform both CALINE3 and CALINE4 in a variety of performance metrics. First, the UCD 2001 model is capable of simulating low wind speed meteorological conditions more effectively than both CALINE models. The UCD 2001 simulations result in significantly less error between observed and predicted pollutant concentrations. In a review of the top forty observed concentrations, the UCD model showed greater agreement with SF6 concentrations and was shown less likely to result in significant over and under predictions.

CALINE Input Variable Uncertainty

In addition to its statistical performance, the UCD model has some operational advantages over the CALINE models. Although the UCD 2001 model is programmatically more complex than the CALINE models, it requires less user input, expertise, and intuition on the part of the modeler. Unlike the CALINE model, the UCD model does not depend on stability or surface roughness. As shown in Chapter 7, CALINE model performance was noticeably different if one used the field measured surface roughness of 3 cm versus the 250 cm value used for model calibration.

Both CALINE models are based on a Gaussian-type equation that requires a uniform wind field. The CALINE input files require the user to specify a single number to represent the wind field whereas UCD 2001 allows the user to specify a wind profile. The CALINE4 user manual indicates that representative wind speed should be estimated by "measuring at 5 to 10 m or assume worst-case [0.5 m/s]. For localized sources and nearby receptors, wind speeds measured at lower elevations (5 m) are desirable. For more diffuse sources and distant receptors, 10 m height is more appropriate" (Benson 1984). Clearly, these instructions are quite open to interpretations on the part of the modeler, for instance, how should one employ measured data if it is collected?

Since the receptor concentration estimate is inversely proportional to wind speed, small differences in determining the representative wind speed elevations can lead to large variations in downwind concentrations. The ambiguity associated with wind speed is a direct consequence of trying to model a wind profile with a single wind speed. For example, if one user selects 10 m as the representative wind height and an different user selected 5 m, differences between the two modeler's concentration estimates could be as great as 50% if one assumed a power wind profile and stable conditions.

The UCD 2001 model requires the user to specify the wind speed at a reference elevation. No additional meteorological data or intuition are required of the modeler to determine the concentration field surrounding a roadway (note: the UCD 2001 temperature and pressure input parameters are used only for unit conversions). In contrast to the CALINE models, if there is no ambiguity in roadway link geometry, vehicle emission factors, or receptor locations, different transportation modelers would estimate identical receptor concentrations with the UCD 2001 model. Ideally, user preference and experience should not have a significant impact on model predictions.

The UCD 2001, An Intuitive Dispersion Model

The UCD 2001 point source model is conceptually simple and physically intuitive. The UCD model simulates vehicular emissions as if they were generated by a volume source above the roadway. The mixing volume extends 2.5 m above the roadway and 3 m to each side of a links traveled way. Emissions from this volume are simulated with an array of point sources bounded by the mixing volume dimensions. This mixing volume approach is both mathematically simplistic and physically intuitive when compared to the CALINE line source approach. In the CALINE models, links are partitioned into a series of ground-based line sources that have been rotated perpendicular to the average wind direction and weighted based on link and wind orientation. The UCD 2001 mixing volume approach results in smooth concentration predictions both downwind and above the roadway given its geometric simplicity. Given the complexity of the CALINE formulation, it is not clear that the concentration field near a roadway link is smooth and well behaved near the finite line sources used to represent vehicle emissions.

The literature suggests that the boundary layer immediately downwind of a roadway is well-mixed and that pollutant transport in this region is dominated by vehicle activity not ambient meteorology. The UCD 2001 formulation is one of the most simplistic models developed that is still consistent with these findings. To achieve this consistency, the UCD 2001 model assumes a neutral wind profile and an eddy diffusivity profile that are independent of meteorological field variables. This modeling approach shows good agreement with the GM dataset.

Possible Extensions of the UCD 2001 Model

The UCD 2001 model simulates vehicular emissions as an array of point sources. At the time of model development, the GM database was the only major line source dispersion study available for model calibration. The vehicular type and usage was near identical for each of the GM sampling periods and was adequately simulated with a mixing zone depth of 2.5 m in the UCD 2001 model. However, one would expect a different sized mixing zone if a significant number of heavy duty vehicles were present. If additional line source calibration data become available, one could easily modify the UCD 2001 model to allow for a different sized mixing zone, or to allow for multiple mixing zones with differing emissions or to include a separate algorithm of for distributing the emissions from heavy duty vehicles. These modifications may be needed to properly simulate slow-moving congested conditions or to model vehicles starting from stop at an intersection. Visual observation of vehicle emissions for these conditions clearly indicate that the bulk of the exhaust plume is not always entrained into the vehicle wake.

In addition, the UCD 2001 model could be integrated with a micro-scale intersection model to simulate pollutant transport from roadways with unsteady vehicular flow rates. The UCD 2001 model internally represents roadway emissions as a collection of point sources. UCD 2001 represents a highway link with a uniform array of point sources, however a non-uniform array could be used to simulate pollutant releases near intersections.

The UCD 2001 model is intended for use within 100 m of a roadway. It is unlikely that significant deposition, coagulation, or chemical transformation of particulate matter (PM) generated from vehicular activity will occur between the tail pipe and

receptors within 100 m. If it can be shown that PM matter does indeed have similar transport characteristics to inert tracers in the near field, the UCD 2001 model could be augmented to allow for estimations of PM concentrations downwind of roadways.

References

"Guideline on Air Quality Models." (1997). 40 CFR Appendix to Part 51.

"Transportation conformity rule amendments: flexibility and streamlining; final rule." (1997). 40 CFR 51 and 93.

Albergel, A., and Jasmin, F. (1998). "3-D simulation of local-scale traffic pollution." *International Journal of Vehicle Design*, 20(1-4), 79-87.

Al-Deek, H., Wayson, R. L., Cooper, D. C., Keely, D., Trynelis, R., Liu, P.-S., Malone, L. C., and Datz, A. "A queuing algorithm for calculating idling emissions in FLINT - the "FLorida INTersection" air quality model." *76th TRB Annual Meeting*, Washington, D.C.

Baker, C. J. (1996). "Outline of a novel method for the prediction of atmospheric pollution dispersal from road vehicles." *Journal of Wind Engineering and Industrial Aerodynamics*, 65(1-3), 395-404.

Batchelor, G. K. (1949). "Diffusion in a field of homogeneous turbulence." *Australian Journal of Scientific Research*, 2, 437-450.

Benson, P. (1980). "Effects of vehicle induced turbulence on vertical dispersion of carbon monoxide near roadways," [Davis, Calif.].

Benson, P. E. (1979). "CALINE3 - A versatile dispersion model for predicting air pollutant levels near highways and arterial streets." *FHWA/CA/TL-79/23*.

Benson, P. E. (1984). "CALINE4, a dispersion model for predicting air pollutant concentrations near roadways." *FHWA/CA/TL-84/15*, California Department of Transportation, Sacramento, CA.

Berkowicz, R. (1997). "Modeling street canyon pollution: model requirements and expectations." *International Journal of Environment and Pollution*, 8(3-6), 609-619.

Buckland, A. T. (1998). "Validation of a street canyon model in two cities." *Environmental Monitoring and Assessment*, 52(1-2), 255-267.

Buckland, A. T., and Middleton, D. R. (1999). "Nomograms for calculating pollution within street canyons." *Atmospheric Environment*, 33(7), 1017-1036.

Cadle, S. H., Chock, D. P., Monson, P. R., and Heuss, J. M. (1977). "General Motors sulfate dispersion experiment: experimental procedures and results." *JAPCA*, 33.

Cadle, S. H., et al. (1976). "Results of the General Motors sulfate dispersion experiment." *GMR-2107*, General Motors Research Laboratories, Waren, MI.

Calder, K. L. (1973). "On Estimating Air Pollution Concentrations From a Highway in an Oblique Wind." *Atmospheric Environment*, 7, 863-868.

Carpenter, W. A., and Clemena, G. G. (1975). "Analysis and comparative evaluation of AIRPOL-4." *VHTRC-75-R55*, Virginia Highway and Transportation Research Council, Charlottesville, VA.

Chabni, A., Le Quere, P., Tenaud, C., and Laatar, H. (1998). "Modeling of pollutant dispersion in urban street canyons by means of a large-eddy simulation approach." *International Journal of Vehicle Design*, 20(1-4), 88-95.

Chan, L. Y., Hung, W. T., and Qin, Y. (1995). "Assessment of Vehicular Emission Dispersion Models Applied in Street Canyons in Guangzhou, Prc." *Environment International*, 21(1), 39-46.

Chock, D. P. (1977a). "General Motors sulfate dispersion experiment - an overview of the wind, temperature, and concentration fields." *Atmospheric Environment*, 11(6), 553-559.

Chock, D. P. (1977b). "General Motors sulfate dispersion experiment: assessment of the EPA HIWAY model." *Journal of the Air Pollution Control Association*, 27(1), 39-45.

Chock, D. P. (1978a). "An advection-diffusion model for pollutant dispersion near roadways." *Journal of Applied Meteorology*, 17(7), 976-89.

Chock, D. P. (1978b). "A simple line-source model for dispersion near roadways." *Atmospheric Environment*, 12(4), 823-9.

Chock, D. P. (1980a). "Comments on "a new model for estimating concentrations of substances emitted from a line source"." *Journal of the Air Pollution Control Association*, 30(1), 52-56.

Chock, D. P. (1980b). "General Motors sulfate dispersion experiment. An analysis of the wind field near a road." *Boundary-Layer Meteorology*, 18(4), 431-51.

Cooper, C. D., and Alley, F. C. (1994). *Air pollution control: a design approach*, Waveland Press, Inc.

Cooper, D. C., Wayson, R. L., Al-Deek, H., Malone, L. C., Liu, P.-S., Keely, D., Trynelis, R., Heriba, M., and Matar, F. (1997). "FLINT - The FLorida INTersection Model." *WPI 0510676*, Civil and Environmental Engineering Dept., Univ. of Central Florida.

Dabberdt, W. F., Hoydysh, W., Schorling, M., Yang, F., and Holynskyj, O. (1995). "Dispersion modeling at urban intersections." *Science of the Total Environment*, 169(1-3), 93-102.

Dabberdt, W. F., and Hoydysh, W. G. (1991). "Street Canyon Dispersion - Sensitivity to Block Shape and Entrainment." *Atmospheric Environment Part a-General Topics*, 25(7), 1143-1153.

Dabberdt, W. F., Shelar, E., Marimont, D., and Skinner, G. (1981). "Analyses, experimental studies, and evaluations of control measures for air flow and air quality on and near highways." *FHWA/RD-81/051*, SRI International, Menlo Park.

Danard, M. B. (1972). "Numerical modeling of carbon monoxide concentrations near a highway." *Journal of Applied Meteorology*, 11, 947-957.

DePaul, F. T., and M., S. C. (1986). "Measurements of wind velocities in a street canyon." *Atmospheric Environment*, 20, 455-459.

DeTar, D. F. (1979). "A new model for estimating concentrations of substances emitted from a line source." *Air Pollution Control Association*, 29(2), 138-141.

Draxler, R. R. (1976). "Determination of atmospheric diffusion parameters." *Atmospheric Environment*, 10(2), 99-105.

Drivas, P. J., and Shair, F. H. (1974). "Dispersion of an instantaneous cross-wind line source of tracer released from an urban highway." *Atmospheric Environment*, 8, 475-485.

Dufort, E. C., and Frankel, S. P. (1953). "Stability conditions in the numerical treatment of parabolic differential equations." *Mathl Tabl. Natn. Res. Coun., Wash.*, 7, 135.

EPA. (1992a). "Guideline for modeling carbon monoxide from roadway intersections." *EPA-454/R-92-005*, EPA, Research Triangle Park, North Carolina.

EPA. (1992b). "User's guide to CAL3QHC version 2.0: a modeling methodology for predicting pollutant concentrations near roadway intersections." *EPA-454/R-92-006*, U.S. Environmental Protection Agency.

EPA. (1995). "User's guide for the ISC3 dispersion models." *EPA-454/B-95-003b*, U.S. EPA OAQPS, Research Triangle Park, North Carolina.

Eskridge, R. E., Binkowski, F. S., Hunt, J. C. R., Clark, T. L., and Demerijian, K. L. (1979). "Highway Modeling. Part II : advection and diffusion of SF6 tracer gas." *Journal of Applied Meteorology*, 18(4), 401-412.

Eskridge, R. E., and Hunt, J. C. R. (1979). "Highway modeling. Part I : prediction of velocity and turbulence fields in the wake of vehicles." *Journal of Applied Meteorology*, 18(4), 387-400.

Eskridge, R. E., Petersen, W. B., and Rao, S. T. (1991). "Turbulent diffusion behind vehicles - effect of traffic speed on pollutant concentrations." *Journal of the Air & Waste Management Association*, 41(3), 312-317.

Eskridge, R. E., Petersen, W. B., Rao, S. T., and Sistla, G. "Turbulent Diffusion Behind Vehicles: Experiments and Verification of Roadway Models." *Air Pollution Control Association*, San Francisco, California.

Eskridge, R. E., and Rao, S. T. (1983). "Measurement and prediction of traffic-induced turbulence and velocity fields near roadways." *Journal of Climate and Applied Meteorology*, 22(8), 1431-43.

Eskridge, R. E., and Rao, S. T. (1986). "Turbulent diffusion behind vehicles: experimentally determined turbulence mixing parameters." *Atmospheric Environment*, 20(5), 851-860.

Eskridge, R. E., and Thompson, R. S. (1982). "Experimental and theoretical study of the wake of a block-shaped vehicle in a shear-free boundary flow." *Atmospheric Environment*, 16(12), 2821-2836.

FHWA. (1997). "Transportation conformity: a basic guide for state and local officials." *FHWA-PD-97-035*, Federal Highway Administration, Federal Transit Administration.

Garza, V. J., Graney, P., Sperling, D., Niemeier, D., Eisinger, D., Kear, T., Chang, D., and Meng, Y. (1997). "Transportation project-level carbon monoxide protocol." *UCD-ITS-RR-97-21*, Institute of Transportation Studies, Davis.

Graf, J., Paffrath, D., Rosler, F. M., Schumann, U., and Seiler, W. (1990). "Experimental and numerical study of the dispersion and transport of automobile exhaust gases from highways." *Science of the Total Environment*, 93(APR), 323-330.

Gronskei, K. E. (1988). "The influence of car speed on dispersion of exhaust gases."

Hargreaves, D. M., and Baker, C. J. (1997). "Gaussian puff model of an urban street canyon." *Journal of Wind Engineering and Industrial Aerodynamics*, 71, 927-939.

Hassan, A. A., and Crowther, J. M. (1998a). "Modeling of fluid flow and pollutant dispersion in a street canyon." *Environmental Monitoring and Assessment*, 52(1-2), 281-297.

Hassan, A. A., and Crowther, J. M. (1998b). "A simple model of pollutant concentrations in a street canyon." *Environmental Monitoring and Assessment*, 52(1-2), 269-280.

Held, A. E., Chang, D. P. Y., and Carroll, J. J. (1998). "Observations and model simulations of carbon monoxide dispersion." *Contract Number 43Y070*, California Department of Transportation, Davis, CA.

Held, A. E., Chang, D. P. Y., and Niemeier, D. A. (2001). "Observations and model simulations of carbon monoxide emission factors from a California highway." *Air & Waste Management*, 51, 121-132.

Herbert, J. M., Johnson, G. T., and Arnfield, A. J. (1997). "Coupling of a scalar dispersion and an urban canyon energy budget model." *Mathematics and Computers in Simulation*, 43(3-6), 277-283.

Hlavinka, M. W., Korpics, J. J., and Bullin, J. A. (1987). "TEXIN2: A versatile model for predicting carbon monoxide concentrations near intersections." *Journal of the Air Pollution Control Association*(July), 819-822.

Hoydysh, W. G., and Dabberdt, W. F. (1988). "Kinematics and Dispersion Characteristics of Flows in Asymmetric Street Canyons." *Atmospheric Environment*, 22(12), 2677-2689.

Hoydysh, W. G., and Dabberdt, W. F. (1994a). "Concentration fields at urban intersections - fluid modeling studies." *Atmospheric Environment*, 28(11), 1849-1860.

Hoydysh, W. G., and Dabberdt, W. F. (1994b). "A fluid modeling study of concentration distributions at urban intersections." *Science of the Total Environment*, 147(MAY), 425-432.

Huang, C.-H. (1979). "A theory of dispersion in turbulent shear." *Atmospheric Environment*, 13, 453-463.

Hunter, L. J., Johnson, G. T., and Watson, I. D. (1992). "An Investigation of 3-Dimensional Characteristics of Flow Regimes Within the Urban Canyon." *Atmospheric Environment Part B-Urban Atmosphere*, 26(4), 425-432.

Johnson, G. T., and Hunter, L. J. (1995). "A Numerical Study of Dispersion of Passive Scalars in City Canyons." *Boundary-Layer Meteorology*, 75(3), 235-262.

Johnson, G. T., and Hunter, L. J. (1999). "Some insights into typical urban canyon airflows." *Atmospheric Environment*, 33(24-25), 3991-3999.

Kamenetsky, E., and Vieru, N. (1995). "Model of Air-Flow and Air-Pollution Concentration in Urban Canyons." *Boundary-Layer Meteorology*, 73(1-2), 203-206.

Kastner-Klein, P., and Plate, E. J. (1999). "Wind-tunnel study of concentration fields in street canyons." *Atmospheric Environment*, 33(24-25), 3973-3979.

Kirsch, J. W., and Mason, B. F. (1975). "Mathematical models for air pollution studies involving the Oregon I205 highway project." *SSS-R-76-2744*, Systems, Science and Software, La Jolla, CA.

Koushki, P. A. (1991). "Evaluation of Street-Canyon Carbon Monoxide - Dispersion Simulation Model." *Journal of Transportation Engineering-Asce*, 117(4), 444-456.

Lanzani, G., and Tamponi, M. (1995). "A Microscale Lagrangian Particle Model For the Dispersion of Primary Pollutants in a Street Canyon - Sensitivity Analysis and First Validation Trials." *Atmospheric Environment*, 29(23), 3465-3475.

Lee, I. Y., and Park, H. M. (1994). "Parameterization of the Pollutant Transport and Dispersion in Urban Street Canyons." *Atmospheric Environment*, 28(14), 2343-2349.

Matzoros, A., and Vanvliet, D. (1992a). "A model of air-pollution from road traffic, based on the characteristics of interrupted flow and junction control, part 2,

model results." *Transportation Research Part a-Policy and Practice*, 26(4), 331-355.

Matzoros, A., and Vanvliet, D. (1992b). "A model of air-pollution from road traffic, based on the characteristics of interrupted flow and junction control, part 1, model description." *Transportation Research Part a-Policy and Practice*, 26(4), 315-330.

McCormick, R. A., and Xintaras, C. (1962). "Variation of carbon monoxide concentrations as related to sampling interval, traffic and meteorological factors." *Journal of Applied Meteorology*, 1, 237-243.

Meroney, R. N., Pavageau, M., Rafailidis, S., and Schatzmann, M. (1996). "Study of line source characteristics for 2-D physical modeling of pollutant dispersion in street canyons." *Journal of Wind Engineering and Industrial Aerodynamics*, 62(1), 37-56.

Nakamura, Y., and Oke, T. R. (1988). "Wind, temperature and stability conditions in an East-West oriented urban canyon." *Atmospheric Environment*, 22, 2691-2700.

Okamoto, S., Lin, F. C., Yamada, H., and Shiozawa, K. (1996). "Evaluation of a two-dimensional numerical model for air quality simulation in a street canyon." *Atmospheric Environment*, 30(23), 3909-3915.

Pavageau, M., and Schatzmann, M. (1999). "Wind tunnel measurements of concentration fluctuations in an urban street canyon." *Atmospheric Environment*, 33(24-25), 3961-3971.

Pearce, W., and Baker, C. J. (1997). "Wind-tunnel investigation of the effect of vehicle motion on dispersion in urban canyons." *Journal of Wind Engineering and Industrial Aerodynamics*, 71, 915-926.

Pitter, R. L. (1976). "User's manual ROADS, PSMOG, VIS1." Oregon Graduate Center, Beaverton, Oregon.

Qin, Y., and Kot, S. C. (1993). "Dispersion of Vehicular Emission in Street Canyons, Guangzhou- City, South China (Prc)." *Atmospheric Environment Part B-Urban Atmosphere*, 27(3), 283-291.

Ragland, K. W., and Peirce, J. J. (1975). "Boundary layer model for air pollutant concentrations due to highway traffic." *Journal of the Air Pollution Control Association*, 25(1), 48-51.

Rao, K. S., Wyngaard, J. C., and Cote, O. R. (1974). "The structure of the two-dimensional internal boundary layer over a sudden change of surface roughness." *Journal of the Atmospheric Sciences*, 31(3), 738-46.

Rao, S. T., and Kienan, M. T. (1980). "Suggestions for improvement of the EPA-HIWAY Model." *Journal of the Air Pollution Control Association*, 3, 60-69.

Rao, S. T., Sedefian, L., and Czapski, U. H. (1979). "Characteristics of turbulence and dispersion of pollutants near major highways." *Journal of Applied Meteorology*, 18, 283-293.

Rao, S. T., Sistla, G., Eskridge, R. E., and Petersen, W. B. (1986). "Turbulent diffusion behind vehicles: evaluation of roadway models." *Atmospheric Environment*, 20(6), 1095-1103.

Rao, S. T., Sistla, G., Keenan, M. T., and Wilson, J. S. (1980). "An evaluation of some commonly used highway dispersion models." *JAPCA*, 30, 239.

Rotach, M. W. (1995). "Profiles of Turbulence Statistics in and Above an Urban Street Canyon." *Atmospheric Environment*, 29(13), 1473-1486.

Sistla, G., Samson, P., Keenan, M., and Rao, S. T. (1979). "A study of pollution dispersion near highways." *Atmospheric Environment*, 13, 669-685.

Stull. (1988). *An introduction to boundary layer meteorology*, Kluwer Academic Publishers.

Sutton, O. G. (1953). *A study of physical processes in the lowest layers of the earth's atmosphere*, McGraw-Hill, New York.

Turner, D. B. (1969). "Workbook of atmospheric dispersion estimates." *AP-26*, Public Health Service.

US EPA. (2000). "Introduction to laws and regulations." http://www.epa.gov/epahome/lawintro.htm.

Ward, C. E., Ranzieri, A. J., and Shirley, E. C. (1977). "CALINE2- an improved microscale model for the dispersion of air pollutants from a line source." *FHWA-RD-77-74*, FHWA, Washington, D.C.

Washington, S., Leonard, J. D., Roberts, C. A., Young, T., Sperling, D., and Botha, J. (1998). "Forecasting vehicle modes of operation needed as input to 'modal' emissions models." *International Journal of Vehicle Design*, 20(1-4), 351-359.

Wilson, J. D., and Swaters, G. E. (1991). "The source area influencing a measurement in the planetary boundary layer - the footprint and the distribution of contact distance." *Boundary-Layer Meteorology*, 55(1-2), 25-46.

Wilson, W. E., Spiller, L. L., Ellestad, T. G., Lamothe, P. J., Dzubay, T. G., Stevens, R. K., Macias, E. S., Fletcher, R. A., Husar, J. D., Husar, R. B., Whitby, K. T., Kittelson, D. B., and Cantrell, B. K. (1977). "General Motors Sulfate Dispersion Experiment: Summary of EPA Measurements." *Journal of the Air Pollution Control Association*, 27(1), 46-51.

Yamartino, R. J., and Wiegand, G. (1986). "Development and evaluation of simple models for the flow, turbulence and pollutant concentration fields within an urban street canyon." *Atmospheric Environment*, 20, 2137-2156.

Zimmerman, J. R., and Thompson, R. S. (1975). "User's guide for HIWAY, a highway air pollution model." *EPA-650/4-74-008*, EPA.

Zoumakis, N. M. (1995). "A note on average vertical profiles of vehicular pollutant concentrations in urban street canyons." *Atmospheric Environment*, 29(24), 3719-3725.

Appendix A. UCD 2001 Simulations of the GM Dataset

Appendix B. CALINE3 Simulations of the GM Dataset Assuming a Surface Roughness of 250 Centimeters

Appendix C. CALINE3 Simulations of the GM Dataset Assuming a Surface Roughness of 3 Centimeters

Appendix D. CALINE4 Simulations of the GM Dataset Assuming a Surface Roughness of 250 Centimeters

Appendix E. CALINE4 Simulations of the GM Dataset Assuming a Surface Roughness of 3 Centimeters